Geochemical Architecture of the Lower- to Middle-crustal Section of a Paleo-island Arc (Kohistan Complex, Jijal–Kamila Area, Northern Pakistan): Implications for the Evolution of an Oceanic Subduction Zone

Bruno Dhuime, Delphine Bosch, Carlos J Garrido, Jean-Louis Bodinier, Olivier Bruguier, Sahid S Hussain, Hamid Dawood

JOURNAL OF PETROLOGY | VOLUME 50 | NUMBER 3 | PAGES 531–569 | 2009 | doi:10.1093/petrology/egp010

Geochemical Architecture of the Lower- to Middle-crustal Section of a Paleo-island Arc (Kohistan Complex, Jijal–Kamila Area, Northern Pakistan): Implications for the Evolution of an Oceanic Subduction Zone

BRUNO DHUIME[1]*, DELPHINE BOSCH[1], CARLOS J. GARRIDO[2], JEAN-LOUIS BODINIER[1], OLIVIER BRUGUIER[1], SAHID S. HUSSAIN[3] AND HAMID DAWOOD[3]

[1]LABORATOIRE GÉOSCIENCES MONTPELLIER, EQUIPE MANTEAU-NOYAU, UMR 5243, CNRS & UNIVERSITÉ DE MONTPELLIER 2, CC 60, 34095 MONTPELLIER CEDEX 05, FRANCE

[2]INSTITUTO ANDALUZ DE CIENCIAS DE LA TIERRA (IACT), CSIC & UGR, FACULTAD DE CIENCIAS, FUENTENUEVA S/N, 18002 GRANADA, SPAIN

[3]PAKISTAN MUSEUM OF NATURAL HISTORY, GARDEN AVENUE, SHAKARPARIAN, 44000 ISLAMABAD, PAKISTAN

RECEIVED MARCH 17, 2008; ACCEPTED FEBRUARY 13, 2009
ADVANCE ACCESS PUBLICATION MARCH 19, 2009

The processes active in the deep crust above an oceanic subduction zone during its evolution have been constrained through a detailed geochemical study (major and trace elements and Sr, Nd and Pb isotopes) of representative samples through an ~30 km thick exhumed crustal section of the Cretaceous Kohistan oceanic island arc (Northern Pakistan). The use of both trace elements and radiogenic isotopes reveals two distinct geochemical suites (suites A and B) within the Jijal–Patan–Kiru–Kamila (JPKK) complex. Suite A is characterized by a progressive enrichment in ^{207}Pb and a decrease in $^{143}Nd/^{144}Nd$ with increasing La_N/Sm_N. Suite B has higher $^{207}Pb/^{204}Pb$ and lower $^{143}Nd/^{144}Nd$ ratios with approximately constant La_N/Sm_N. By combining trace elements with different partitioning behaviour it is demonstrated that there is an increasing contribution of the subduction component in the magmas with time. It is also possible to distinguish a slab component imprint carried by aqueous fluids from one corresponding to sediment melts. Intrusive granites are abundant in the upper levels of the JPKK section. All were generated at the arc root level (Jijal crustal section) during dehydration-melting of hornblende-rich plutonic rocks. A three-stage geodynamic model is proposed for the evolution of the arc over a period of ~30 Myr. The first stage (~117–105 Ma) starts with the onset of subduction, which was followed by the building of the volcanic arc. The second stage (~105–99 Ma to ~96–91 Ma) corresponds to a major igneous event, which was characterized by abundant magma underplating and granulite-facies metamorphism at the arc base. Recycling of the residual–cumulative lower crust into the convective asthenospheric mantle was efficient during this stage, and was probably related to thermo-mechanical erosion of the base of the crust. The last stage (~95–85 Ma) corresponds to a period of low magmatic activity, which marked the end of the intra-oceanic subduction. This is related to the formation of a 'cold blanket' above the slab surface as a result of thermo-mechanical erosion of the cold walls of the subduction zone (i.e. the upper part of the slab and the base of the overriding plate), and corner flow dragging the cold material into the zone of melt generation. Ultimately, a voluminous magmatic pulse occurred around 85 Ma (forming the Chilas complex), before arc–continent collision.

KEY WORDS: *arc magmas; geochemistry; island arc; Kohistan; Sr, Nd, Pb isotopes*

*Corresponding author. Present address: Department of Earth Sciences, University of Bristol, Wills Memorial Building, Queens Road, Bristol BS8 1RJ, UK. Telephone: +44 (0)117 95 45 247. Fax: +44 (0)117 92 53 385. E-mail: B.Dhuime@bristol.ac.uk

INTRODUCTION

Subduction is a major geodynamic process in the evolution of the Earth. Active margins represent key sites for recycling of sediments from the Earth's surface to the mantle, contributing to upper mantle heterogeneity. Moreover, subduction zones have been considered as the main site for the formation of juvenile crust in the Phanerozoic (e.g. McLennan & Taylor, 1985; Rudnick, 1995; Condie & Chomiak, 1996). Thus the characterization of arc magmas, their evolution in space and time, and the relationship between arc magmatism and continental crust formation have been major research topics in petrology and geochemistry during the last three decades.

Most island arc lavas are thought to originate from magmas formed during partial melting of the sub-arc peridotitic mantle wedge in response to flux melting triggered by aqueous fluids and/or silicate melts from the subducting plate (Nicholls & Ringwood, 1973; Ringwood, 1974; Gill, 1981; Arculus & Powell, 1986; Tatsumi *et al.*, 1986; Ellam & Hawkesworth, 1988; Tatsumi, 1989; McCulloch & Gamble, 1991; Davies & Stevenson, 1992; Hawkesworth *et al.*, 1993; Pearce & Parkinson, 1993; Plank & Langmuir, 1993; Woodhead *et al.*, 1993; Arculus, 1994; Stolper & Newman, 1994). Fluids and/or melts derived from both the sediment and variably altered oceanic crust portions of the slab modify the composition of the sub-arc mantle wedge (Tera *et al.*, 1986; Ellam & Hawkesworth, 1988; von Huene & Scholl, 1993; Miller *et al.*, 1994; Kamenetsky *et al.*, 1997). The mantle wedge is generally thought to have an initial composition similar to the depleted MORB mantle source (DMM) of mid-ocean ridge basalts (MORB) (Perfit *et al.*, 1980; Hawkesworth, 1982; White & Patchett, 1984; Tatsumi *et al.*, 1986; Davidson, 1987; Ewart & Hawkesworth, 1987; Ryerson & Watson, 1987), although a more enriched source similar to that of ocean island basalts (OIB) has been proposed in some cases (e.g. Morris & Hart, 1983; Woodhead, 1989; Crawford *et al.*, 1995; Peate *et al.*, 1997).

Island arc basalts are distinguished from other basalts (e.g. MORB and OIB) by their enrichment in large ion lithophile elements (LILE) and, to a lesser extent, in light rare earth elements (LREE) relative to high field strength elements (HFSE) (e.g. Gill, 1981; Pearce, 1982; Hawkesworth *et al.*, 1991, 1993). To explain the distinctive geochemical characteristics of island arc basalts, many studies have argued for a multi-component model involving contributions from the mantle wedge and from one or more 'subduction components' conveyed by aqueous fluids and/or silicate melts (e.g. Kay, 1980; Ellam & Hawkesworth, 1988; Miller *et al.*, 1994; Gamble *et al.*, 1996; Turner *et al.*, 1996; Elliott *et al.*, 1997; Hawkesworth *et al.*, 1997a, 1997*b*; Turner *et al.*, 1997; Münker, 2000; Garrido *et al.*, 2005). However, many uncertainties remain, notably concerning the extent of slab–mantle interaction, and the decoupling between fluids and melts derived from the slab (e.g. Hawkesworth *et al.*, 1991, 1993; McCulloch & Gamble, 1991; Saunders *et al.*, 1991; Davies & Stevenson, 1992; Plank & Langmuir, 1993; Woodhead *et al.*, 1993).

The processes active in subduction zones and their temporal evolution can be followed indirectly via the study of erupted lavas or of well-preserved, exhumed, paleo-arc sections such as the Jurassic Talkeetna arc in Alaska (e.g. Barker & Grantz, 1982; DeBari & Coleman, 1989) and the Cretaceous Kohistan arc in North Pakistan (e.g. Bard, 1983; Treloar *et al.*, 1996). This study provides the first detailed geochemical study of the Kohistan arc that combines major element, transition metal, REE and incompatible element analysis of whole-rocks with high-precision Sr, Nd and Pb isotopic data for whole-rocks and mineral separates. It is based on representative samples collected across an ~30 km lower- to middle-crustal section of the Kohistan Arc Complex (KAC, Northern Pakistan, Fig. 1). We specifically focus on the geochemical variations across a section of the arc and on the determination of genetic relationships between the various rock types exposed. The aims are to define the source(s) of the arc magmatism and the processes of magmatic evolution and arc building through time.

Our results suggest an evolutionary continuum between contributions from three main components in the source (i.e. 'DMM-like' asthenospheric mantle, subducted sediments and altered oceanic crust). The precise characterization of trace element distribution in the arc crust reveals that the subduction component was conveyed by slab fluids during the first phase of arc magmatism with subsequent evolution of the subduction zone characterized by the superimposition and the amplification of a 'slab melt' component in the source of the younger magmas. Based on our geochemical data and radiometric ages from previous studies, we propose a three-stage geodynamic model of arc evolution, starting with subduction initiation and leading up to arc–continent collision.

TECTONIC AND GEOLOGICAL SETTING

The Kohistan Arc Complex is located in northern Pakistan, between the Karakoram (Asian) plate to the north and the Indian plate to the south (Fig. 1). It is separated from these blocks by two major faults; the Main Karakoram Thrust (or Northern Suture) and the Main Mantle Thrust (or Indus Suture), respectively. The KAC constitutes the exhumed section of a Cretaceous intra-oceanic island arc formed during the northward subduction of the Neo-Tethys ocean beneath the Karakoram

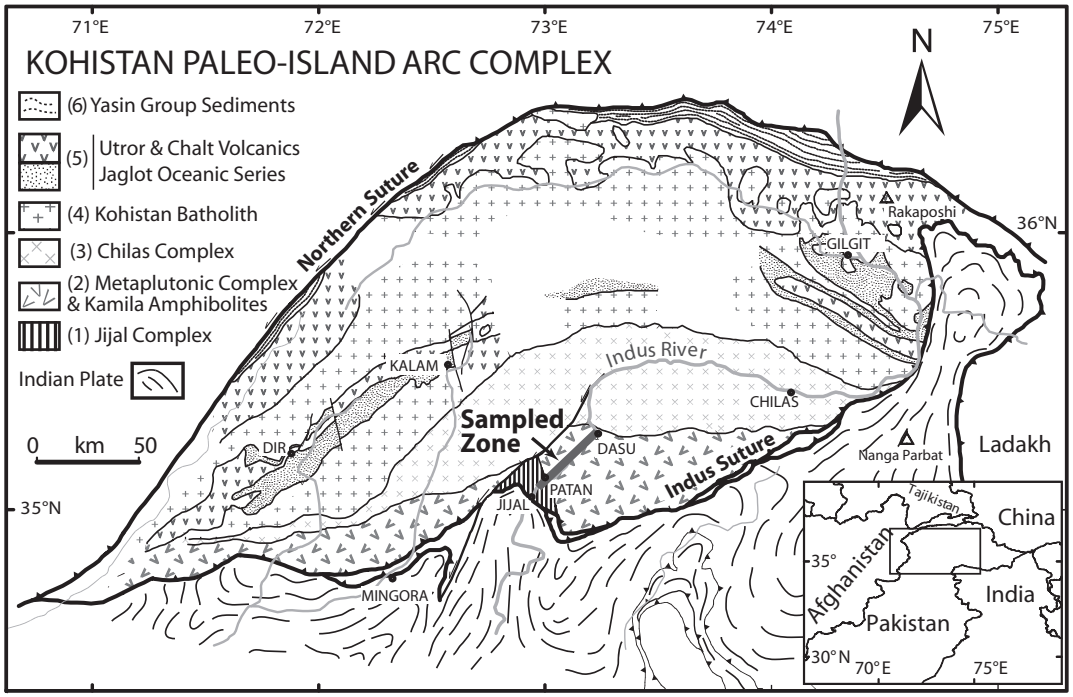

Fig. 1. Simplified geological map of the Kohistan Island Arc Complex (KAC, Northern Pakistan), modified after Burg *et al.* (1998). (1) Jijal ultramafic–mafic complex; (2) Kamila amphibolite belt or 'metaplutonic complex'; (3) intrusive Chilas ultramafic–mafic complex (~85 Ma); (4) Kohistan Batholith; (5) Jurassic to Cretaceous metasedimentary and metavolcanic units of the Jaglot and Utror–Chalt groups; (6) Albian–Aptian volcano-sedimentary Yasin group. The sampled zone between Jijal–Patan and Dasu is shown in more detail in Fig. 3.

plate (Tahirkheli, 1979; Bard *et al.*, 1980; Coward *et al.*, 1982, 1986; Bard, 1983). The KAC is subdivided into six distinct units (Jijal complex; 'Kamila amphibolite belt' or 'metaplutonic complex'; Chilas complex; Kohistan Batholith; Jaglot and Utror–Chalt groups; Yasin group) from south to north along a transect spanning ~200 km (Fig. 1). This study focuses on the Jijal complex and the overlying metaplutonic complex (Fig. 2), that represent the lower and mid- to upper sections, respectively, of an ~30 km thick crust accreted during the island arc building stage between ~117 Ma and 85 Ma (Le Fort *et al.*, 1983; Schärer *et al.*, 1984; Petterson & Windley, 1985; Pudsey, 1986; Treloar *et al.*, 1989; Debon & Khan, 1996; Mikoshiba *et al.*, 1999; Yamamoto & Nakamura, 2000; Fraser *et al.*, 2001; Schaltegger *et al.*, 2002; Yamamoto *et al.*, 2005; Garrido *et al.*, 2006; Dhuime *et al.*, 2007).

The Jijal complex consists of a lower ultramafic and an upper mafic section (Jan, 1979; Bard *et al.*, 1980; Jan & Howie, 1981; Miller & Christensen, 1994; Burg *et al.*, 1998; Garrido *et al.*, 2006, 2007). The ultramafic section formed at 117 ± 7 Ma (Dhuime *et al.*, 2007) during melt–rock reaction between lithospheric mantle and REE-depleted 'boninite-like' melts (Dhuime *et al.*, 2007; Garrido *et al.*, 2007). The transition between the spinel-bearing peridotites of the ultramafic section (dunites, wehrlites and pyroxenites) and the gabbroic rocks of the mafic section (mainly garnet-bearing gabbros, also referred to as 'garnet granulites' in the literature) represents the mantle–crust transition of the KAC (Bard, 1983; Miller *et al.*, 1991; Burg *et al.*, 1998; Dhuime *et al.*, 2007; Garrido *et al.*, 2007). The crustal section of the Jijal complex was metamorphosed to form high-pressure granulites ($T = 700$–$950°C$, $P > 1$ GPa) at ~91–96 Ma (Yamamoto, 1993; Yamamoto & Nakamura, 1996, 2000; Yoshino *et al.*, 1998; Ringuette *et al.*, 1999; Anczkiewicz & Vance, 2000; Anczkiewicz *et al.*, 2002).

The metaplutonic complex (Zeilinger, 2002) crops out along the Karakoram highway (Fig. 2). It represents a thick pile of metabasic rocks that was metamorphosed and variably deformed under amphibolite-facies conditions (i.e. 550–650°C and 0·9–1·0 GPa; Tahirkheli *et al.*, 1979; Bard, 1983; Jan, 1988; Treloar *et al.*, 1989, 1990; Khan *et al.*, 1993; Zeilinger, 2002), prior to 83 ± 1 Ma [Ar–Ar cooling age on hornblende after Treloar *et al.* (1990)]. Most of these rocks were originally laccoliths and they are interlayered with rocks interpreted as either former volcanic or volcano-sedimentary formations or remnants of oceanic crust (Bard *et al.*, 1980; Coward *et al.*, 1986; Jan, 1988; Khan *et al.*, 1993; Treloar *et al.*, 1996; Bignold *et al.*, 2006).

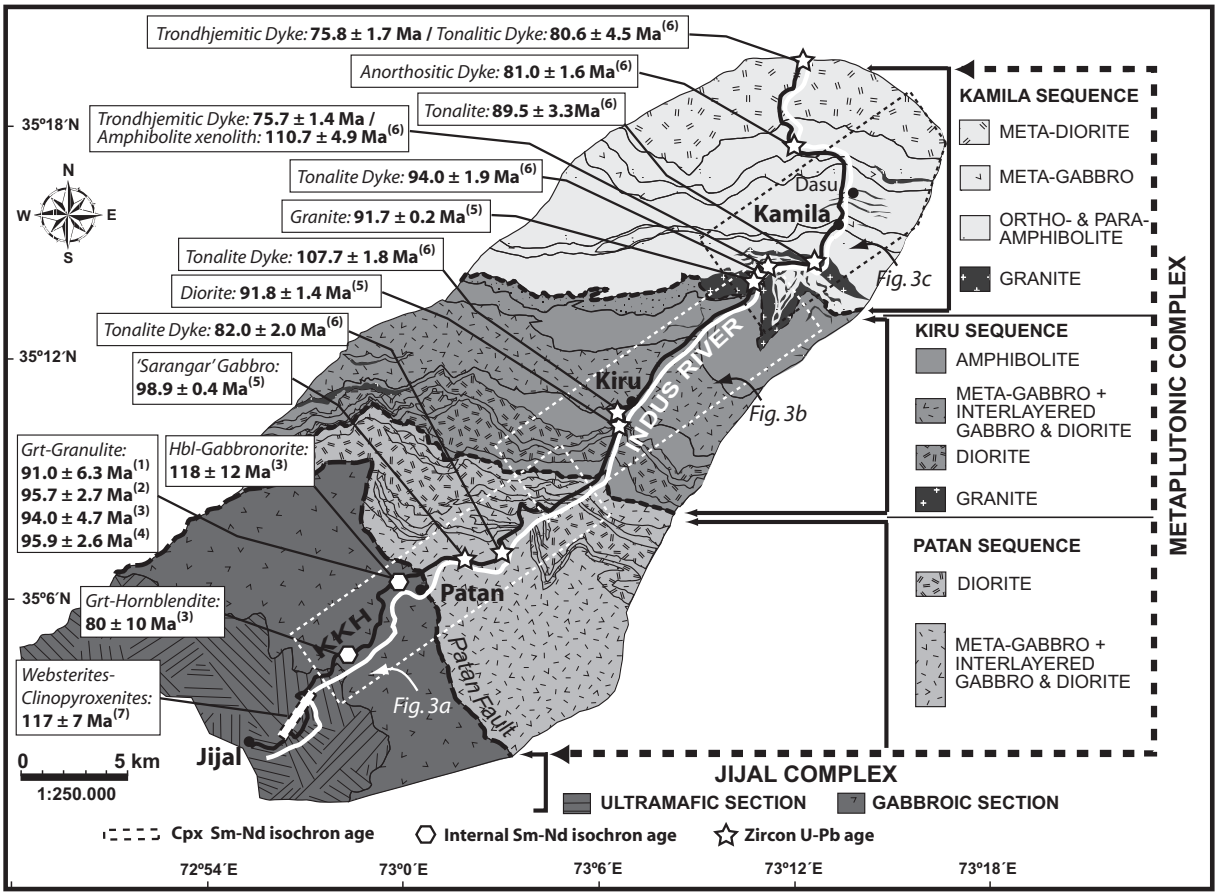

Fig. 2. Simplified geological map of the Jijal–Patan–Kiru–Kamila (JPKK) transect of the Kohistan arc along the Indus valley, modified after Zeilinger (2002) and Garrido *et al.* (2006). Published radiometric ages are reported after: [(1)]Yamamoto & Nakamura (1996); [(2)]Anczkiewicz & Vance (1997); [(3)]Yamamoto & Nakamura (2000); [(4)]Anczkiewicz *et al.* (2002); [(5)]Schaltegger *et al.* (2002); [(6)]Yamamoto *et al.* (2005); [(7)]Dhuime *et al.* (2007). Grt, garnet; Hbl, hornblende; Cpx, clinopyroxene.

FIELD RELATIONS AND SAMPLE SELECTION

The Jijal complex (mafic crustal section)

The mafic section of the Jijal complex constitutes the lowermost exposed crustal levels of the KAC (Figs 2 and 3a). This ~3 km thick granulite section is dominated by garnet-bearing metagabbroic rocks (garnet granulite). Scarce hornblende-bearing gabbronorites present in the top of the section are inferred to represent the magmatic protolith for the garnet granulites (Bard, 1983; Yamamoto, 1993; Yoshino *et al.*, 1998; Yamamoto & Nakamura, 2000; Garrido *et al.*, 2006). Hornblendite lenses (10–100 m thick) are enclosed in the garnet granulites. These rocks are more abundant at the base of the section and show, at outcrop scale, modal variations between (± clinopyroxene)–garnet-hornblendite and hornblende-garnetite. Detailed petrological–geochemical (Garrido *et al.*, 2006) and Sr–Nd–Pb isotopic studies (Dhuime *et al.*, 2007, Fig. 3a) have already been undertaken on the mafic section of the Jijal complex.

The Patan–Kiru–Kamila metaplutonic complex

The metaplutonic complex can be subdivided into three sequences; these are, from bottom to top, the Patan, Kiru and Kamila sequences (Fig. 2). Samples were collected along a SW–NE transect that is roughly orthogonal to the arc stratification.

The Patan sequence

The Patan sequence forms an ~7 km thick pile of interlayered metagabbros and metadiorites, and is heterogeneously deformed along anastomosing shear zone networks (Figs 2 and 3a). The 'Sarangar gabbro' at the base of the Patan sequence constitutes up to 50% of the entire sequence. It is a thick, massive gabbroic body of

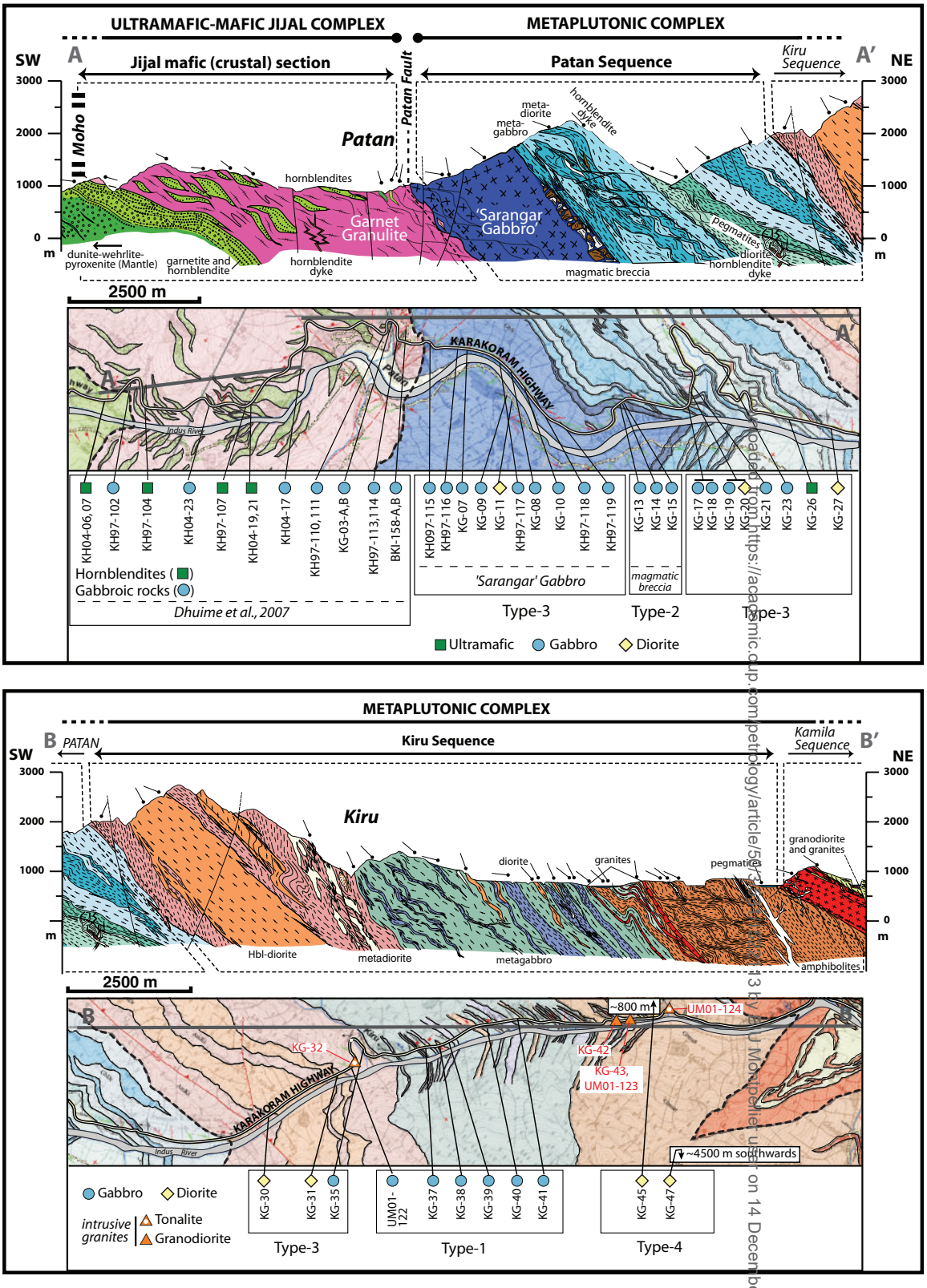

Fig. 3. Geological cross-section and associated geological map showing sample type and location through the JPKK crustal section of the Kohistan arc, modified after Zeilinger (2002) Geometric symbols reflect SiO_2 content [ultramafic: $SiO_2 \leq 45\%$; gabbro: $45\% < SiO_2 \leq 55\%$; diorite: $55\% < SiO_2 \leq 63\%$; 'intrusive granites' (tonalites and granodiorites): $SiO_2 > 63\%$]. The location of the volcanic–plutonic rocks as a function of their trace element characteristics, from Type-1 to Type-5 (see Fig. 4), is also indicated. (a) Section from the lower garnet granulite zone of the Jijal complex to the Patan sequence of the metaplutonic complex [including samples of Dhuime *et al.* (2007)]; (b) section through the Kiru sequence of the metaplutonic complex; (c) section through the Kamila sequence of the metaplutonic complex (i.e. the uppermost section of the metaplutonic complex, close to the contact with the intrusive Chilas complex). The black ellipse indicates the projected position of the UM01-133 to -135 samples (out of map) along the CC' cross-section.

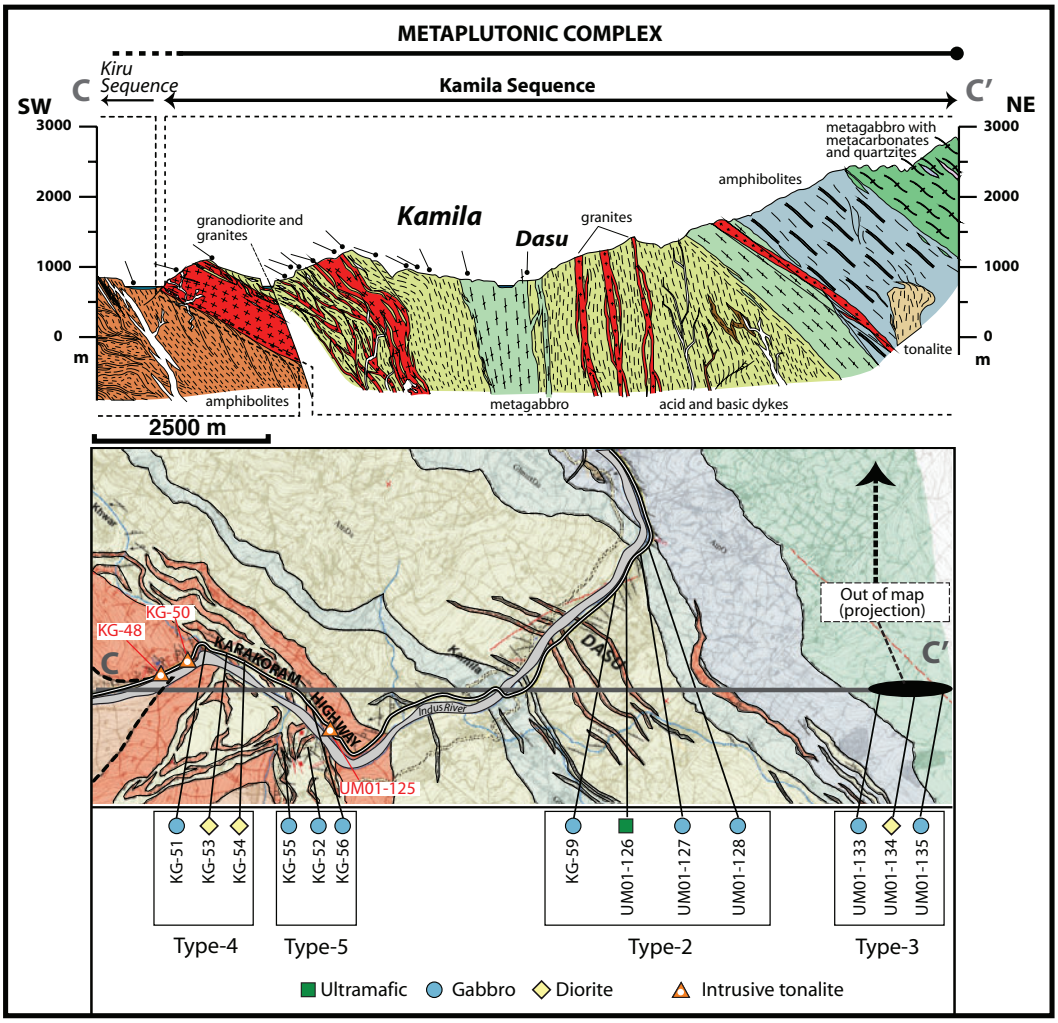

Fig. 3. Continued

coarse-grained meta-gabbro or gabbrodiorite with locally preserved igneous layering (Zeilinger, 2002). The Sarangar gabbro is intrusive into the underlying Jijal garnet-bearing metagabbros (Zeilinger, 2002). The top of the Patan sequence consists of metagabbro, diorite and hornblendite sills of various thicknesses, which are occasionally intruded by pegmatite and hornblendite dykes. The contact between these units and the underlying Sarangar gabbro forms an ~100 m thick magmatic breccia that includes gabbroic to tonalitic facies rocks.

Twenty-two representative samples from the Patan sequence were selected (Fig. 3a and Table 1): 10 Sarangar gabbros (KH97-115, KH97-116, KG-07, KG-09, KG-11, KH97-117, KG-08, KG-10, KH97-118 and KH97-119); four magmatic breccias (KG-13a, KG-13b, KG-14 and KG-15); and eight metaplutonic samples from the upper Patan sequence (KG-17, KG-18, KG-19, KG-20, KG-21, KG-23, KG-26 and KG-27).

The Kiru sequence

The contact between the Patan and Kiru sequences is irregular, and it is characterized by interfingered slices from both formations (Zeilinger, 2002). The Kiru sequence forms an ~7 km thick pile of strongly deformed, imbricated sills with compositions that range from gabbroic to dioritic (Figs 2 and 3b). Its lower part contains fine-grained and layered rocks from gabbroic to dioritic facies [the 'Kiru amphibolites' of Zeilinger (2002)], which are intruded by coarse- to medium-grained hornblende-rich metadiorites. A thick pile of interlayered gabbros (with rare enclosed metacarbonates lenses) and diorites showing various degrees of amphibolitization and deformation occurs further up section. The top of the Kiru sequence [the 'Mandraza amphibolites' of Zeilinger (2002)] is composed of coarse- to medium-grained metagabbros or metadiorites and is interlayered with fine-grained hornblende-rich rocks. Intrusive pegmatites and granites

Table 1: Major and trace elements for the JPKK crustal section

	Type-1 plutonics–volcanics					
Lat. (N):	35°10′51·25″	35°11′30·01″	35°11′35·81″	35°11′40·99″	35°12′06·01″	35°12′21·49″
Long. (E):	73°06′33·26″	73°07′09·62″	73°07′16·72″	73°07′20·86″	73°07′35·80″	73°07′52·57″
Sample:	UM01-122	KG-37	KG-38	KG-39	KG-40	KG-41
Unit:	Kiru	Kiru	Kiru	Kiru	Kiru	Kiru
Rock type:	Gabbro	Gabbro	Gabbro	Gabbro	Gabbro	Gabbro
Geochemical suite:	A	A	A	A	A	A
wt %						
SiO_2	49·81	46·23	48·12	47·11	46·96	48·35
TiO_2	0·70	0·18	0·22	0·30	1·40	0·56
Al_2O_3	15·82	19·37	18·32	17·02	15·79	16·72
FeO_T	7·79	5·67	3·72	6·95	11·65	6·94
MnO	0·16	0·11	0·08	0·12	0·20	0·13
MgO	8·52	9·35	8·59	9·82	7·26	8·50
CaO	12·42	13·86	16·93	13·50	12·14	14·34
Na_2O	1·83	1·47	0·88	1·54	2·25	1·57
K_2O	0·11	0·08	0·02	0·03	0·03	0·06
P_2O_5	0·09	0·01	0·01	0·01	0·02	0·01
LOI	1·53	2·17	1·84	2·55	0·96	1·71
Total	98·78	98·50	98·73	98·95	98·66	98·89
Mg-no.	66	75	80	72	53	69
ppm						
Sc	37	26	43	34	42	46
Ti	3212	1341	1629	1730	8677	4030
V	164	128	157	136	415	242
Ni	121	179	175	179	64	133
Cr	263	323	426	363	175	238
Rb	1·70	1·75	0·45	0·58	0·77	1·11
Sr	187	119	120	103	171	140
Y	19·7	5·03	5·97	5·82	13·3	10·5
Zr-XRF	22·0	9·6	9·4	9·2	14·0	12·4
Nb	1·52	0·11	0·03	0·16	0·24	0·06
Cs	0·03	0·07	0·02	0·03	0·02	0·05
Ba	16·5	13·0	4·80	9·33	9·71	11·6
La	2·40	0·43	0·28	0·28	0·48	0·39
Ce	7·01	1·06	0·86	0·88	1·61	1·21
Pr	1·20	0·17	0·17	0·19	0·33	0·25
Nd	6·94	1·02	1·12	1·23	2·33	1·70
Sm	2·39	0·41	0·48	0·58	1·07	0·77
Eu	0·90	0·31	0·34	0·41	0·86	0·50
Gd	3·37	0·70	0·85	1·01	1·88	1·38
Tb	0·59	0·13	0·15	0·19	0·34	0·26
Dy	4·22	0·93	1·10	1·37	2·46	1·89
Ho	0·88	0·19	0·23	0·29	0·50	0·39
Er	2·53	0·53	0·62	0·83	1·38	1·03
Tm	0·37	0·07	0·09	0·11	0·19	0·15
Yb	2·39	0·46	0·53	0·72	1·18	0·90
Lu	0·37	0·07	0·08	0·11	0·19	0·14
Ta	0·11	0·01	0·00	0·01	0·02	0·00
Pb	0·46	0·29	0·21	1·27	0·25	0·48
Th	0·04	0·02	0·01	0·01	0·01	0·01
U	0·02	0·02	0·01	0·002	0·01	0·02
ΣREE (ppm)	35·6	6·49	6·89	8·20	14·8	11·0
Eu^*	0·97	1·73	1·62	1·60	1·84	1·47
La_N	10·1	1·82	1·18	1·19	2·04	1·63
Yb_N	14·0	2·69	3·12	4·22	6·94	5·28
Ce_N/Yb_N	0·82	0·64	0·45	0·34	0·38	0·37
La_N/Sm_N	0·65	0·68	0·38	0·31	0·29	0·32

(continued)

Table 1: Continued

	Type-2 plutonics–volcanics					
Lat. (N):	35°07′42·78″	35°07′42·78″	35°07′43·18″	35°07′43·86″	35°16′55·16″	35°17′09·72″
Long. (E):	73°02′48·88″	73°02′48·88″	73°02′49·24″	73°02′49·31″	73°13′27·91″	73°13′24·02″
Sample:	KG-13a	KG-13b	KG-14	KG-15	KG-59	UM01-126
Unit:	Patan	Patan	Patan	Patan	Kamila	Kamila
Rock type:	Gabbro	Gabbro	Gabbro	Gabbro	Gabbro	UB
Geochemical suite:	A	A	A	A	A	A
wt %						
SiO_2	48·60	46·76	45·33	44·05	44·73	42·40
TiO_2	1·13	1·03	1·63	1·31	1·29	1·99
Al_2O_3	22·16	18·45	18·83	10·56	19·85	14·35
FeO_T	6·37	9·29	11·04	14·65	10·00	11·54
MnO	0·08	0·13	0·15	0·24	0·14	0·14
MgO	3·06	6·41	5·22	12·30	5·91	12·87
CaO	10·25	10·34	10·48	10·24	10·83	10·69
Na_2O	4·02	2·96	2·88	1·23	2·78	2·32
K_2O	0·15	0·15	0·18	0·15	0·20	0·24
P_2O_5	0·26	0·15	0·41	0·09	0·10	0·05
LOI	1·50	1·46	0·89	1·42	2·63	1·78
Total	97·58	97·13	97·04	96·24	98·46	98·37
Mg-no.	46	55	46	60	51	66
ppm						
Sc	23	41	41	73	21	51
Ti	6199	5862	8907	7145	7787	10761
V	232	313	304	418	287	395
Ni	10	32	18	76	53	173
Cr	34	85	35	150	82	209
Rb	0·87	0·60	0·71	0·63	1·15	0·93
Sr	560	427	375	34	533	171
Y	14·5	19·7	23·5	33·7	19·3	22·3
Zr-XRF	25·5	28·8	31·5	45·4	46·6	47·0
Nb	0·86	0·84	1·65	1·27	1·41	1·73
Cs	0·07	0·05	0·07	0·03	0·04	0·02
Ba	89·4	50·3	60·0	21·5	32·8	25·4
La	3·21	2·40	5·20	1·37	3·34	2·55
Ce	8·75	7·23	15·7	6·51	10·3	8·92
Pr	1·34	1·20	2·52	1·37	1·80	1·70
Nd	7·55	6·96	14·1	9·00	10·7	10·4
Sm	2·22	2·35	4·23	3·45	3·28	3·46
Eu	0·94	0·95	1·32	0·98	1·28	1·28
Gd	3·01	3·25	5·41	4·99	4·10	4·69
Tb	0·48	0·53	0·86	0·85	0·64	0·77
Dy	3·14	3·62	5·78	5·93	4·08	5·21
Ho	0·62	0·73	1·18	1·24	0·81	1·03
Er	1·62	2·00	3·30	3·46	2·11	2·82
Tm	0·22	0·27	0·46	0·50	0·29	0·37
Yb	1·27	1·58	2·86	3·02	1·79	2·32
Lu	0·19	0·24	0·45	0·47	0·28	0·35
Ta	0·03	0·03	0·08	0·06	0·07	0·09
Pb	1·88	1·23	1·14	5·29	0·78	1·17
Th	0·12	0·06	0·22	0·01	0·04	0·04
U	0·05	0·04	0·08	0·03	0·03	0·03
ΣREE (ppm)	34·5	33·3	63·3	43·1	44·8	45·8
Eu^*	1·11	1·05	0·84	0·72	1·07	0·97
La_N	13·5	10·1	21·9	5·8	14·1	10·8
Yb_N	7·44	9·3	16·8	17·8	10·5	13·6
Ce_N/Yb_N	1·92	1·27	1·52	0·60	1·61	1·07
La_N/Sm_N	0·93	0·66	0·79	0·26	0·66	0·48

(continued)

Table 1: Continued

	Type-2 plutonics–volcanics		Type-3 plutonics–volcanics			
Lat. (N):	35°17′15·84″	35°17′21·80″	35°06′56·12″	35°07′04·46″	35°07′07·28″	35°07′15·64″
Long. (E):	73°13′25·28″	73°13′25·70″	73°00′26·02″	73°00′46·26″	73°00′52·38″	73°01′16·20″
Sample:	UM01-127	UM01-128	KH97-115	KH97-116[1]	KG-07[1]	KH97-117[1]
Unit:	Kamila	Kamila	Patan	Patan	Patan	Patan
Rock type:	Gabbro	Gabbro	Gabbro	Gabbro	Gabbro	Gabbro
Geochemical suite:	A	A	B, group B1	B, group B1	B, group B1	B, group B1
wt %						
SiO_2	44·73	51·78	48·18	51·62	52·14	53·66
TiO_2	1·12	1·05	0·71	0·88	0·82	0·79
Al_2O_3	21·66	19·65	18·22	16·60	17·49	17·08
FeO_T	9·61	8·08	10·26	9·34	9·05	8·96
MnO	0·19	0·18	0·18	0·18	0·17	0·19
MgO	3·30	4·13	6·18	5·15	5·52	4·92
CaO	11·06	8·42	10·95	9·46	9·78	9·32
Na_2O	3·55	4·15	2·14	3·76	2·09	2·43
K_2O	0·09	0·24	0·29	0·69	0·49	0·38
P_2O_5	0·58	0·17	0·03	0·18	0·11	0·14
LOI	2·42	0·66	1·12	1·08	0·90	0·63
Total	98·31	98·51	98·26	98·94	98·56	98·49
Mg-no.	38	48	52	49	52	49
ppm						
Sc	13	16	38	37	32	34
Ti	6535	5793	—	—	4993	—
V	119	139	245	262	249	253
Ni	3	8	20	23	30	19
Cr	3	3	80	79	176	73
Rb	0·39	1·14	1·51	3·71	2·77	1·61
Sr	573	551	253	235	293	242
Y	25·7	21·5	12·3	20·8	15·0	20·7
Zr-XRF	120	32·0	25·0	48·2	44·1	38·9
Nb	2·71	4·13	0·87	2·04	1·24	2·16
Cs	0·26	0·05	0·02	0·24	0·16	0·06
Ba	34·1	50·3	108	233	138	156
La	4·63	7·13	3·68	7·65	5·59	8·32
Ce	15·2	19·2	7·64	16·5	13·1	17·9
Pr	2·69	3·04	1·12	2·39	1·73	2·55
Nd	15·7	16·4	5·21	10·9	8·34	11·4
Sm	4·67	4·87	1·54	2·99	2·25	2·99
Eu	1·71	1·50	0·77	1·08	0·81	1·06
Gd	5·71	5·55	2·09	3·76	2·86	3·69
Tb	0·90	0·82	0·36	0·62	0·48	0·61
Dy	5·95	5·25	2·55	4·32	3·33	4·26
Ho	1·19	0·99	0·55	0·92	0·69	0·91
Er	3·42	2·76	1·62	2·62	2·04	2·58
Tm	0·49	0·38	0·25	0·39	0·30	0·39
Yb	3·21	2·54	1·62	2·53	1·99	2·59
Lu	0·50	0·39	0·28	0·42	0·33	0·43
Ta	0·13	0·23	0·05	0·11	0·09	0·12
Pb	10·2	1·98	1·47	6·57	3·06	3·27
Th	0·07	0·07	0·12	0·26	0·21	0·13
U	0·04	0·03	0·04	0·08	0·06	0·05
ΣREE (ppm)	66·0	70·9	29·3	57·0	43·8	59·7
Eu^*	1·01	0·88	1·31	0·99	0·98	0·98
La_N	19·5	30·1	15·5	32·3	23·6	35·1
Yb_N	18·9	14·9	9·55	14·9	11·7	15·3
Ce_N/Yb_N	1·32	2·10	1·31	1·81	1·82	1·92
La_N/Sm_N	0·64	0·95	1·54	1·65	1·61	1·80

(continued)

Table 1: Continued

	Type-3 plutonics–volcanics					
Lat. (N):	35°07′14·23″	35°07′12·54″	35°06′59·54″	35°06′58·90″	35°07′10·55″	35°07′07·96″
Long. (E):	73°01′22·73″	73°01′35·58″	73°01′38·78″	73°01′45·16″	73°01′54·89″	73°02′22·84″
Sample:	KG-08	KG-10	KG-09[1]	KG-11[1]	KH97-118[1]	KH97-119[1]
Unit:	Patan	Patan	Patan	Patan	Patan	Patan
Rock type:	Gabbro	Gabbro	Gabbro	Diorite	Gabbro	Gabbro
Geochemical suite:	B, group B1	B, group B1	B, group B1	B, group B1	B, group B1	B, group B1
wt %						
SiO_2	49·80	52·49	53·91	53·49	53·15	51·99
TiO_2	0·81	0·80	0·95	0·84	1·05	0·69
Al_2O_3	17·65	17·57	19·28	16·62	16·70	18·19
FeO_T	10·30	8·68	9·48	9·12	8·95	9·15
MnO	0·19	0·16	0·16	0·17	0·16	0·18
MgO	5·90	5·03	4·68	4·93	4·81	5·57
CaO	10·47	9·62	10·17	9·10	9·45	10·45
Na_2O	1·73	2·27	2·26	2·32	2·41	1·96
K_2O	0·44	0·41	0·24	0·34	0·45	0·31
P_2O_5	0·06	0·21	0·13	0·09	0·17	0·08
LOI	0·61	0·87	0·63	1·08	1·12	0·04
Total	97·96	98·11	101·89	98·10	98·42	98·62
Mg-no.	50	51	47	49	49	52
ppm						
Sc	35	34	27	33	33	25
Ti	4856	3674	4486	4081	—	—
V	270	235	266	301	221	250
Ni	24	22	18	20	16	19
Cr	88	105	121	94	61	94
Rb	3·20	3·36	0·97	1·02	2·51	2·85
Sr	291	272	266	256	238	232
Y	15·6	16·2	15·5	14·4	18·6	15·7
Zr-XRF	49·0	42·7	43·3	35·8	43·0	31·8
Nb	0·97	0·76	1·11	0·60	1·78	1·22
Cs	0·12	0·08	0·06	0·09	0·11	0·09
Ba	185	115	80·5	71·7	139	120
La	5·24	6·41	5·49	4·18	6·65	4·43
Ce	11·9	15·3	12·6	9·77	15·5	10·2
Pr	1·58	2·06	1·70	1·36	2·10	1·34
Nd	7·71	10·1	8·40	6·75	10·3	6·70
Sm	2·18	2·73	2·38	1·99	2·80	1·84
Eu	0·86	1·06	0·93	0·79	1·09	0·73
Gd	2·81	3·38	3·06	2·60	3·66	2·34
Tb	0·48	0·55	0·50	0·45	0·61	0·39
Dy	3·35	3·80	3·49	3·14	4·16	2·79
Ho	0·71	0·78	0·73	0·66	0·87	0·58
Er	2·13	2·27	2·14	1·91	2·51	1·71
Tm	0·31	0·32	0·31	0·28	0·37	0·26
Yb	2·14	2·16	1·99	1·85	2·41	1·65
Lu	0·34	0·35	0·33	0·30	0·39	0·27
Ta	0·07	0·06	0·08	0·04	0·12	0·07
Pb	2·51	2·75	2·30	1·70	2·88	1·95
Th	0·12	0·67	0·29	0·17	0·42	0·29
U	0·05	0·19	0·09	0·09	0·13	0·08
ΣREE (ppm)	41·7	51·3	44·1	36·0	53·4	35·3
Eu^*	1·07	1·07	1·05	1·07	1·04	1·08
La_N	22·1	27·1	23·2	17·6	28·1	18·7
Yb_N	12·6	12·7	11·7	10·9	14·2	9·70
Ce_N/Yb_N	1·54	1·97	1·77	1·47	1·78	1·72
La_N/Sm_N	1·55	1·51	1·49	1·36	1·53	1·55

(continued)

Table 1: Continued

	Type-3 plutonics–volcanics					
Lat. (N):	35°08′06·94″	35°08′06·90″	35°08′14·02″	35°08′14·02″	35°08′16·01″	35°08′18·82″
Long. (E):	73°03′30·92″	73°03′30·53″	73°03′25·70″	73°03′25·70″	73°03′24·08″	73°03′22·28″
Sample:	KG-17	KG-18	KG-19a	KG-19b	KG-20	KG-21
Unit:	Patan	Patan	Patan	Patan	Patan	Patan
Rock type:	Gabbro	Gabbro	Gabbro	Gabbro	Gabbro	Gabbro
Geochemical suite:	B, group B2	B, group B2	B, group B2	B, group B2	B, group B2	B, group B2
wt %						
SiO_2	53·08	50·78	48·36	45·76	57·74	52·54
TiO_2	0·92	1·04	1·09	1·00	0·70	0·75
Al_2O_3	17·44	18·12	18·51	19·33	16·64	16·97
FeO_T	9·21	10·31	11·01	11·42	6·78	8·86
MnO	0·19	0·21	0·24	0·23	0·15	0·15
MgO	4·37	4·93	5·34	5·64	4·46	3·29
CaO	9·15	9·80	10·10	10·97	9·06	12·94
Na_2O	2·54	2·59	2·60	2·50	2·60	0·40
K_2O	0·28	0·29	0·20	0·33	0·19	
P_2O_5	0·17	0·19	0·20	0·21	0·15	0·16
LOI	0·69	0·15	0·18	0·59	0·27	2·79
Total	98·04	98·41	97·83	97·98	98·74	98·85
Mg-no.	46	46	46	47	54	40
ppm						
Sc	33	36	37	31	27	26
Ti	5921	6039	6183	6051	4062	4510
V	305	276	359	357	222	227
Ni	11	9	12	13	35	17
Cr	28	40	30	14	43	196
Rb	0·68	0·65	0·23	0·58	0·24	0·02
Sr	306	291	329	327	243	667
Y	26·8	24·8	21·7	22·5	24·3	12·3
Zr-XRF	75·9	68·2	54·6	44·4	87·2	39·1
Nb	1·97	2·28	1·76	1·54	1·57	1·41
Cs	0·01	0·01	0·004	0·01	0·01	0·01
Ba	88·5	86·9	63·0	81·2	56·3	9·81
La	9·26	9·38	7·34	8·22	6·00	6·16
Ce	23·6	24·1	18·3	21·1	15·8	14·2
Pr	3·09	3·37	2·41	2·80	2·18	1·85
Nd	14·7	16·3	11·5	13·2	10·7	8·66
Sm	3·72	4·15	2·98	3·30	2·92	2·13
Eu	1·23	1·35	1·18	1·38	1·02	0·89
Gd	4·33	4·95	3·54	3·77	3·55	2·53
Tb	0·70	0·81	0·57	0·61	0·60	0·41
Dy	4·76	5·56	3·84	4·07	4·09	2·80
Ho	0·99	1·15	0·80	0·85	0·84	0·57
Er	2·85	3·31	2·30	2·43	2·47	1·66
Tm	0·42	0·48	0·34	0·36	0·37	0·24
Yb	2·70	3·23	2·17	2·29	2·33	1·60
Lu	0·43	0·52	0·36	0·38	0·37	0·25
Ta	0·12	0·12	0·09	0·07	0·09	0·08
Pb	2·03	2·03	1·60	1·91	0·96	3·11
Th	0·09	0·06	0·12	0·25	0·06	0·07
U	0·03	0·03	0·04	0·08	0·03	0·03
ΣREE (ppm)	72·8	78·7	57·6	64·7	53·2	43·9
Eu^*	0·94	0·91	1·11	1·20	0·96	1·17
La_N	39·1	39·6	31·0	34·7	25·3	26·0
Yb_N	15·9	19·0	12·8	13·5	13·7	9·41
Ce_N/Yb_N	2·43	2·08	2·34	2·56	1·88	2·47
La_N/Sm_N	1·61	1·46	1·59	1·61	1·33	1·87

(continued)

Table 1: Continued

	Type-3 plutonics–volcanics					
Lat. (N):	35°08′41·03″	35°08′41·21″	35°08′54·64″	35°09′52·20″	35°10′39·47″	35°11′03·41″
Long. (E):	73°03′30·85″	73°04′36·44″	73°05′08·52″	73°06′07·81″	73°06′29·05″	73°06′34·70″
Sample:	KG-23	KG-26	KG-27	KG-30	KG-31	KG-35
Unit:	Patan	Patan	Patan	Kiru	Kiru	Kiru
Rock type:	Gabbro	UB	Diorite	Diorite	Diorite	Gabbro
Geochemical suite:	B, group B2	B, group B2	B, group B2	A	A	A
wt %						
SiO_2	53·41	41·83	54·56	58·48	56·98	52·40
TiO_2	1·11	1·07	0·96	0·59	0·57	0·40
Al_2O_3	18·35	20·58	16·74	18·19	18·94	17·97
FeO_T	8·96	12·95	8·82	5·17	5·92	7·02
MnO	0·27	0·18	0·20	0·11	0·15	0·15
MgO	3·75	6·03	4·51	2·58	2·70	6·92
CaO	8·20	12·26	8·57	7·17	7·40	10·19
Na_2O	2·90	1·08	2·37	4·15	3·84	2·87
K_2O	0·16	0·13	0·20	0·50	0·43	0·43
P_2O_5	0·31	0·27	0·23	0·22	0·22	0·10
LOI	0·83	1·31	1·02	1·44	1·87	0·96
Total	98·25	97·69	98·18	98·60	99·02	99·41
Mg-no.	43	45	48	47	45	64
ppm						
Sc	31	33	28	11	10	22
Ti	6714	6829	5970	3360	3175	2745
V	208	445	212	137	104	135
Ni	7	7	21	14	17	79
Cr	18	13	45	121	247	64
Rb	0·91	0·94	1·40	4·04	3·58	8·81
Sr	300	350	285	641	426	209
Y	36·3	17·6	20·5	12·0	15·6	16·8
Zr-XRF	73·2	21·8	37·3	127	94·3	115
Nb	2·01	0·87	1·70	2·39	2·81	2·90
Cs	0·05	0·11	0·01	0·15	0·14	0·15
Ba	45·4	30·1	67·0	172	130	73·4
La	7·48	4·92	6·31	7·27	8·52	7·88
Ce	18·7	13·0	15·1	18·4	21·2	18·6
Pr	2·59	1·83	2·06	2·56	2·91	2·33
Nd	13·0	9·12	10·5	11·7	13·4	10·1
Sm	3·41	2·27	2·73	2·62	2·95	2·22
Eu	1·41	0·85	1·17	0·90	1·02	0·78
Gd	4·39	2·67	3·29	2·69	3·20	2·51
Tb	0·73	0·42	0·51	0·40	0·49	0·41
Dy	5·45	2·87	3·45	2·52	3·29	2·83
Ho	1·22	0·59	0·71	0·50	0·67	0·59
Er	3·77	1·68	1·97	1·45	1·95	1·72
Tm	0·58	0·25	0·27	0·21	0·29	0·26
Yb	3·83	1·54	1·71	1·38	1·95	1·81
Lu	0·65	0·25	0·28	0·22	0·33	0·30
Ta	0·08	0·04	0·08	0·13	0·13	0·18
Pb	1·13	0·78	1·39	3·61	2·99	1·40
Th	0·07	0·16	0·26	0·13	0·14	0·70
U	0·04	0·07	0·11	0·09	0·04	0·22
ΣREE (ppm)	67·1	42·2	50·1	52·9	62·2	52·3
Eu^*	1·12	1·05	1·19	1·02	1·01	1·01
La_N	31·6	20·7	26·6	30·7	36·0	33·3
Yb_N	22·5	9·07	10·0	8·13	11·5	10·6
Ce_N/Yb_N	1·35	2·33	2·47	3·70	3·02	2·85
La_N/Sm_N	1·42	1·40	1·49	1·80	1·86	2·29

(continued)

Table 1: Continued

	Type-3 plutonics–volcanics			Type-4 plutonics–volcanics		
Lat. (N):	35°18′55·70″	35°21′00·30″	35°22′24·40″	35°11′49·88″	35°13′37·49″	35°14′38·22″
Long. (E):	73°11′31·10″	73°12′13·50″	73°12′15·80″	73°11′42·90″	73°08′47·18″	73°10′45·41″
Sample:	UM01-133	UM01-134	UM01-135	KG-47	KG-45	KG-51
Unit:	Kamila	Kamila	Kamila	Kiru	Kiru	Kamila
Rock type:	Gabbro	Diorite	Gabbro	Diorite	Diorite	Gabbro
Geochemical suite:	B, group B3	B, group B3	B, group B3	A	A	A
wt %						
SiO_2	52·08	54·66	51·16	56·99	54·66	51·55
TiO_2	0·72	0·90	0·82	0·65	0·44	0·59
Al_2O_3	19·01	16·34	16·16	15·18	20·72	18·81
FeO_T	7·34	7·70	8·40	7·04	5·44	6·92
MnO	0·15	0·16	0·18	0·12	0·13	0·15
MgO	5·72	5·33	6·99	5·13	2·79	5·35
CaO	10·06	8·10	9·18	7·85	8·37	9·63
Na_2O	3·07	3·21	2·86	2·79	3·36	2·54
K_2O	0·42	0·52	0·36	0·31	0·40	0·77
P_2O_5	0·10	0·18	0·11	0·12	0·15	0·11
LOI	0·00	1·53	2·04	2·70	2·41	2·12
Total	98·67	98·63	98·26	98·88	98·87	98·54
Mg-no.	58	55	60	56	48	58
ppm						
Sc	21	25	27	29	6	22
Ti	3936	5843	4820	4460	2011	4137
V	132	220	206	220	74	160
Ni	48	75	108	61	11	29
Cr	72	257	164	101	87	10
Rb	3·25	1·41	1·26	9·01	10·1	21·3
Sr	604	288	349	129	393	217
Y	11·2	16·6	14·6	16·2	7·05	13·8
Zr-XRF	31	90	70	73·5	26·1	40·5
Nb	1·41	2·78	2·14	1·19	2·09	2·23
Cs	0·13	0·15	1·24	0·19	0·24	0·36
Ba	118	145	101	84·1	164	191
La	6·46	9·26	6·08	5·18	7·51	6·68
Ce	14·3	20·4	14·1	12·6	16·3	14·9
Pr	1·90	2·56	1·96	1·66	2·00	1·80
Nd	8·8	11·6	9·4	7·95	9·10	7·89
Sm	2·14	2·77	2·47	2·06	2·10	1·88
Eu	0·84	0·95	0·89	0·79	0·77	0·81
Gd	2·46	3·27	2·96	2·59	2·11	2·34
Tb	0·38	0·52	0·48	0·43	0·29	0·38
Dy	2·51	3·44	3·24	3·03	1·70	2·54
Ho	0·50	0·69	0·66	0·63	0·32	0·51
Er	1·46	1·89	1·87	1·73	0·84	1·37
Tm	0·20	0·28	0·27	0·26	0·12	0·20
Yb	1·34	1·78	1·80	1·66	0·78	1·34
Lu	0·22	0·28	0·28	0·27	0·12	0·22
Ta	0·10	0·20	0·14	0·08	0·14	0·17
Pb	3·54	4·52	4·38	1·41	4·26	1·85
Th	0·25	0·06	0·06	0·80	0·73	2·08
U	0·06	0·02	0·02	0·17	0·24	0·54
ΣREE (ppm)	43·5	59·8	46·5	40·8	44·1	42·8
Eu^*	1·11	0·97	1·01	1·05	1·11	1·17
La_N	27·2	39·1	25·7	21·8	31·7	28·2
Yb_N	7·9	10·5	10·6	9·76	4·58	7·86
Ce_N/Yb_N	2·97	3·18	2·17	2·11	5·82	3·09
La_N/Sm_N	1·95	2·16	1·59	1·63	2·31	2·29

(continued)

Table 1: Continued

	Type-4 plutonics–volcanics		Type-5 plutonics–volcanics		
Lat. (N):	35°14′40·24″	35°14′43·48″	35°14′19·57″	35°14′30·08″	35°14′47·94″
Long. (E):	73°10′54·16″	73°11′07·30″	73°12′00·54″	73°12′11·09″	73°11′50·60″
Sample:	KG-53	KG-54	KG-52	KG-55	KG-56
Unit:	Kamila	Kamila	Kamila	Kamila	Kamila
Rock type:	Diorite	Diorite	Gabbro	Gabbro	Gabbro
Geochemical suite:	A	A	A	A	A
wt %					
SiO_2	61·43	57·65	49·35	47·11	49·45
TiO_2	0·51	0·81	0·79	0·94	0·89
Al_2O_3	14·20	16·58	20·75	19·02	16·73
FeO_T	5·90	7·30	7·74	9·86	10·58
MnO	0·14	0·15	0·15	0·19	0·22
MgO	5·54	3·29	3·18	4·29	5·45
CaO	6·93	7·21	8·67	9·52	10·64
Na_2O	2·60	2·73	3·08	2·38	1·47
K_2O	1·01	0·83	1·91	1·88	1·05
P_2O_5	0·13	0·18	0·47	0·74	0·18
LOI	1·46	1·55	2·64	2·53	2·42
Total	99·85	98·28	98·73	98·46	99·08
Mg-no.	63	44	42	44	48
ppm					
Sc	23	25	17	19	34
Ti	3547	5275	5595	5610	5462
V	158	216	215	264	401
Ni	100	13	6	7	23
Cr	444	44	9	16	30
Rb	28·7	25·4	54·1	50·4	34·5
Sr	170	255	865	690	761
Y	15·4	27·2	23·3	27·4	29·6
Zr-XRF	88·0	88·9	107	73·7	108
Nb	3·12	3·15	4·89	5·42	7·42
Cs	0·28	0·49	0·96	0·93	0·46
Ba	242	150	1445	1014	600
La	10·8	11·7	63·5	46·2	71·1
Ce	23·1	26·9	107	89·4	125
Pr	2·65	3·37	10·7	9·85	12·6
Nd	11·1	15·3	39·9	39·8	46·1
Sm	2·36	3·69	6·33	7·02	7·25
Eu	0·80	1·23	2·21	2·17	2·25
Gd	2·63	4·37	5·66	6·56	6·43
Tb	0·42	0·72	0·76	0·92	0·93
Dy	2·79	4·86	4·60	5·54	5·77
Ho	0·57	1·01	0·89	1·08	1·15
Er	1·55	2·89	2·34	2·91	3·25
Tm	0·24	0·43	0·33	0·41	0·49
Yb	1·52	2·77	2·02	2·47	3·15
Lu	0·25	0·46	0·32	0·39	0·51
Ta	0·27	0·22	0·20	0·19	0·38
Pb	1·08	2·07	4·76	3·42	4·76
Th	3·00	2·50	9·87	7·29	13·0
U	0·58	0·68	1·13	1·55	1·65
ΣREE (ppm)	60·8	79·6	246	215	286
Eu^*	0·97	0·94	1·10	0·96	0·99
La_N	45·7	49·2	268	195	300
Yb_N	8·95	16·3	11·9	14·5	18·5
Ce_N/Yb_N	4·21	2·69	14·7	10·1	11·1
La_N/Sm_N	2·97	2·04	6·48	4·24	6·33

(continued)

Table 1: Continued

	Intrusive granites				
Lat. (N):	35°10′55·34″	35°13′27·92″	35°14′15·47″	35°14′30·62″	35°14′42·22″
Long. (E):	73°06′30·92″	73°09′20·85″	73°10′36·08″	73°10′42·49″	73°12′12·31″
Sample:	KG-32	UM01-124[1]	KG-48	KG-50[1]	UM01-125[1]
Unit:	Kiru	Kiru	Kamila	Kamila	Kamila
Rock type:	Tonalite	Tonalite	Tonalite	Tonalite	Tonalite
wt %					
SiO_2	63·27	64·72	74·03	67·88	71·20
TiO_2	0·43	0·38	0·11	0·21	0·22
Al_2O_3	20·02	17·40	14·88	16·56	15·37
FeO_T	2·36	3·46	1·29	2·35	2·35
MnO	0·04	0·10	0·03	0·06	0·07
MgO	1·04	1·32	0·54	0·86	0·73
CaO	7·08	5·84	2·81	4·52	3·38
Na_2O	4·31	3·48	4·35	3·88	3·77
K_2O	0·15	0·90	0·75	1·15	1·28
P_2O_5	0·14	0·13	0·03	0·09	0·05
LOI	0·34	1·60	0·89	1·54	1·18
Total	99·18	99·33	99·71	99·10	99·60
Mg-no.	44	40	43	39	36
ppm					
Sc	3	7	1	2	1
Ti	3070	—	562	1415	872
V	49	41	12	30	11
Ni	7	2	3	3	1
Cr	15	27	47	39	1
Rb	5·06	33·5	22·3	44·0	48·7
Sr	399	386	289	332	364
Y	4·48	5·75	1·02	2·59	2·84
Zr-XRF	122	78·0	89·7	73·7	70·0
Nb	2·22	2·50	1·03	1·82	5·55
Cs	0·22	0·43	0·31	0·51	0·48
Ba	120	431	343	516	889
La	4·44	10·5	2·81	11·0	50·9
Ce	10·7	21·0	5·15	20·3	93·7
Pr	1·36	2·35	0·55	2·02	8·29
Nd	6·09	9·64	2·17	7·44	28·8
Sm	1·27	1·94	0·38	1·11	3·43
Eu	0·50	0·77	0·26	0·58	0·82
Gd	1·13	1·80	0·32	0·90	2·02
Tb	0·14	0·23	0·04	0·10	0·19
Dy	0·77	1·36	0·23	0·54	0·78
Ho	0·14	0·25	0·04	0·10	0·11
Er	0·36	0·69	0·12	0·26	0·25
Tm	0·05	0·10	0·02	0·04	0·03
Yb	0·33	0·68	0·13	0·24	0·22
Lu	0·05	0·11	0·02	0·04	0·04
Ta	0·18	0·17	0·06	0·09	0·21
Pb	1·56	3·25	2·81	2·60	5·08
Th	0·57	2·21	0·42	2·08	13·96
U	0·14	0·45	0·04	0·32	0·77
ΣREE (ppm)	27·3	51·5	12·2	44·6	190
Eu*	1·24	1·24	2·22	1·73	0·87
La_N	18·7	44·4	11·9	46·3	214·6
Yb_N	1·95	4·02	0·75	1·41	1·26
Ce_N/Yb_N	8·95	8·56	11·2	23·6	121
La_N/Sm_N	2·26	3·50	4·83	6·39	9·58

(continued)

Table 1: Continued

	Intrusive granites		
Lat. (N):	35°13′02·32″	35°13′07·28″	35°13′05·52″
Long. (E):	73°08′55·68″	73°09′01·48″	73°09′02·75″
Sample:	KG-42[1]	KG-43	UM01-123[1]
Unit:	Kiru	Kiru	Kiru
Rock type:	Granodiorite	Granodiorite	Granodiorite
wt %			
SiO_2	74·35	74·80	74·09
TiO_2	0·05	0·05	0·03
Al_2O_3	14·95	14·66	14·87
FeO_T	1·09	0·90	0·82
MnO	0·18	0·22	0·15
MgO	0·27	0·25	0·26
CaO	2·20	2·13	1·80
Na_2O	3·56	3·13	2·90
K_2O	1·57	1·86	2·28
P_2O_5	0·07	0·05	0·04
LOI	0·97	0·99	1·22
Total	99·26	99·04	98·46
Mg-no.	31	33	36
ppm			
Sc	1	2	3
Ti	257	222	—
V	5	9	21
Ni	9	6	2
Cr	209	105	24
Rb	50·4	53·2	63·6
Sr	206	148	154
Y	9·79	13·3	8·02
Zr-XRF	42·0	47·5	38·0
Nb	5·89	6·88	7·12
Cs	1·12	0·98	1·13
Ba	853	773	841
La	8·35	6·95	6·38
Ce	17·3	14·6	13·3
Pr	1·94	1·67	1·53
Nd	7·61	6·56	6·17
Sm	1·62	1·69	1·46
Eu	0·35	0·28	0·29
Gd	1·70	1·98	1·67
Tb	0·26	0·35	0·25
Dy	1·79	2·41	1·54
Ho	0·35	0·45	0·27
Er	1·01	1·28	0·74
Tm	0·16	0·20	0·11
Yb	1·11	1·37	0·83
Lu	0·19	0·22	0·14
Ta	0·65	0·75	0·75
Pb	15·65	8·22	11·90
Th	2·05	1·60	1·61
U	0·56	0·54	0·36
ΣREE (ppm)	43·7	40·0	34·7
Eu*	0·65	0·46	0·57
La_N	35·2	29·3	26·9
Yb_N	6·54	8·03	4·88
Ce_N/Yb_N	4·31	2·97	4·45
La_N/Sm_N	3·32	2·66	2·82

*Sample names from Garrido *et al*. (2006).Rock types are established as a function of the SiO_2 content of the rocks. UM: ultramafic ($SiO_2 \leq 45\%$); gabbros: gabbros *sensu stricto* and gabbrodiorites [$45 < SiO_2$ (wt %) ≤ 55]; diorites [$55 < SiO_2$ (wt %) ≤ 63]; intrusive granites (tonalites and granodiorites, $SiO_2 > 63\%$). Because zircons, expressed as an accessory mineral phase in granitoids, were not completely dissolved during the ICP-MS acid digestion procedure, Zr values were taken from the XRF analyses. 'Suite A' and 'suite B' are defined based on combined trace element and isotopic analysis. —, not analyzed; LOI, loss on ignition; N, chondrite-normalized, after Sun & McDonough (1989). Mg-number = $100 \times MgO/(MgO + FeO_{Total})$, on a molar basis.

are common in the Kiru sequence and are most abundant in the upper section.

Eleven plutonic and volcanic rocks samples were selected (Fig. 3b and Table 1): three 'Kiru amphibolite' samples (KG-30, KG-35, UM01-122); one metadiorite taken from a large sill intrusive into the Kiru amphibolites (KG-31); five gabbros from the thick pile of interlayered gabbro–diorite found above the Kiru amphibolites (KG-37, KG-38, KG-39, KG-40, KG-41); and two diorites from the 'Mandraza amphibolites' (KG-45, KG-47). In addition, five intrusive granitic rocks were sampled: one tonalite intrusive into the Kiru amphibolites (KG-32); one tonalite (UM01-124) and three granodiorites (KG-42, KG-43, UM01-123) intrusive into the Mandraza amphibolites (Fig. 3b and Table 1).

The Kamila sequence

The Kamila sequence (>10 km thick) represents the uppermost crustal level investigated in this study (Figs 2 and 3c). It comprises various types of fine-grained and layered amphibolite (i.e. ortho-amphibolites, metapelites, metavolcanic rocks and carbonates), which are heavily intruded by amphibolitized rocks of gabbroic to granitic composition. These amphibolites may be remnants of an upper crustal sequence (Zeilinger, 2002). One thick (~500 m) metagabbroic body is intrusive into the amphibolites, which are in turn intruded by numerous pegmatites or dykes and by large granite bodies. The largest granite (up to 1 km thick) is located at the bottom of the Kamila sequence and is also intrusive into the underlying Mandraza amphibolites of the Kiru sequence. The upper amphibolites are overlain by massive coarse-grained metadiorites that are associated with metacarbonates and quartzites.

Thirteen plutonic or volcanic rocks samples were selected (Fig. 3c and Table 1): six amphibolite samples taken from the sequence base (KG-51, KG-53, KG-54, KG-55, KG-52, KG-56); two amphibolites from the top of the section (KG-59, UM01-126); two metagabbros from the thick gabbroic body intrusive into the amphibolites (UM01-127, UM01-128); and three metagabbros or diorites from the uppermost part of the Kamila sequence, near the contact with the intrusive Chilas complex (UM01-133, UM01-134, UM01-135). In addition, three intrusive tonalites (KG-48, KG-50 and UM01-125) were sampled from the bottom of the Kamila sequence (Fig. 3c and Table 1).

ANALYTICAL METHODS

Rock samples were crushed and then pulverized in an agate mill for whole-rock analyses. Plagioclases and clinopyroxenes were extracted from 100–150 μm mineral fractions using a Frantz magnetic separator, and were then carefully hand-picked to avoid composite grains and inclusions.

Whole-rock major elements were analyzed by X-ray fluorescence (XRF) on a Philips PW1404/10 instrument at the CIC (University of Granada, Spain). The system was calibrated using 24 international standards to ensure accuracy and the calibration was periodically monitored using four internal standards. The reproducibility of the major element data is 0·3% absolute. Trace elements and REE abundances in whole-rocks and minerals were analyzed by inductively coupled plasma mass spectrometry (ICP-MS) using a VG Plasmaquad II system at the University of Montpellier II. The results from the international rock standards BEN ($n = 13$) and UBN ($n = 13$) yielded limits of detection below 1·5 ppb and a relative standard deviation (RSD) of 4–7%, except for Rb, Sr, Nb, Zr, and Ta (RSD ~7–15%).

Before undertaking the acid digestion for the Sr, Nd and Pb isotopic analyses, clinopyroxenes were leached for 30 min in 6N HCl at 80°C and plagioclases were leached for 15 min in 2·5N HCl at 60°C. All whole-rocks were leached for 30 min with 6N HCl at 80°C. After the leaching steps, the residues were rinsed three times in purified milli-Q H_2O. The Sr, Nd and Pb separation procedures were slightly modified from those of Manhès *et al.* (1980) and Pin *et al.* (1994). The total blank contents for Pb, Sr and Nd were less than 65, 60 and 30 pg, respectively, for a 100 mg sample. Pb and Nd isotopic compositions were measured by multicollector (MC)-ICP-MS using the VG Plasma 54 and the Nu 500 systems at the Ecole Normale Supérieure in Lyon (France). The Pb isotopic compositions were measured with an external precision of ~100–150 ppm for $^{206, 207, 208}Pb/^{204}Pb$, using the Tl normalization method described by White *et al.* (2000). The NIST 981 standard was measured every two samples, and the Nd isotopic measurements were bracketed between the 'Lyon in-house' Nd standard every two samples. This Nd standard is a 500 ppb dilution of the JMC commercial solution, batch 801149A (Luais *et al.*, 1997) with an average of $^{143}Nd/^{144}Nd = 0{\cdot}512134 \pm 24$ (2σ) ($n = 102$). The Sr isotopic compositions were measured on a Finnigan Triton TI mass spectrometer at the Laboratoire de Géochimie GIS of Nîmes (France). The results from the NBS 987 Sr standard yielded a mean value of $^{87}Sr/^{86}Sr = 0{\cdot}710256 \pm 10$ (2σ) ($n = 22$). The initial isotopic compositions of the entire dataset were corrected for *in situ* decay, assuming an age of ~100 Ma according to the U–Pb zircon ages obtained by Schaltegger *et al.* (2002) relating to the main period of magmatism in the KAC.

RESULTS

Major and trace elements

The major and trace element compositions of 55 samples from the JPKK crustal section are reported in Table 1. Two groups of rocks can be distinguished as a function of their tectonic emplacement: (1) plutonic-volcanic rocks of ultramafic to dioritic composition; (2) later rocks

intrusive into group (1) of quartz-diorite to granitic composition, referred to as 'intrusive granites'.

Plutonic-volcanic rocks

We have subdivided the plutonic-volcanic rocks into five 'types' on the basis of their trace element compositions. These are referred to as 'Type-1' to 'Type-5' rocks in Table 1 and Figs 3 and 4.

Chondrite-normalized REE patterns and primitive mantle-normalized trace element patterns are reported in Fig. 4. The transition from Type-1 to Type-5 patterns is mainly characterized by the enrichment of highly incompatible elements (HIE) [i.e. LILE (Cs, Rb, Ba, Pb, Sr), LREE, Th and U] in relation to HFSE (Nb, Ta, Zr).

Type-1 rocks are gabbroic [$48 < SiO_2$ (wt %) < 51] on an anhydrous basis; see Table A in the Supplementary Data, available for downloading at http://www.petrology.oxfordjournals.org] with a large range in Mg-number values ($53 <$ Mg-number < 80) and low REE contents [$6{\cdot}5 < \sum$REE (ppm) < 36]. Five samples appear to be cumulates, characterized by strong REE depletion [$6{\cdot}5 < \sum$REE (ppm) < 15], highly fractionated REE patterns with a strong LREE/MREE (middle REE) depletion ($0{\cdot}34 < Ce_N/Yb_N < 0{\cdot}64$; $1{\cdot}2 < La_N < 2{\cdot}0$; $2{\cdot}7 < Yb_N < 6{\cdot}9$ and $0{\cdot}29 < La_N/Sm_N < 0{\cdot}68$), and a marked positive Eu anomaly [$1{\cdot}5 < Eu^* < 1{\cdot}8$; $Eu^* = 2 \times Eu_N/(Sm_N + Gd_N)$] that is correlated with positive Sr and Pb anomalies in primitive mantle normalized trace element patterns (Fig. 4). One sample (UM01-122) is distinguished by a weakly fractioned REE pattern ($Ce_N/Yb_N = 0{\cdot}82$), a slight depletion in LREE ($La_N/Sm_N = 0{\cdot}65$) and no Eu anomaly ($Eu^* = 0{\cdot}97$). A liquid–cumulate relationship between this sample and the clinopyroxene from the cumulate sample (KG-37) is suggested by their complementary REE patterns (Fig. 5).

In Harker variation diagrams (Fig. 6), the Type-1 rocks deviate from the global trend defined by modern island arc lavas. For a given SiO_2content, Type-1 samples have lower TiO_2, Zr, FeO_T and $Na_2O + K_2O$, and higher CaO and MgO contents. All of the samples except one (KG-40) plot in the calc-alkaline field of the Mg-number vs SiO_2 diagram.

Type-2 rocks have ultramafic to gabbroic compositions [$44 < SiO_2$ (wt %) < 53] with primitive to highly differentiated Mg-number values ($38 <$ Mg-number < 66). Compared with Type-1, the Type-2 samples are significantly enriched in REE ($33 < \sum$REE (ppm) < 71), show slightly fractionated, 'N-MORB-like' REE patterns ($0{\cdot}6 < Ce_N/Yb_N < 2{\cdot}1$; $6 < La_N < 30$; $7 < Yb_N < 19$) with variable LREE/MREE depletion ($0{\cdot}26 < La_N/Sm_N < 0{\cdot}95$). They have slightly negative to positive Eu anomalies ($0{\cdot}7 < Eu^* < 1{\cdot}1$).

In Harker variation diagrams, the Type-2 samples are scattered and deviate from the modern island arc lavas trend (Fig. 6). In the $Na_2O + K_2O$ vs SiO_2 diagram, they display a slight enrichment in total alkalis compared with the main trend of the data. All Type-2 samples plot in the tholeiitic domain in the Mg-number vs SiO_2 diagram.

Type-3 rocks have ultramafic to dioritic compositions [$43 < SiO_2$ (wt %) < 60] with variable Mg-number from primitive to highly differentiated values ($40 <$ Mg-number < 64). Compared with the Type-2 samples, Type-3

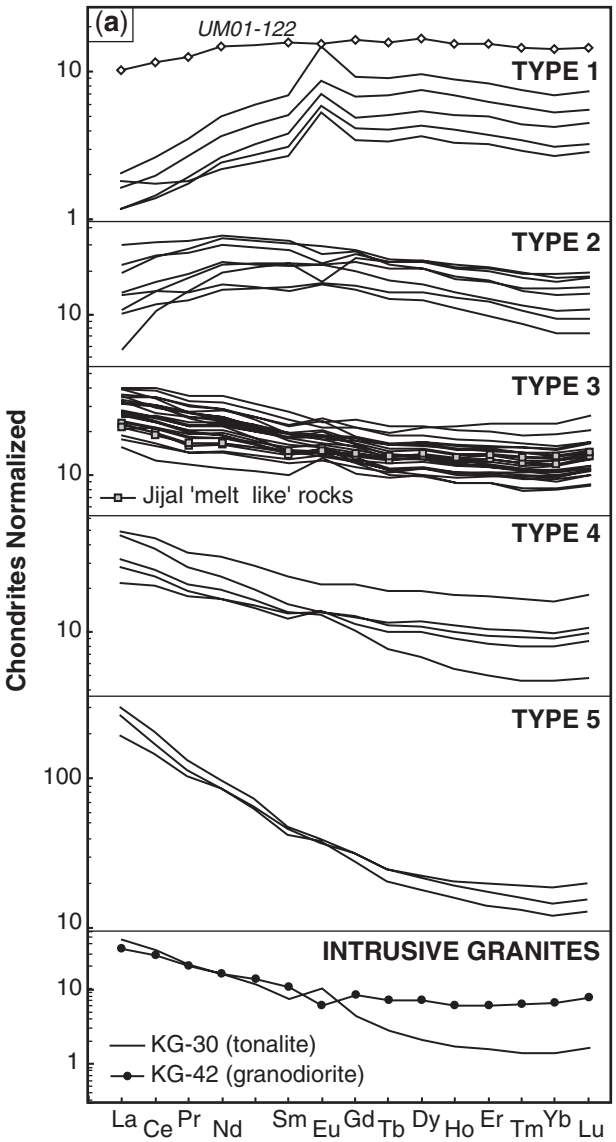

Fig. 4. (a) Chondrite-normalized REE patterns and (b) primitive mantle-normalized extended trace element diagrams of JPKK crustal section rocks (including plutonic–volcanic rocks and intrusive granites). Normalization values after Sun & McDonough (1989). Five main types of patterns (Type-1 to Type-5) are distinguished for the plutonic–volcanic rocks throughout the ~30 km arc crust section (see text for explanation). Only one representative pattern for each type of granite is plotted in (b). The trace element patterns of the Type-3 rocks are similar to those of gabbros and diorites from the Chilas complex (Jagoutz *et al.*, 2006; Takahashi *et al.*, 2006).

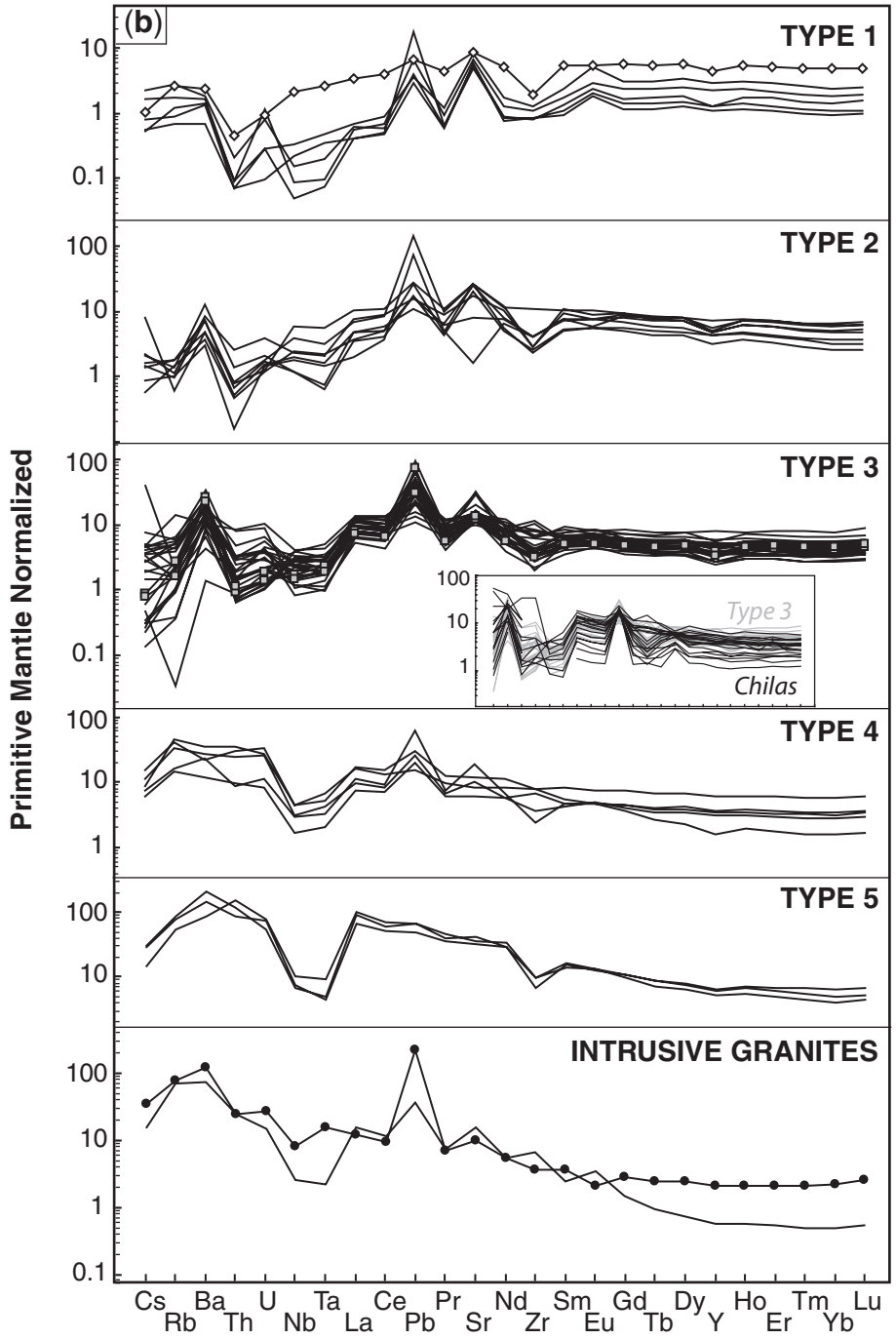

Fig. 4. Continued

rocks have similar $\sum$REE values [$30 < \text{REE (ppm)} < 79$] but display stronger LREE/HREE and LREE/MREE enrichments ($1{\cdot}3 < Ce_N/Yb_N < 3{\cdot}7$; $1{\cdot}3 < La_N/Sm_N < 2{\cdot}3$). The Eu anomalies are slightly negative to slightly positive ($0{\cdot}9 < Eu^* < 1{\cdot}3$), and there are Sr and Pb positive spikes in the mantle-normalized trace element patterns (Fig. 4).

Trace element patterns of the gabbros and diorites from the Chilas complex (Jagoutz *et al.*, 2006; Takahashi *et al.*, 2006) are reported in the inset of Fig. 4b for comparison. These patterns are similar to the Type-3 patterns and show marked HFSE anomalies that are typical features of arc magmas.

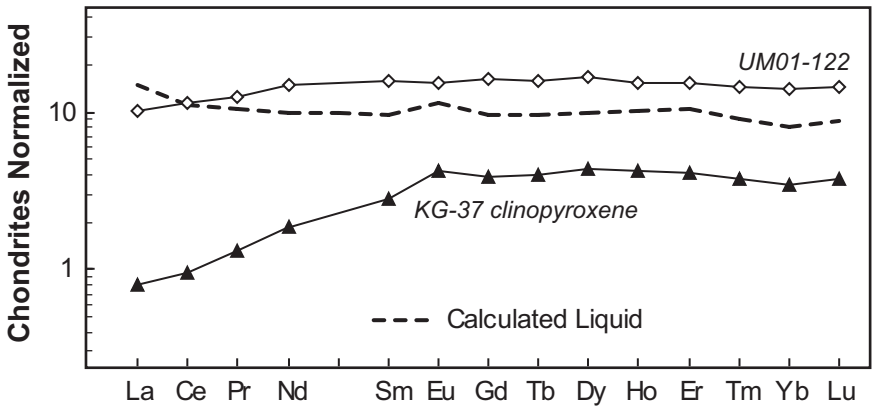

Fig. 5. Chondrite-normalized REE pattern of the calculated liquid in equilibrium with the KG-37 cumulate sample compared with that of UM01-122. The composition of the liquid has been calculated from dissolution ICP-MS data, for an ~10 mg clinopyroxene fraction from KG-37, and using clinopyroxene–melt distribution coefficients of Hart & Dunn (1993). Normalization values after Sun & McDonough (1989).

In the Harker variation diagrams (Fig. 6), the Type-3 samples roughly follow the trend of modern island arc lavas. In the Mg-number vs SiO_2 diagram, two groups of samples can be distinguished: (1) a group located in the tholeiitic domain, formed by the Jijal and Patan samples (except for KG-20); (2) a calc-alkaline group, formed by one Patan sample (KG-20) and by rocks from the Kiru and Kamila sequences (see Table 1).

Type-4 rocks show more differentiated compositions [$54 < SiO_2$ (wt %) < 62]; four of the five samples are dioritic in composition (Table 1). This is consistent with the Mg-number values of these rocks ($44 <$ Mg-number < 63). When compared with Type-2 and -3, Type-4 samples display similar $\sum$REE values [$41 < \sum$REE (ppm) < 81] but are characterized by a stronger LREE/HREE and LREE/MREE enrichment ($2{\cdot}1 < Ce_N/Yb_N < 5{\cdot}8$; $1{\cdot}6 < La_N/Sm_N < 3{\cdot}0$), and by an overall enrichment in the most incompatible elements (Cs–U segment in Fig. 4b). These rocks show no marked Eu anomalies ($0{\cdot}9 < Eu^* < 1{\cdot}2$), but weak positive to prominent Pb and Sr spikes. Samples from this group plot roughly in the Type-3–modern island arc lavas field in the Harker diagrams (Fig. 6) and clearly show a calc-alkaline character in the Mg-number vs SiO_2 diagram.

Type-5 rocks are restricted to the Kamila sequence and are located in the field close to the Type-4 samples (Fig. 3c). Type-5 samples have a gabbroic composition [$49 < SiO_2$ (wt %) < 51] and differentiated Mg-number values ($42 <$ Mg-number < 48). These samples are notably distinguished from the Type-4 rocks by an extreme enrichment in REE [$215 < \sum$REE (ppm) < 286], a strong enrichment of LREE relative to HREE and MREE ($10 < Ce_N/Yb_N < 15$; $4{\cdot}2 < La_N/Sm_N < 6{\cdot}5$), an overall enrichment in the most incompatible elements (Cs–U segment in Fig. 4b) and no marked Eu, Sr or Pb anomalies. Type-5 samples roughly plot in an intermediate position between the Type-2 and Type-3 groups in Fig. 6.

Intrusive granites

Three granites have been analyzed and are reported in Table 1; a further five samples were analysed by Garrido *et al.* (2006). According to those workers, two types of granitoid can be distinguished in the Kiru–Kamila section, tonalites and granodiorites. Overall, tonalites are characterized by a strong fractionation of LREE/HREE ($6{\cdot}5 < Ce_N/Yb_N < 121$) and a positive Eu anomaly ($1{\cdot}2 < Eu^* < 2{\cdot}2$; Fig. 4). The granodiorites are distinguished by a weaker LREE/HREE fractionation ($3{\cdot}0 < Ce_N/Yb_N < 4{\cdot}5$) and a marked negative Eu anomaly ($0{\cdot}5 < Eu^* < 0{\cdot}7$; Fig. 4).

All the granites plot along the modern island arc lavas trend for TiO_2, CaO, FeO_T, MgO and $Na_2O + K_2O$, and in the calc-alkaline area in the Mg-number vs SiO_2 diagram (Fig. 6).

Sr, Nd and Pb isotope compositions

Sr, Nd and Pb isotopic data are reported in Table 2 along with data from Dhuime *et al.* (2007) for 17 samples from the crustal section of the Jijal complex (i.e. 'Jijal gabbroic rocks', including hornblende gabbronorites and garnet granulites; and 'Jijal hornblendites', including rocks from the hornblendite–garnetite transition; see Fig. 3a). In addition to the leached-whole rock analyses, the isotopic compositions of clinopyroxenes and plagioclases have also been determined for some samples (Table 2).

Plutonic-volcanic rocks

In a Nd–Sr isotope diagram (Fig. 7), the leached-whole rocks and clinopyroxenes from Type-1 to Type-5 rocks define a very large domain ($0{\cdot}51261 < {}^{143}Nd/{}^{144}Nd_{(i)}$

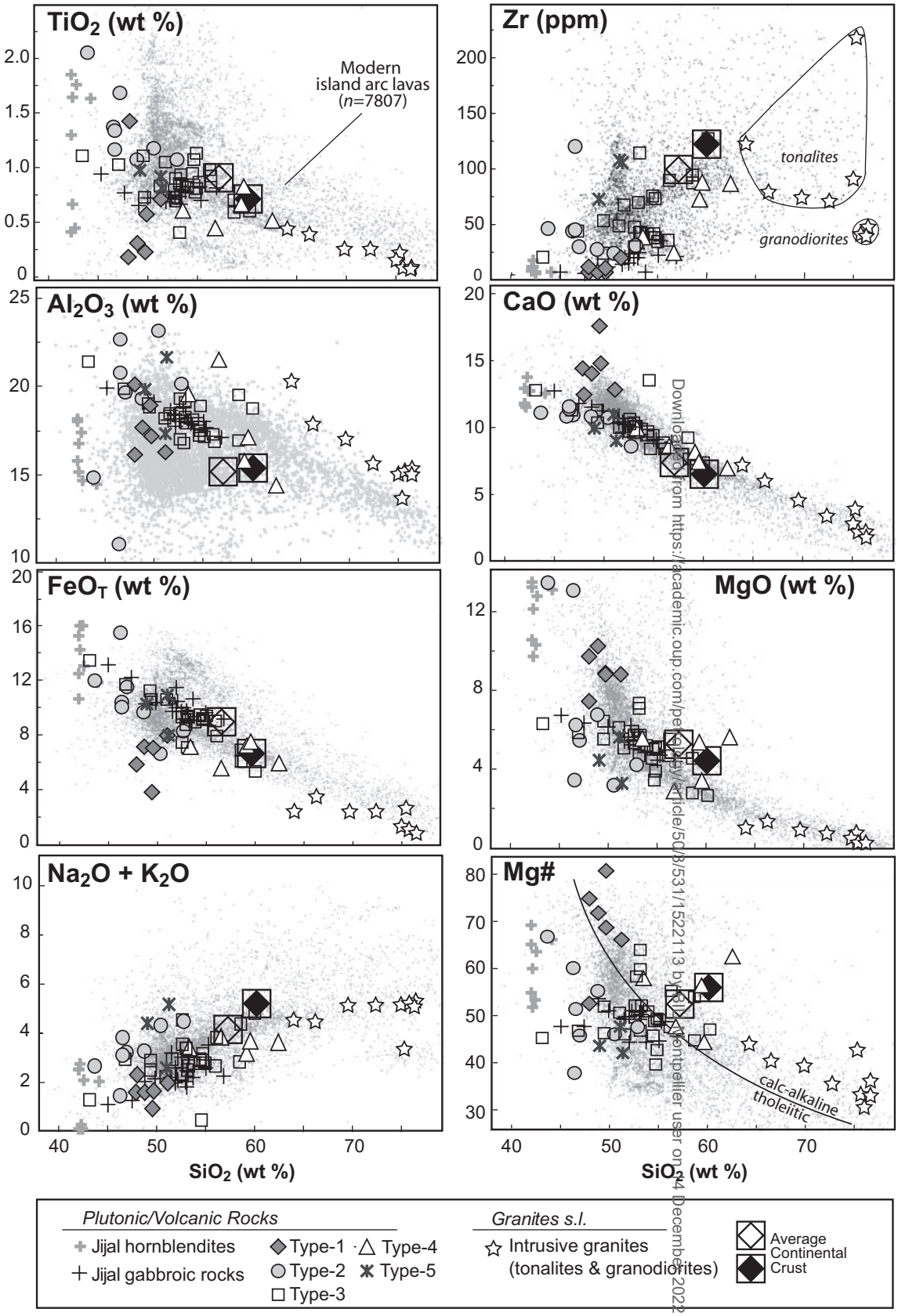

Fig. 6. Harker variation diagrams for JPKK crustal section rocks. The Jijal 'hornblendites' (i.e. hornblendite–garnetite) and Jijal 'gabbroic rocks' (i.e. hornblende gabbronorites and garnet granulites) compositions are from Garrido *et al.* (2006) and Dhuime *et al.* (2007). The grey array of data points corresponds to the modern island arc lavas field ($n = 7807$, after http://georoc.mpch-mainz.gwdg.de/georoc/Entry.html). Squares including diamonds indicate average continental crust compositions after Taylor & McLennan (1985) (white diamond) and Rudnick & Fountain (1995) (black diamond). Calc-alkaline–tholeiitic transition is after Miyashiro (1974).

Table 2: Isotope compositions for the JPKK crustal rocks

Sample	Unit	Mineral	$^{87}Rb/^{86}Sr$	$^{87}Sr/^{86}Sr$	$^{87}Sr/^{86}Sr_{(i)}$	$\varepsilon Sr_{(i)}$	$^{147}Sm/^{144}Nd$	$^{143}Nd/^{144}Nd$	$^{143}Nd/^{144}Nd_{(i)}$	$\varepsilon Nd_{(i)}$	$^{206}Pb/^{204}Pb$	$^{207}Pb/^{204}Pb$	$^{208}Pb/^{204}Pb$	$^{206}Pb/^{204}Pb_{(i)}$	$^{207}Pb/^{204}Pb_{(i)}$	$^{208}Pb/^{204}Pb_{(i)}$
Geochemical suite 'A'																
Type-1 trace element patterns																
UM01-122	Kiru	WR	0·026	0·703211 ± 7	0·70317	−17·2	0·208	0·512984 ± 4	0·51285	6·6	18·0698 ± 8	15·5185 ± 8	38·1074 ± 18	18·028	15·516	38·081
KG-37	Kiru	WR	0·043	0·703173 ± 5	0·70311	−18·0	0·243	0·513164 ± 24	0·51301	9·6	18·1982 ± 27	15·5456 ± 24	38·2779 ± 67	18·140	15·543	38·258
		Cpx	0·459	0·703694 ± 3	0·70304	−19·1	0·297	0·513094 ± 30	0·51290	7·6	—	—	—	—	—	—
		Pl	0·011	0·703132 ± 5	0·70312	−18·0	0·236	0·512997 ± 42	0·51284	6·5	18·1324 ± 22	15·5127 ± 19	38·1950 ± 49	18·131	15·513	38·194
KG-40	Kiru	WR	0·013	0·703140 ± 6	0·70312	−17·9	0·276	0·513092 ± 14	0·51291	7·8	18·1195 ± 17	15·5235 ± 16	38·1849 ± 35	18·097	15·522	38·175
		Pl	0·001	0·703117 ± 2	0·70312	−18·0	—	—	—	—	18·0866 ± 42	15·4923 ± 36	38·1221 ± 93	18·087	15·492	38·122
Type-2 trace element patterns																
KG-59	Kamila	WR	0·006	0·703676 ± 3	0·70367	−10·2	0·185	0·512940 ± 5	0·51282	6·0	18·3130 ± 8	15·5511 ± 7	38·3763 ± 18	18·273	15·549	38·358
UM01-128	Kamila	WR	0·006	0·703627 ± 13	0·70362	−10·9	0·179	0·512973 ± 19	0·51286	6·7	18·2367 ± 6	15·5306 ± 6	38·2788 ± 16	18·224	15·530	38·268
		Pl	0·001	0·703610 ± 3	0·70361	−11·0	0·102	0·512929 ± 13	0·51286	6·8	18·1923 ± 5	15·5325 ± 5	38·2280 ± 16	18·192	15·532	38·228
KG-13a	Patan	WR	0·005	0·703730 ± 1	0·70372	−9·4	0·178	0·512890 ± 11	0·51277	5·1	18·3656 ± 4	15·5538 ± 4	38·4861 ± 14	18·342	15·553	38·466
		Pl	0·003	0·703729 ± 6	0·70373	−9·4	0·322	0·513103 ± 12	0·51289	7·4	18·3553 ± 8	15·5479 ± 8	38·4641 ± 25	18·355	15·548	38·464
KG-14	Patan	WR	0·005	0·703733 ± 5	0·70373	−9·3	0·182	0·512887 ± 7	0·51277	5·0	18·3286 ± 7	15·5456 ± 6	38·4423 ± 17	18·258	15·542	38·380
		Pl	0·001	0·703727 ± 9	0·70373	−9·4	0·093	0·512917 ± 62	0·51286	6·7	18·2994 ± 10	15·5382 ± 9	38·3974 ± 22	18·299	15·538	38·397
Type-3 trace element patterns																
KG-30	Kiru	WR	0·018	0·703607 ± 6	0·70358	−11·4	0·134	0·512903 ± 8	0·51281	5·9	18·2996 ± 8	15·5510 ± 7	38·3361 ± 24	18·275	15·550	38·325
KG-31	Kiru	WR	0·024	0·703617 ± 3	0·70358	−11·4	0·133	0·512913 ± 5	0·51283	6·1	18·2746 ± 5	15·5350 ± 5	38·3433 ± 14	18·261	15·534	38·328
		Pl	0·030	0·703606 ± 2	0·70356	−11·6	0·102	0·513023 ± 11	0·51296	8·7	18·2526 ± 10	15·5265 ± 8	38·3083 ± 24	18·252	15·526	38·308
Type-4 trace element patterns																
KG-45	Kamila	WR	0·075	0·703727 ± 6	0·70362	−10·8	0·139	0·512871 ± 7	0·51278	5·2	18·3911 ± 6	15·5470 ± 3	38·5107 ± 11	18·336	15·544	38·455
KG-47	Kamila	WR	0·202	0·703830 ± 8	0·70354	−12·0	0·156	0·512853 ± 4	0·51275	4·7	18·3593 ± 5	15·5527 ± 5	38·5179 ± 13	18·240	15·547	38·334
KG-51	Kamila	WR	0·283	0·703968 ± 3	0·70357	−11·6	0·144	0·512923 ± 9	0·51283	6·2	18·6839 ± 9	15·5717 ± 8	38·8825 ± 21	18·398	15·558	38·517
		Pl	—	—	—	—	—	—		—	18·5005 ± 44	15·5513 ± 36	38·5045 ± 92	18·389	15·546	38·485
Type-5 trace element patterns																
KG-52	Kamila	WR	0·181	0·704070 ± 7	0·70381	−8·1	0·096	0·512793 ± 3	0·51273	4·3	18·8707 ± 8	15·5740 ± 8	39·4558 ± 23	18·634	15·563	38·773
KG-55	Kamila	WR	0·211	0·704125 ± 8	0·70382	−7·9	0·107	0·512809 ± 5	0·51274	4·4	19·0924 ± 4	15·5917 ± 4	39·5890 ± 13	18·638	15·570	38·884
KG-56	Kamila	WR	0·131	0·703954 ± 3	0·70377	−8·8	0·095	0·512805 ± 6	0·51274	4·5	18·9767 ± 5	15·5939 ± 4	39·6994 ± 13	18·630	15·577	38·795
Jijal hornblendite–garnetite lenses (Dhuime et al., 2007)																
KH04-06*	Jijal	WR	0·014	0·703664 ± 2	0·70364	−10·5	0·260	0·512987 ± 6	0·51282	6·0	18·4444 ± 7	15·5861 ± 6	38·5832 ± 17	18·442	15·586	38·581
KH04-07*	Jijal	WR	0·011	0·703753 ± 2	0·70374	−9·2	0·394	0·513078 ± 8	0·51282	6·0	18·4664 ± 35	15·5842 ± 31	38·5695 ± 78	18·452	15·584	38·564
KH04-19*	Jijal	WR	0·005	0·703759 ± 2	0·70375	−9·0	0·466	0·513067 ± 8	0·51276	4·9	18·4321 ± 17	15·5744 ± 16	38·5550 ± 40	18·399	15·573	38·547
KH04-21*	Jijal	WR	0·009	0·703713 ± 2	0·70370	−9·7	0·242	0·512968 ± 6	0·51281	5·8	18·3772 ± 7	15·5638 ± 6	38·4886 ± 23	18·370	15·563	38·483
KH97-104*	Jijal	WR	0·023	0·703603 ± 3	0·70357	−11·6	0·246	0·512969 ± 16	0·51281	5·8	18·3327 ± 6	15·5430 ± 6	38·4251 ± 16	18·319	15·542	38·417
		Hbl	0·025	0·703590 ± 3	0·70355	−11·8	0·247	0·512974 ± 9	0·51281	5·9	18·3467 ± 7	15·5410 ± 6	38·4446 ± 16	18·341	15·541	38·441
KH97-107*	Jijal	WR	0·009	0·703772 ± 2	0·70376	−8·9	0·230	0·512924 ± 18	0·51277	5·1	18·4126 ± 7	15·5776 ± 7	38·5405 ± 20	18·404	15·577	38·535
		Hbl	0·012	0·703776 ± 2	0·70376	−8·9	0·234	0·512941 ± 15	0·51279	5·4	18·4774 ± 6	15·5811 ± 7	38·6292 ± 16	18·474	15·581	38·626

(continued)

Table 2: Continued

Sample	Unit	Group	Mineral	$^{87}Rb/^{86}Sr$	$^{87}Sr/^{86}Sr$	$^{87}Sr/^{86}Sr_{(i)}$	$\varepsilon Sr_{(i)}$	$^{147}Sm/^{144}Nd$	$^{143}Nd/^{144}Nd$	$^{143}Nd/^{144}Nd_{(i)}$	$\varepsilon Nd_{(i)}$	$^{206}Pb/^{204}Pb$	$^{207}Pb/^{204}Pb$	$^{208}Pb/^{204}Pb$	$^{206}Pb/^{204}Pb_{(i)}$	$^{207}Pb/^{204}Pb_{(i)}$	$^{208}Pb/^{204}Pb_{(i)}$
Geochemical suite 'B'																	
(Type-3 trace element patterns only)																	
Jijal gabbroic rocks (Dhuime et al., 2007)																	
KH97-102*	Jijal	B1	WR	0·002	0·704016 ± 3	0·70401	–5·3	0·195	0·512932 ± 15	0·51280	5·7	18·5735 ± 24	15·5870 ± 19	38·7628 ± 53	18·565	15·587	38·760
			Pl	0·010	0·704035 ± 2	0·70402	–5·2	—	—	—	—	—	—	—	—	—	—
KH04-23*	Jijal	B1	WR	0·001	0·703995 ± 4	0·70399	–5·5	0·187	0·512932 ± 3	0·51281	5·8	18·5398 ± 5	15·5839 ± 5	38·7144 ± 15	18·533	15·584	38·714
KH04-17*	Jijal	B1	WR	0·012	0·703991 ± 3	0·70397	–5·8	0·177	0·512962 ± 11	0·51285	6·5	18·5349 ± 5	15·5812 ± 6	38·7067 ± 14	18·516	15·580	38·691
KH97-110*	Jijal	B1	WR	0·002	0·703942 ± 2	0·70394	–6·3	0·216	0·512933 ± 29	0·51279	5·5	18·5144 ± 8	15·5761 ± 7	38·6761 ± 18	18·507	15·576	38·672
KH97-111*	Jijal	B1	WR	0·001	0·703925 ± 10	0·70392	–6·5	0·218	0·512929 ± 14	0·51279	5·4	18·5190 ± 11	15·5843 ± 10	38·6967 ± 27	18·515	15·584	38·695
			Cpx	0·004	0·703937 ± 3	0·70393	–6·4	0·143	0·512895 ± 5	0·51280	5·7	18·4957 ± 32	15·5746 ± 16	38·6604 ± 53	18·487	15·574	38·656
			Pl	0·000	0·703938 ± 3	0·70394	–6·3	0·058	0·512872 ± 9	0·51283	6·3	18·5207 ± 9	15·5802 ± 8	38·6899 ± 25	18·521	15·580	38·690
KG-03-A*	Jijal	B1	WR	0·007	0·703953 ± 10	0·70394	–6·3	0·185	0·512962 ± 21	0·51284	6·4	18·5323 ± 9	15·5829 ± 9	38·7036 ± 25	18·518	15·582	38·692
KH97-114*	Jijal	B1	WR	0·007	0·703938 ± 4	0·70393	–6·5	0·177	0·512897 ± 13	0·51278	5·3	18·5299 ± 6	15·5830 ± 8	38·7108 ± 22	18·513	15·582	38·697
			Cpx	0·021	0·703958 ± 6	0·70393	–6·5	0·125	0·512949 ± 14	0·51287	6·9	18·5273 ± 16	15·5781 ± 12	38·7493 ± 33	18·518	15·578	38·675
			Pl	0·003	0·703937 ± 5	0·70393	–6·4	0·046	0·512863 ± 10	0·51283	6·3	18·5330 ± 7	15·5819 ± 9	38·7085 ± 24	18·533	15·582	38·708
BKI-158-B*	Jijal	B1	WR	0·012	0·703926 ± 2	0·70391	–6·7	0·188	0·512948 ± 8	0·51282	6·1	18·5446 ± 6	15·5832 ± 6	38·7090 ± 15	18·515	15·582	38·682
			Cpx	0·071	0·703944 ± 7	0·70384	–7·7	0·135	0·512914 ± 4	0·51283	6·1	18·5505 ± 13	15·5752 ± 10	38·8200 ± 30	18·520	15·574	38·697
			Pl	0·005	0·703909 ± 15	0·70390	–6·8	0·051	0·512795 ± 15	0·51276	4·9	18·5259 ± 9	15·5791 ± 7	38·6921 ± 24	18·526	15·579	38·692
KG-03-B*	Jijal	B1	WR	0·010	0·703958 ± 18	0·70394	–6·3	0·176	0·512942 ± 14	0·51283	6·2	18·5236 ± 3	15·5861 ± 5	38·6805 ± 16	18·516	15·586	38·674
KH97-113*	Jijal	B1	WR	0·016	0·703969 ± 5	0·70395	–6·2	0·178	0·512925 ± 8	0·51281	5·8	18·5281 ± 4	15·5763 ± 5	38·6853 ± 14	18·501	15·575	38·661
			Cpx	0·002	0·704256 ± 3	0·70425	–1·9	0·144	0·512935 ± 4	0·51284	6·4	18·5800 ± 5	15·5828 ± 4	38·7711 ± 12	18·564	15·582	38·764
			Pl	0·001	0·703937 ± 4	0·70394	–6·4	0·068	0·512795 ± 22	0·51275	4·7	18·5312 ± 10	15·5806 ± 8	38·7077 ± 29	18·531	15·581	38·708
			Hbl	0·141	0·704104 ± 2	0·70390	–6·8	0·201	0·512940 ± 5	0·51281	5·8	18·5731 ± 16	15·5788 ± 11	38·7593 ± 29	18·529	15·577	38·699
BKI-158-A*	Jijal	B1	WR	0·013	0·703922 ± 2	0·70390	–6·8	0·190	0·512924 ± 15	0·51280	5·6	18·5363 ± 5	15·5827 ± 3	38·7026 ± 10	18·517	15·582	38·683
			Cpx	0·048	0·703971 ± 3	0·70390	–6·8	0·217	0·512925 ± 5	0·51278	5·3	18·6269 ± 8	15·5873 ± 6	38·8318 ± 17	18·553	15·584	38·727
			Pl	0·001	0·703908 ± 5	0·70391	–6·8	0·071	0·512840 ± 9	0·51279	5·5	18·5300 ± 10	15·5776 ± 7	38·6933 ± 24	18·529	15·578	38·693
Patan–Kiru–Kamila section																	
KH97-116	Patan	B1	Pl	0·013	0·703933 ± 5	0·70391	–6·7	0·096	0·512851 ± 10	0·51279	5·4	18·5059 ± 7	15·5845 ± 7	38·6646 ± 23	18·505	15·584	38·664
KG-07	Patan	B1	WR	0·027	0·703939 ± 9	0·70390	–6·9	0·163	0·512868 ± 7	0·51276	4·9	18·5233 ± 4	15·5887 ± 4	38·6998 ± 11	18·503	15·588	38·678
KH97-117	Patan	B1	Pl	0·004	0·703929 ± 2	0·70392	–6·5	0·095	0·512814 ± 11	0·51275	4·7	18·4990 ± 6	15·5848 ± 6	38·6612 ± 18	18·499	15·585	38·661

(continued)

Table 2: Continued

Sample	Unit	Group	Mineral	$^{87}Rb/^{86}Sr$	$^{87}Sr/^{86}Sr$	$^{87}Sr/^{86}Sr_{(i)}$	$\varepsilon Sr_{(i)}$	$^{147}Sm/^{144}Nd$	$^{143}Nd/^{144}Nd$	$^{143}Nd/^{144}Nd_{(i)}$	$\varepsilon Nd_{(i)}$	$^{206}Pb/^{204}Pb$	$^{207}Pb/^{204}Pb$	$^{208}Pb/^{204}Pb$	$^{206}Pb/^{204}Pb_{(i)}$	$^{207}Pb/^{204}Pb_{(i)}$	$^{208}Pb/^{204}Pb_{(i)}$
KG-11	Patan	B1	WR	0·011	0·703933 ± 3	0·70392	−6·6	0·177	0·512876 ± 5	0·51276	4·9	18·5484 ± 5	15·5878 ± 5	38·7064 ± 13	18·495	15·585	38·674
			Pl	0·006	0·703918 ± 8	0·70391	−6·7	—	—	—	—	18·5120 ± 10	15·5851 ± 9	38·6685 ± 24	18·512	15·585	38·668
KH97-118	Patan	B1	WR	0·031	0·703963 ± 9	0·70392	−6·6	0·165	0·512862 ± 11	0·51275	4·7	18·5423 ± 6	15·5808 ± 6	38·6916 ± 18	18·497	15·579	38·645
KH97-119	Patan	B1	Cpx	0·036	0·703978 ± 5	0·70393	−6·5	0·166	0·512853 ± 22	0·51274	4·5	18·5673 ± 28	15·5709 ± 22	38·7619 ± 67	18·528	15·569	38·714
			Pl	0·017	0·703899 ± 2	0·70387	−7·2	0·071	0·512814 ± 9	0·51277	5·0	18·5212 ± 7	15·5842 ± 8	38·6834 ± 25	18·520	15·584	38·681
KG-17	Patan	B1	Pl	0·006	0·703961 ± 7	0·70395	−6·1	—	—	—	—	18·5411 ± 7	15·6016 ± 7	38·6562 ± 18	18·527	15·601	38·642
KG-18	Patan	B2	WR	0·006	0·703976 ± 3	0·70397	−5·9	0·154	0·512831 ± 8	0·51273	4·3	18·5529 ± 7	15·6098 ± 6	38·6813 ± 16	18·541	15·609	38·671
			Pl	0·000	0·703976 ± 4	0·70398	−5·8	0·055	0·512923 ± 20	0·51289	7·3	18·5481 ± 6	15·6066 ± 5	38·6643 ± 15	18·548	15·607	38·664
KG-26	Patan	B2	WR	0·008	0·703988 ± 3	0·70398	−5·8	0·150	0·512810 ± 5	0·51271	3·9	18·6037 ± 9	15·6085 ± 9	38·7327 ± 22	18·521	15·604	38·665
			Pl	0·072	0·703920 ± 4	0·70382	−8·1	—	—	—	—	18·5121 ± 6	15·5853 ± 5	38·6632 ± 18	18·512	15·585	38·663
UM01-133	Kamila	B3	WR	0·016	0·703806 ± 2	0·70378	−8·5	0·147	0·512789 ± 7	0·51269	3·5	18·5042 ± 7	15·6173 ± 8	38·6839 ± 24	18·487	15·617	38·661
			Cpx	0·136	0·703920 ± 3	0·70373	−9·3	0·174	0·512761 ± 9	0·51265	2·7	18·5280 ± 7	15·6195 ± 5	38·7473 ± 14	18·490	15·618	38·674
			Pl	0·003	0·703788 ± 2	0·70378	−8·5	0·062	0·512672 ± 11	0·51263	2·3	18·5054 ± 9	15·6213 ± 11	38·6890 ± 28	18·505	15·621	38·689
UM01-134	Kamila	B3	WR	0·014	0·704172 ± 2	0·70415	−3·3	0·144	0·512701 ± 2	0·51261	1·9	18·5329 ± 4	15·6336 ± 4	38·7585 ± 12	18·528	15·633	38·755
			Pl	0·009	0·704162 ± 3	0·70415	−3·3	0·075	0·512724 ± 16	0·51267	3·2	18·5348 ± 5	15·6309 ± 5	38·7509 ± 16	18·535	15·631	38·751
UM01-135	Kamila	B3	WR	0·010	0·704041 ± 2	0·70403	−5·1	0·158	0·512783 ± 7	0·51268	3·3	18·5023 ± 5	15·6220 ± 5	38·7001 ± 14	18·498	15·622	38·696
			Pl	0·005	0·704038 ± 2	0·70403	−5·0	0·082	0·512762 ± 10	0·51271	3·8	18·5095 ± 6	15·6237 ± 6	38·7151 ± 21	18·510	15·624	38·715
Intrusive granites																	
KG-32	Kiru	tonalites	WR	0·037	0·703467 ± 3	0·70342	−13·8	0·126	0·512973 ± 12	0·51289	7·4	18·3052 ± 7	15·5431 ± 8	38·4528 ± 30	18·220	15·539	38·334
			Pl	0·011	0·703440 ± 5	0·70342	−13·6	0·104	0·512971 ± 17	0·51290	7·6	18·2548 ± 12	15·5300 ± 11	38·3494 ± 28	18·237	15·529	38·305
UM01-124	Kiru	tonalites	WR	0·251	0·704070 ± 7	0·70371	−9·5	0·122	0·512844 ± 13	0·51276	4·9	18·6553 ± 6	15·5791 ± 8	38·9798 ± 23	18·519	15·572	38·758
			Pl	0·201	0·704013 ± 3	0·70373	−9·3	0·202	0·513459 ± 13	0·51333	15·9	18·4901 ± 5	15·5687 ± 6	38·6670 ± 18	18·487	15·569	38·666
KG-50	Kamila	tonalites	WR	0·383	0·704045 ± 4	0·70350	−12·6	0·090	0·512851 ± 7	0·51279	5·5	18·4857 ± 8	15·5666 ± 8	38·7705 ± 26	18·366	15·561	38·510
			Pl	0·549	0·704117 ± 6	0·70334	−14·9	—	—	—	—	18·4207 ± 26	15·5571 ± 24	38·5697 ± 62	18·412	15·557	38·566
UM01-125	Kamila	tonalites	WR	0·387	0·704097 ± 7	0·70355	−11·9	0·072	0·512844 ± 12	0·51280	5·6	18·7555 ± 5	15·5813 ± 5	39·9073 ± 18	18·603	15·574	38·998
			Pl	0·359	0·704025 ± 2	0·70352	−12·3	0·125	0·512860 ± 24	0·51278	5·2	18·5868 ± 18	15·5709 ± 14	38·9269 ± 40	18·571	15·570	38·923
KG-42	Kiru	granodiorites	WR	0·707	0·704806 ± 7	0·70380	−8·3	0·129	0·512948 ± 21	0·51286	6·9	18·3914 ± 5	15·5650 ± 6	38·4811 ± 15	18·356	15·563	38·439
UM01-123	Kiru	granodiorites	WR	1·196	0·705672 ± 9	0·70397	−5·8	0·143	0·512976 ± 6	0·51288	7·3	18·3781 ± 5	15·5545 ± 5	38·5478 ± 15	18·349	15·553	38·504
			Pl	0·266	0·704238 ± 3	0·70386	−7·4	0·137	0·512922 ± 6	0·51283	6·3	18·3560 ± 8	15·5544 ± 7	38·4954 ± 24	18·327	15·553	38·486

*Sample names from Dhuime *et al.* (2007).Abbreviations are given in Table 1. WR, whole-rock; Cpx, clinopyroxene; Pl, plagioclase; Hbl, hornblende. —, not analyzed. The initial ratios were calculated at $t_0 = 100$ Ma according to Schaltegger *et al.* (2002). The $\varepsilon_{Sr(i)}$ and $\varepsilon_{Nd(i)}$ values were calculated using $(^{87}Sr/^{86}Sr)_{CHUR(100\ Ma)} = 0{\cdot}704384$ and $(^{143}Nd/^{144}Nd)_{CHUR(100Ma)} = 0{\cdot}512511$, respectively. Errors for the Sr, Nd and Pb isotopic ratios are given at the 2σ level and refer to the last significant digits.

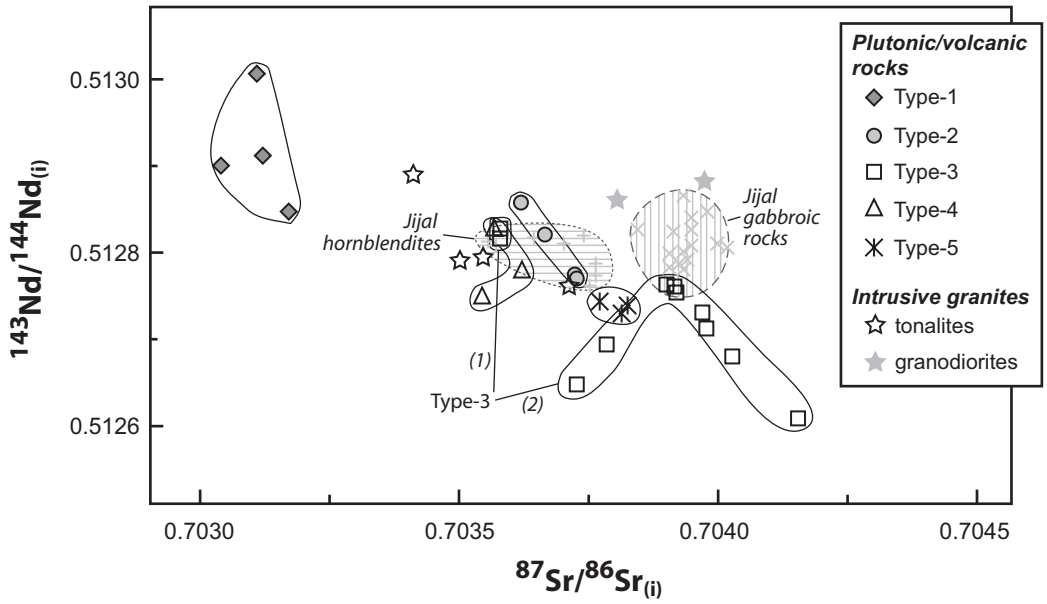

Fig. 7. Nd–Sr isotope diagram for the JPKK crustal section (initial compositions recalculated at $t_0 = 100$ Ma). Only whole-rock and clinopyroxene data (where available) are plotted. The Jijal crustal section fields of 'hornblendites' (i.e. hornblendite–garnetite) and 'gabbroic rocks' (i.e. hornblende gabbronorites and garnet granulites) are from Dhuime *et al.* (2007). The classification of plutonic–volcanic rocks (Types 1–5) and intrusive granites is determined based on their trace element compositions (see explanation in the text and Fig. 4).

$< 0{\cdot}51301$; $0{\cdot}70304 < {}^{87}Sr/{}^{86}Sr_{(i)} < 0{\cdot}70430$) that broadly encompasses the Jijal crustal section ($0{\cdot}51276 < {}^{143}Nd/{}^{144}Nd_{(i)} < 0{\cdot}51287$; $0{\cdot}70355 < {}^{87}Sr/{}^{86}Sr_{(i)} < 0{\cdot}70401$) (Table 2). Type-1 rocks define a distinct field with depleted Nd and Sr isotopic compositions ($0{\cdot}51285 < {}^{143}Nd/{}^{144}Nd_{(i)} < 0{\cdot}51301$; $0{\cdot}70304 < {}^{87}Sr/{}^{86}Sr_{(i)} < 0{\cdot}70317$). Types-2, -4 and -5 together define a limited field ($0{\cdot}51274 < {}^{143}Nd/{}^{144}Nd_{(i)} < 0{\cdot}51286$; $0{\cdot}70357 < {}^{87}Sr/{}^{86}Sr_{(i)} < 0{\cdot}70377$) that is isotopically enriched relative to the Type-1 rocks. Type-3 samples plot in a wide Nd–Sr isotopic domain ($0{\cdot}51261 < {}^{143}Nd/{}^{144}Nd_{(i)} < 0{\cdot}51283$; $0{\cdot}70357 < {}^{87}Sr/{}^{86}Sr_{(i)} < 0{\cdot}70415$) that partly overlaps the field of the Type-2, -4 and -5 rocks. Two groups are distinguished: (1) a small group which is overlapped by the fields of the Type-4 samples and the Jijal hornblendites; (2) samples that have enriched Nd and Sr isotopic compositions (see Fig. 7).

In Pb–Pb isotope diagrams (Fig. 8) the leached-whole rocks and plagioclase separates from Type-1 to Type-5 rocks define a large domain ($18{\cdot}028 < {}^{206}Pb/{}^{204}Pb_{(i)} < 18{\cdot}638$) that encompasses the Jijal crustal section field ($18{\cdot}319 < {}^{206}Pb/{}^{204}Pb_{(i)} < 18{\cdot}565$). In the $^{208}Pb/^{204}Pb$ vs $^{206}Pb/^{204}Pb$ diagram (Fig. 8a), all of the samples plot along a straight line, above and roughly parallel to the Northern Hemisphere Reference Line (NHRL). An increase of the Pb isotopic ratios is observed from the Type-1 samples ($18{\cdot}028 < {}^{206}Pb/{}^{204}Pb_{(i)} < 18{\cdot}140$) to the Type-2 ($18{\cdot}192 < {}^{206}Pb/{}^{204}Pb_{(i)} < 18{\cdot}355$), Type-4 ($18{\cdot}240 < {}^{206}Pb/{}^{204}Pb_{(i)} < 18{\cdot}398$) and Type-5 samples ($18{\cdot}630 < {}^{206}Pb/{}^{204}Pb_{(i)} < 18{\cdot}638$). As already noted for the Nd–Sr diagram (Fig. 7), the Type-3 samples define two groups that are particularly well differentiated in the $^{207}Pb/^{204}Pb$ vs $^{206}Pb/^{204}Pb$ diagram (Fig. 8b): (1) a small group with depleted compositions ($18{\cdot}252 < {}^{206}Pb/{}^{204}Pb_{(i)} < 18{\cdot}275$; $15{\cdot}492 < {}^{207}Pb/{}^{204}Pb_{(i)} < 15{\cdot}577$), forming a field within the main data array, which trends more or less parallel to the NHRL; (2) an enriched group ($18{\cdot}487 < {}^{206}Pb/{}^{204}Pb_{(i)} < 18{\cdot}548$; $15{\cdot}579 < {}^{207}Pb/{}^{204}Pb_{(i)} < 15{\cdot}633$) that shows significantly radiogenic $^{207}Pb/^{204}Pb_{(i)}$ for near-constant $^{206}Pb/^{204}Pb_{(i)}$ and plots within a sub-vertical field, scattering away from the main, NHRL-parallel data trend, towards higher $^{207}Pb/^{204}Pb$ values. A negative correlation is observed between the $^{207}Pb/^{204}Pb$ and $^{143}Nd/^{144}Nd$ ratios for these samples (not shown).

Intrusive granites

The tonalites define the largest range of isotopic variation ($0{\cdot}51276 < {}^{143}Nd/{}^{144}Nd_{(i)} < 0{\cdot}51289$; $0{\cdot}70342 < {}^{87}Sr/{}^{86}Sr_{(i)} < 0{\cdot}70371$; $18{\cdot}220 < {}^{206}Pb/{}^{204}Pb_{(i)} < 18{\cdot}603$) with a spread that encompasses the field defined by the granodiorites in the Pb–Pb diagrams (Fig. 8) but is distinguished by lower $^{87}Sr/^{86}Sr$ ratios in the Nd–Sr diagram (Fig. 7). The field containing all of the intrusive granites is encompassed by the plutonic–volcanic rock field in the Nd–Sr and $^{207}Pb/^{204}Pb$ vs $^{206}Pb/^{204}Pb$ diagrams (Figs 7 and 8b), but

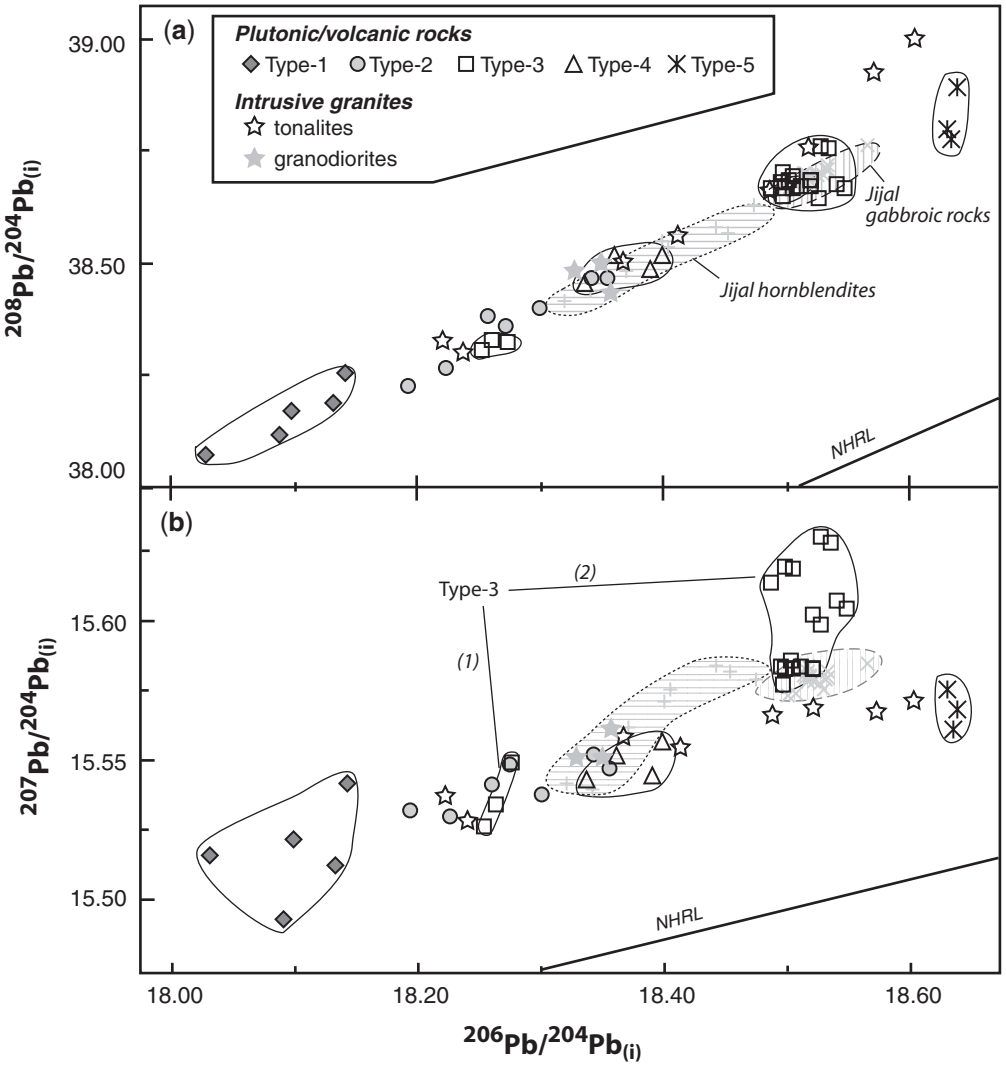

Fig. 8. Variation of $^{208}Pb/^{204}Pb$ (a) and $^{207}Pb/^{204}Pb$ (b) vs $^{206}Pb/^{204}Pb$ for the JPKK crustal section (initial isotopic compositions recalculated at $t_0 = 100$ Ma). Only whole-rock and plagioclase data (where available) are plotted. Fields as in Fig. 7. NHRL, Northern Hemisphere Reference Line (Hart, 1984).

in the $^{208}Pb/^{204}Pb$ vs $^{206}Pb/^{204}Pb$ plot, the tonalite extends towards slightly higher $^{208}Pb/^{204}Pb$ values at the high $^{206}Pb/^{204}Pb$ end of the data array (Fig. 8a). This feature is ascribed to the very low U/Th (and high Th content) of some of the tonalite samples (see Table 1).

DISCUSSION

Relative contribution of the subduction component in the JPKK section

The chemical and Nd–Sr–Pb isotopic diversity of primitive island arc magmas is usually attributed to the composition of the mantle wedge with a variable overprint of components derived from the subducting slab (i.e. altered oceanic crust, subducted oceanic and fore-arc sediments). From a geochemical point of view, this subduction component is characterized by a relative enrichment in LILE, U, Pb and, to a lesser extent, LREE and Th relative to HFSE and HREE. The enrichment in these incompatible trace elements is accounted for by their higher solubility in slab-derived fluids or melts that transfer these elements from the slab into the overlying mantle wedge where the subduction-related magmas are generated (e.g. Ellam & Hawkesworth, 1988).

The relative contribution and nature of the subduction component in the several plutonic–volcanic rock types that we have identified in the JPKK section can be gauged by comparing the primitive mantle normalized trace element pattern of each type to that of average

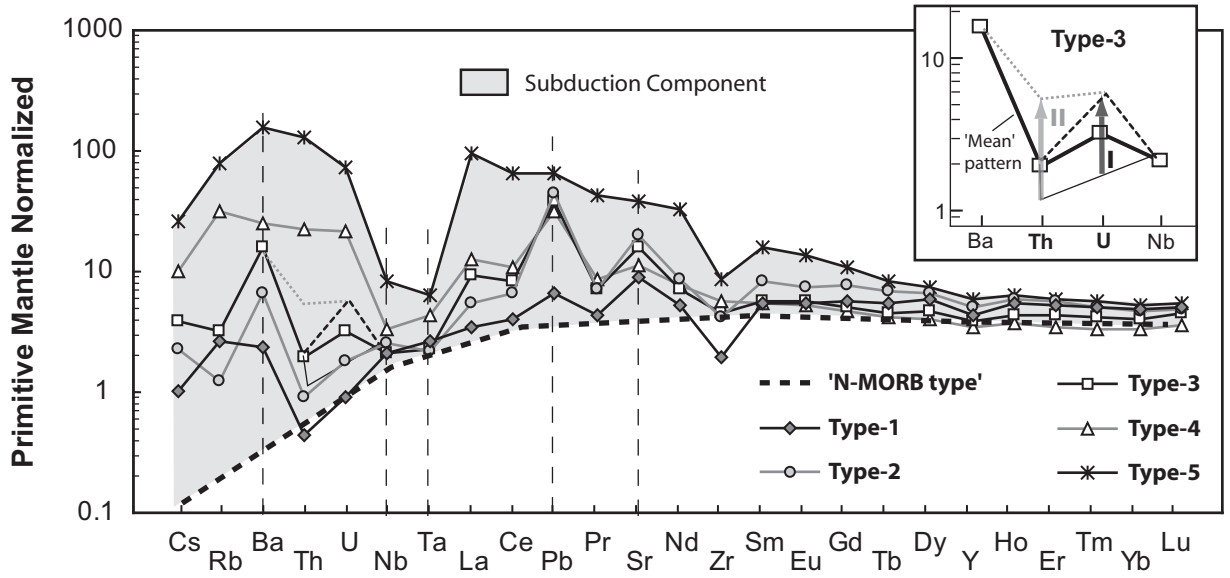

Fig. 9. Evolution of trace element characteristics in the JPKK crustal section. Concentrations are mean values for each type, and normalized to primitive mantle values after Sun & McDonough (1989). The evolution from Type-1 to Type-5 trace element patterns reflects the progressive contribution of a subduction component to the source of the arc magmas (see text). The inset indicates the behaviour of Th and U for the Type-3 samples, which can be classified into three sub-types: (1) those with no Th–U anomaly (thin Th–U segment), which is typically also observed for Types-1 and -2; (2) those with a marked positive U anomaly and no notable Th enrichment (black dashed line and arrow I). Given the lower distribution coefficient of U in fluids compared with the LILE, the U enrichment is interpreted as an indicator of a strong increase in a 'slab fluid' component in the magma source. (3) Trace element patterns with both U and Th enrichment (grey dotted line and arrow II). Given that Th is known to be immobile in aqueous fluids, the Th enrichment would suggest the contribution of a 'slab melt' component to the mantle source. This is consistent with the strong LREE enrichment observed. The 'mean pattern' for Type-3 samples is represented by the thick black line.

N-MORB (e.g. Hofmann, 1988; Sun & McDonough, 1989) representative of a partial melt of a DMM mantle wedge source (Fig. 9). The significant increase from Type-1 to -5 in the LILE content, concomitant with relatively higher contents of Pb, Sr and LREE, and the development of a HFSE (Nb, Ta) negative anomaly from Type-3 to Type-5, may be accounted for by an increasing contribution of a subduction component in the source (Fig. 9, grey shaded area). On the basis of the different chemical behaviour of the various trace elements plotted, it is possible to distinguish between a contribution from a subduction component dominated by aqueous fluids (i.e. the 'slab fluid' component) and one by sediment melts (i.e. the 'slab melt' component). For example, fluid component involvement can be visualized on normalized trace element diagrams by a slight enrichment of LILE, which are highly mobile in aqueous fluids (Kogiso *et al.*, 1997; Tatsumi & Kogiso, 1997) compared with HFSE and LREE. This can also be monitored using ratios of elements with similar partition coefficients during mantle melting but contrasting behaviours in aqueous fluids [e.g. Ba/La, U/Th and Pb/Ce (Brenan *et al.*, 1995; Elliott *et al.*, 1997; Hawkesworth *et al.*, 1997*a*, 1997*b*; Plank *et al.*, 2006]. The variable contribution of a fluid and/or melt component in the different pattern types of the JPKK section can be portrayed in plots showing the U/Th and Pb/Ce ratios as a function of ratios of REE with different compatibility in melts (e.g. La/Yb) (Fig. 10). In these plots the major participation of a slab fluid component is observed for samples from Type-1 and Type-2, reflected by high U/Th and Pb/Ce ratios associated with low La/Yb ratios. An increasing contribution of a slab melt component from Type-3 to Type-5 is manifest by a pronounced negative Nb–Ta anomaly relative to LILE and LREE, higher contents of LILE and Th, and REE enrichment correlated with an increasing fractionation of LREE relative to HREE (Fig. 9). In the U/Th and Pb/Ce vs La/Yb diagrams (Fig. 10), the involvement of the slab melt component is reflected by a decrease of the U/Th and Pb/Ce ratios associated with an increase of the La/Yb ratio.

Studies on high-pressure and ultrahigh-pressure metamorphic terranes (e.g. Hermann *et al.*, 2006), along with experimental studies (Hermann & Green, 2001; Spandler *et al.*, 2007; Hermann & Spandler, 2008), have shown that aqueous fluids released at the blueschist- to eclogite-facies transition contain only moderate amounts of LILE, Sr and Pb and do not transport significant amounts of LREE, U and Th. Fluid-present melting of sediments on top of the slab is required to transfer significant amounts of trace elements from the slab to the mantle wedge; with

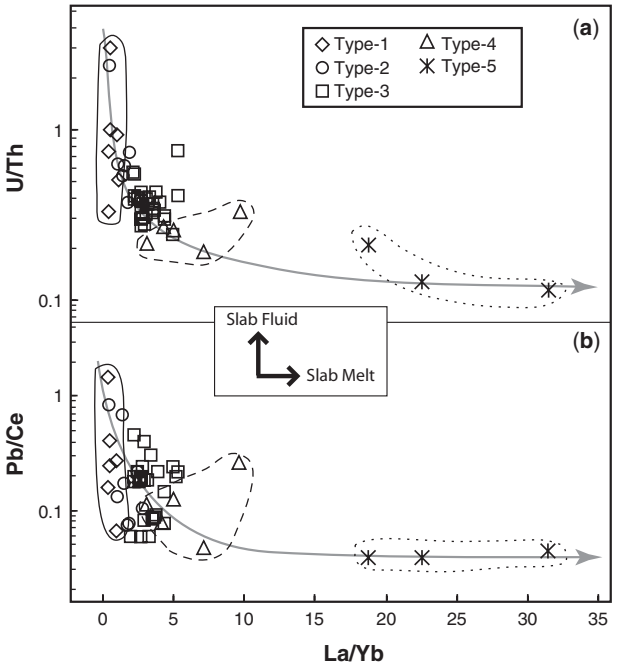

Fig. 10. (a) U/Th vs La/Yb and (b) Pb/Ce vs La/Yb for samples from the JPKK crustal section.

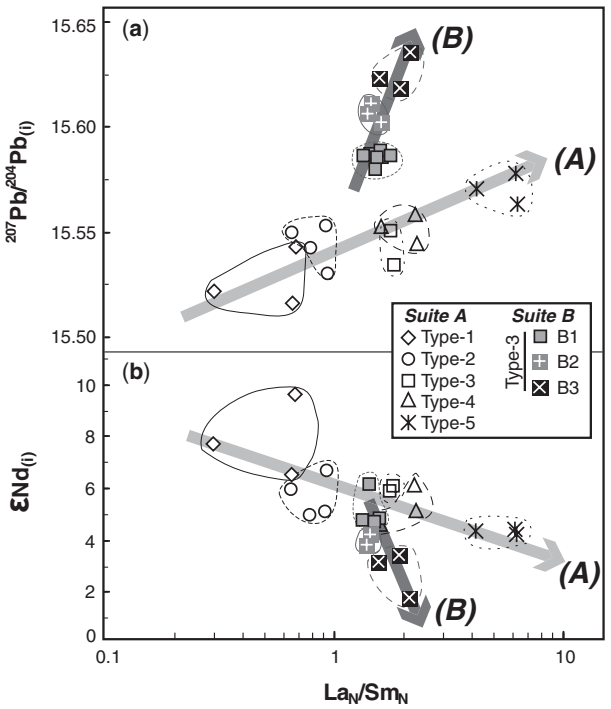

Fig. 11. (a) $^{207}Pb/^{204}Pb$ vs La_N/Sm_N and (b) ε_{Nd} vs La_N/Sm_N diagrams for non-cumulative rocks from the JPKK crustal section (at $t_0 = 100$ Ma). Two geochemical suites, 'A' (pale grey arrow) and 'B' (dark grey arrow) have been distinguished (see text for explanation).

a top slab temperature in the range of 700–900°C at subarc depths (Hermann *et al.*, 2006; Hermann & Spandler, 2008). The hydrous, granitic melts produced during slab melting are not significantly enriched in LREE because of the presence of allanite in the residue above 750°C (Hermann & Green, 2001; Klimm *et al.*, 2008). Consequently, the strong LREE enrichment observed in the Type-3 REE patterns, progressively increasing in the Type-4 and Type-5 patterns, may indicate high melting degrees of slab sediments to consume LREE-rich phases such as allanite.

The JPKK trace element signatures unambiguously indicate an increasing contribution of a subduction component from Type-1 to -5, with a relatively higher contribution of a slab fluid component from Type-1 to -3, and an increasing involvement of a slab melt component from Type-3 to -5. Because the timescale for the transfer of aqueous fluids through the mantle wedge is significantly shorter than that for sediment melts (Hawkesworth *et al.*, 1997*a*, 1997*b*; Turner & Hawkesworth, 1997; Turner *et al.*, 1997), it is conceivable that the parental magmas of Types-3 to -5 were generated later than those of Types-1 and -2 during the mature stage of evolution of the Kohistan subduction zone.

Evidence for two geochemical and temporal magmatic suites in the JPKK section

A plot of La_N/Sm_N vs $^{207}Pb/^{204}Pb_{(i)}$ and $^{143}Nd/^{144}Nd_{(i)}$ (expressed as εNd_i) reveals the existence of two distinct geochemical suites (hereafter referred to as suites A and B; Fig. 11), as follows.

(1) Suite A encompasses samples from Types-1, -2, -4 and -5 and the isotopically depleted Type-3 samples (i.e. high εNd and low $^{207}Pb/^{204}Pb$ ratios). There is a progressive increase in $^{207}Pb/^{204}Pb$ (and reduction in εNd) with increasing La_N/Sm_N from Type-1 to -5 rocks.

(2) Suite B encompasses the isotopically enriched samples of Type-3. It differs from suite A by its higher $^{207}Pb/^{204}Pb$ and lower $^{143}Nd/^{144}Nd$ at similar La_N/Sm_N. We further differentiate within this suite three groups of samples (B1, B2 and B3; Fig. 11) characterized by an increasing enrichment of ^{207}Pb relative to ^{204}Pb combined with decreasing $^{143}Nd/^{144}Nd$ from group B1 to B3.

Suites A and B are emplaced at distinct levels of the JPKK section (Fig. 12). Suite A rocks are mainly located in the middle–upper arc section, whereas suite B rocks are located either in the lower arc crust (groups B1 and B2) or in the uppermost arc crust (group B3).

The existence of two suites with distinct and correlated trace element and isotopic characteristics suggests that these geochemical signatures were imposed on their

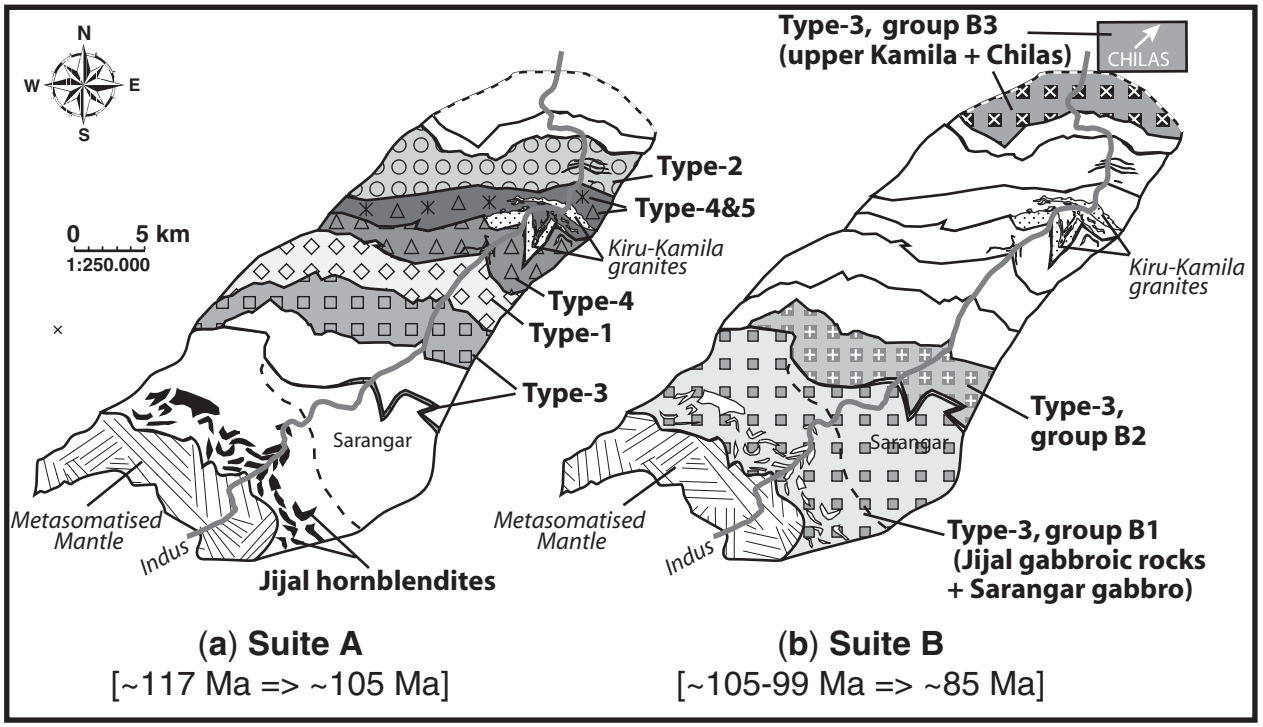

Fig. 12. Simplified maps of the JPKK crustal section indicating the rocks from (a) suite A and (b) suite B (see text for explanation). The position of the metasomatized mantle (Jijal dunite–wehrlite–pyroxenite in contact with the granulitic lower arc crust), together with the granites intrusive into the Kiru–Kamila sequences, is shown for comparison.

parental magmas from their mantle sources and were not the result of late dehydration-melting processes during intra-crustal metamorphism. Samples from the Jijal complex considered to have undergone dehydration-melting that modified their original trace element signature (Garrido *et al.*, 2006; Padrón-Navarta *et al.*, 2008) have been excluded from comparison with these suites. Jijal garnet hornblendites show isotopic characteristics akin to Type-2, -3 and -4 samples of suite A (Table 2). They are interpreted as the deep plutonic equivalent of shallower samples from Type-2 to Type-4 (Dhuime *et al.*, 2006, 2007; Garrido *et al.*, 2006). On the other hand, Jijal gabbroic rocks show isotopic compositions akin to the less-enriched samples of suite B (i.e. group Bl; Table 2), suggesting a common source.

Published ages for samples of suite A are limited (see Fig. 2). Yamamoto *et al.* (2005) reported a secondary ionization mass spectrometry (SIMS) U–Pb zircon age of $107{\cdot}7 \pm 1{\cdot}8$ Ma for a tonalite dike intrusive into rocks with Type-1 and -3 signatures and an age of $110{\cdot}7 \pm 4{\cdot}9$ Ma for an amphibolite xenolith in granites intrusive into Type-4 and -5 rocks. Such results are consistent with an older age for samples from suite A (i.e. >100 Ma), with an upper age bound set by subduction initiation at ~117 Ma (Dhuime *et al.*, 2007), and a lower age bound of ~105 Ma established by the oldest ages of the intrusive rocks.

Suite B samples of group Bl, characterized by the lowest $^{207}Pb/^{204}Pb$ ratio of this suite, are from the 'Sarangar gabbro' unit, for which Schaltegger *et al.* (2002) have reported a precise magmatic U–Pb zircon age of $98{\cdot}9 \pm 0{\cdot}4$ Ma. This unit intrudes and overlies the upper gabbroic rocks of the Jijal section, which are isotopically akin to group Bl. Precise ages for the Jijal gabbroic rocks are lacking: their intrusive age can be bracketed between 118 ± 12 Ma (the Sm/Nd age of a hornblende gabbronorite; Yamamoto & Nakamura, 2000) and ~96 Ma (the maximum age for the granulite-facies metamorphism; Anczkiewicz & Vance, 1997; Anczkiewicz *et al.*, 2002). These ages indicate a younger age for group Bl samples, between ~105 Ma (minimum age of the Jijal gabbros) and ~99 Ma (Sarangar gabbro). The minimum emplacement age for the most enriched samples of suite B (group B3) is $80{\cdot}6 \pm 4{\cdot}5$ Ma (U–Pb zircon age of an intrusive tonalite; Yamamoto *et al.*, 2005). The Chilas complex, which intrudes and shares many geochemical similarities with group B3 (see Figs 4, 13 and 14), yields ~85 Ma zircon U–Pb ages (Zeitler *et al.*, 1981; Schaltegger *et al.*, 2002), indicating a short time lag between the intrusion of the group B3 and Chilas magmas. Although no age is available for group B2, its $^{207}Pb/^{204}Pb$ and Nd isotopic compositions plot intermediate between the Bl and B3 groups and might indicate a transitional magmatic stage

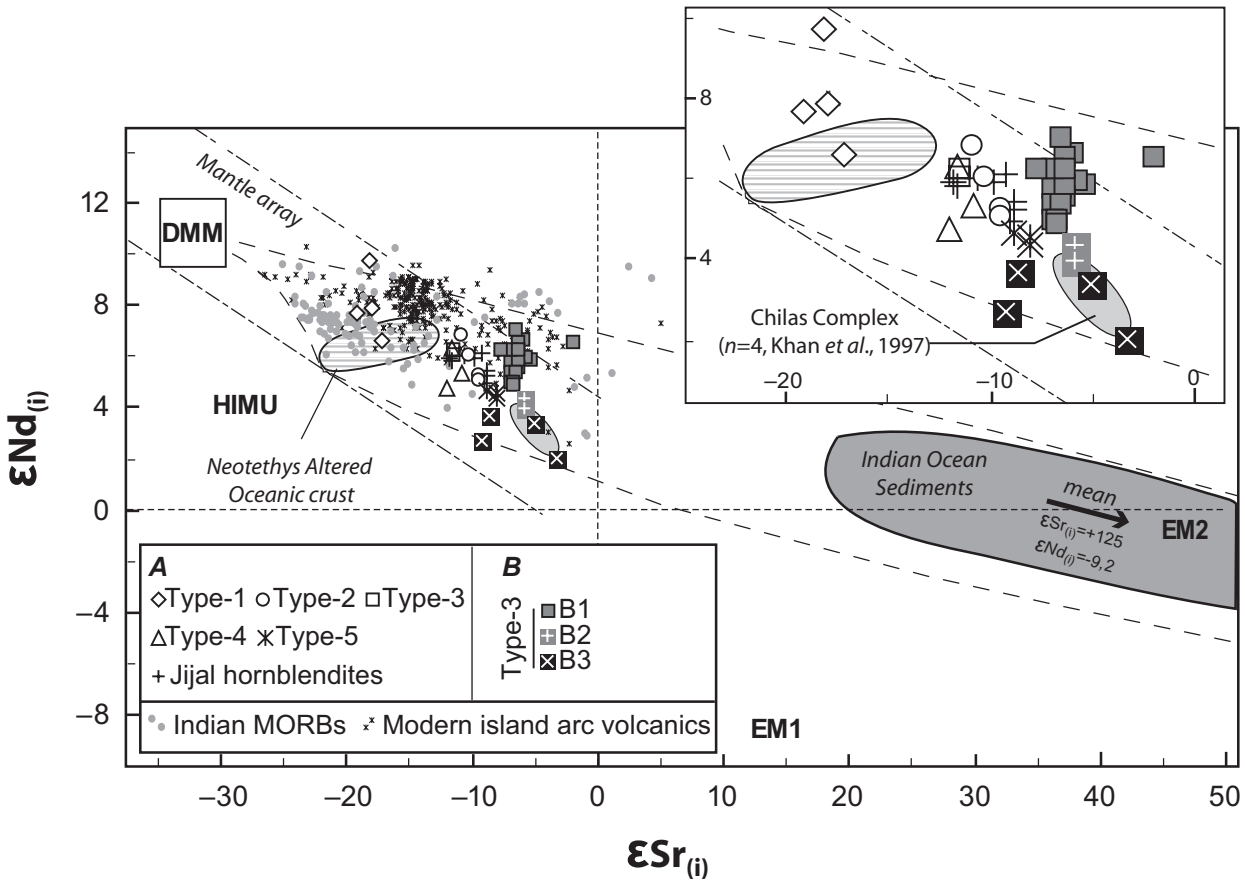

Fig. 13. ε_{Nd} vs ε_{Sr} ($t_0 = 100$ Ma) variation in the JPKK crustal section. Shown for comparison are data for Indian Ocean sediments (Ben Othman *et al.*, 1989; Plank & Langmuir, 1998), the Neotethys altered oceanic crust (Mahoney *et al.*, 1998), Indian MORB (Mahoney *et al.*, 1998, 2002, $n = 120$), modern island arc lavas (GEOROC compilation, http://georoc.mpch-mainz.gwdg.de/georoc/Entry.html, $n = 389$) and the Chilas complex (Khan *et al.*, 1997, $n = 4$). The Chilas complex has enriched isotopic compositions similar to those of the B3 group. The range of Nd–Sr variation for the Chilas complex is slightly broader than that defined by Khan *et al.* (1997): Mikoshiba *et al.* (1999) reported $\varepsilon_{Sr(i)}$ values between −6·9 and +1·5 ($n = 24$) and Jagoutz *et al.* (2006) obtained $\varepsilon_{Nd(i)}$ values between +4·2 and +5·1 ($n = 12$). The compositions of the DMM (Depleted MORB Mantle), HIMU (high $\mu = {}^{238}U/{}^{204}Pb$), EM1 (Enriched Mantle 1) and EM2 (Enriched Mantle 2) mantle end-members are from Zindler & Hart (1986), Hart (1988) and Hofmann (2003). NHRL, Northern Hemisphere Reference Line (Hart, 1984). The dashed lines indicate mixing between DMM, subducted sediment and altered oceanic crust end-members and have been calculated using the methods of Faure (1986) and the following parameters: DMM: Sr = 11·3 ppm and Nd = 1·12 ppm (Eisele *et al.*, 2002); Indian Ocean sediments: Sr = 100–200 ppm and Nd = 15–30 ppm (Ben Othman *et al.*, 1989; Plank & Langmuir, 1998); altered oceanic crust: Sr = 100–300 ppm and Nd = 15–30 ppm (Mahoney *et al.*, 2002).

with intrusion ages between those of groups Bl and B3 (i.e. between 105–99 Ma and 85 Ma). Intrusion ages of ~105–99 Ma, ~95 Ma and ~85 Ma are proposed as approximate ages for groups Bl, B2 and B3, respectively.

Origin of intrusive granites in the JKPP section

Garrido *et al.* (2006) have proposed that the Kiru–Kamila intrusive granites were generated by dehydration-melting of different amphibole-bearing lithologies within the Jijal crustal section. Our isotopic data (Figs 7 and 8; Table 2) show that the isotopic signature of these granites is consistent with a combination of sources located in the arc root of the crustal section (i.e. Jijal hornblendites and Jijal–Patan gabbroic rocks), with variable contributions from the granites' host-rocks. This latter contribution predominates, for example, in sample UM01-125, which has a Pb isotope composition consistent with contamination by Type-5 host-rocks (Table 2). Our data suggest that the granite magmas underwent variable assimilation and interaction with their host-rocks during their ascent and emplacement from the lower crust.

Comparison with other intra-oceanic arcs

In terms of their Sr–Nd–Pb isotope compositions, samples from both suites A and B plot within a triangular domain delimited by the DMM reservoir, Indian Ocean sediments

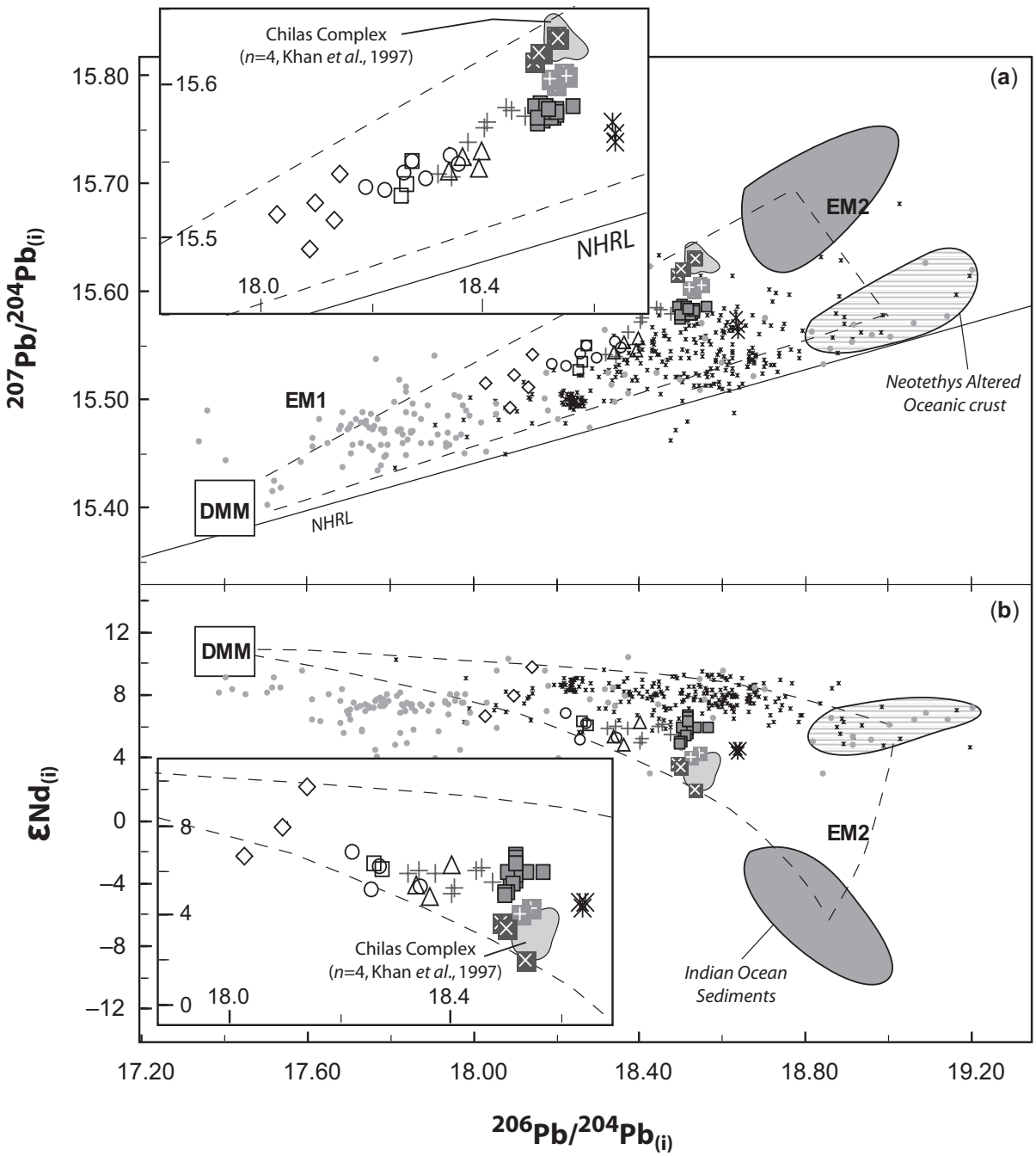

Fig. 14. Variation of $^{207}Pb/^{204}Pb$ vs $^{206}Pb/^{204}Pb$ and ε_{Nd} vs $^{206}Pb/^{204}Pb$ ($t_0 = 100$ Ma) for the JPKK crustal section. The various fields and end-members are the same as in Fig. 13. The mixing lines between the DMM, sediments and altered oceanic crust end-members are calculated after Faure (1986), using the following parameters: DMM: Nd = 1·12 ppm and Pb = 0·050 ppm (Eisele *et al.*, 2002); Indian Ocean sediments: Nd = 15–30 ppm and Pb = 1·5–30 ppm (Ben Othman *et al.*, 1989; Plank & Langmuir, 1998); altered oceanic crust: Nd = 15–30 ppm and Pb = 1–3 ppm (Mahoney *et al.*, 2002). NHRL, Northern Hemisphere Reference Line (Hart, 1984).

and Neotethyan altered oceanic crust (Figs 13 and 14). Previous studies of intra-oceanic arcs worldwide (e.g. Marianas, Tonga–Kermadec, Izu–Bonin) have often interpreted such geochemical characteristics as a result of three-component mixing in which the sediment-related subduction input is determined either by the amount of sediment dragged down to the zone of magma formation and/or the thickness of the sedimentary cover on the

subducting oceanic crust (e.g. Gamble *et al.*, 1996; Regelous *et al.*, 1997) or in terms of nature of the sedimentary component; that is, whether it is pelagic or detrital in origin (e.g. Chauvel *et al.*, 2009). The importance of the nature and composition of the mantle wedge before fluid or melt addition from the subducting slab has also been considered (e.g. Ewart *et al.*, 1998; Woodhead *et al.*, 1998; Pearce *et al.*, 2007). Until now, there have been few insights into the mechanisms by which fluids or silicate melts are added to the mantle wedge, particularly with respect to their timing in relation to the dynamic evolution of the subduction zone (Hawkesworth *et al.*, 1997*a*, 1997*b*). It is noteworthy that of the many variables that can play an important role in controlling the geochemical signatures of arc lavas, the most important are intrinsic to the particular arc system and involve both physical–dynamic and geochemical parameters.

The fossil Kohistan arc constitutes one of the best examples in which the trends exhibited by various geochemical tracers can be explained by combining both geochemical and physical–dynamic parameters, in particular during drastic changes in the subduction regime. The following section summarizes the evolution we propose for the JPKK section in relation to both geodynamic and geochemical parameters.

A three-stage geodynamical evolution model for the KAC

Combination of our new trace element and Sr–Nd–Pb isotopic data with previous results (Dhuime *et al.*, 2007; Garrido *et al.*, 2007) and available geochronological data (Zeitler *et al.*, 1981; Yamamoto & Nakamura, 1996, 2000; Anczkiewicz & Vance, 1997; Anczkiewicz *et al.*, 2002; Schaltegger *et al.*, 2002; Yamamoto *et al.*, 2005; Dhuime *et al.*, 2007) allows us to propose a three-stage model for the evolution of the Kohistan island arc magmatism.

Stage 1 (≥117 Ma to ~105 Ma): subduction initiation and growth of the volcanic arc

This stage encompasses the initiation of an intra-oceanic subduction system and the onset of subduction (Fig. 15a, Stages 1-a and 1-b, respectively). Initiation of subduction most probably occurred near a mid-ocean ridge transform fault or fracture zone, separating young, thin lithosphere from old, thick lithosphere (Stern & Bloomer, 1992; Stern, 2004; Fig. 15a, Stage 1-a). Subduction started at around 117 Ma (Dhuime *et al.*, 2007; Fig. 15a, Stage 1-b). Extension in the overlying lithosphere (the 'proto fore-arc') was associated with LREE-depleted and high-(LILE, $^{207}Pb/^{204}Pb$, $^{87}Sr/^{86}Sr$) 'boninite-like' magmatism that interacted with the pre-existing lithospheric mantle, giving rise to the Jijal dunite–wehrlite–pyroxenite sequence (Dhuime *et al.*, 2007; Garrido *et al.*, 2007).

The mantle component involved in the genesis of the suite A rocks may represent ambient asthenosphere.

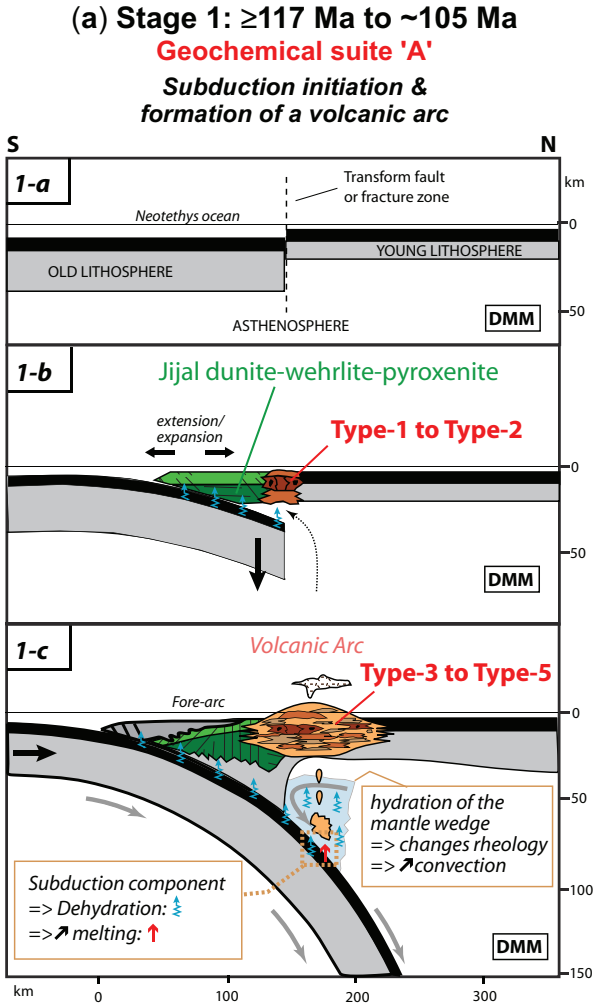

Fig. 15. Three-stage schematic evolution of the Kohistan arc from ~117 to 85 Ma. (a) Stage l; (b) Stage 2; (c) Stage 3. (See text for detailed explanation.)

The gradual enrichment of LILE, REE and the Nd–Sr–Pb isotope composition observed from Type-1 to Type-2 may reflect the increasing but limited contribution of a slab component. Further growth of the arc occurred subsequently by intrusion of Type-3 magmas with an island arc tholeiite geochemical signature, representing ~8–10% of the JPKK section (Fig. 15a, Stage 1-c). The enrichment in fluid-immobile elements characteristic of Type-3 samples (Figs 9 and 10) suggests that at this stage the subduction component was dominated by a slab melt rather than a slab fluid. The progressive building of the volcanic arc is characterized by the increase in the slab melt component in Type-4 and Type-5 rocks, which together represent approximately 10% of the total thickness of the JPKK crustal section. The enrichment in the Nd–Sr–Pb isotopic compositions observed in suite A is consistent with a progressive increase in the subduction contribution as the

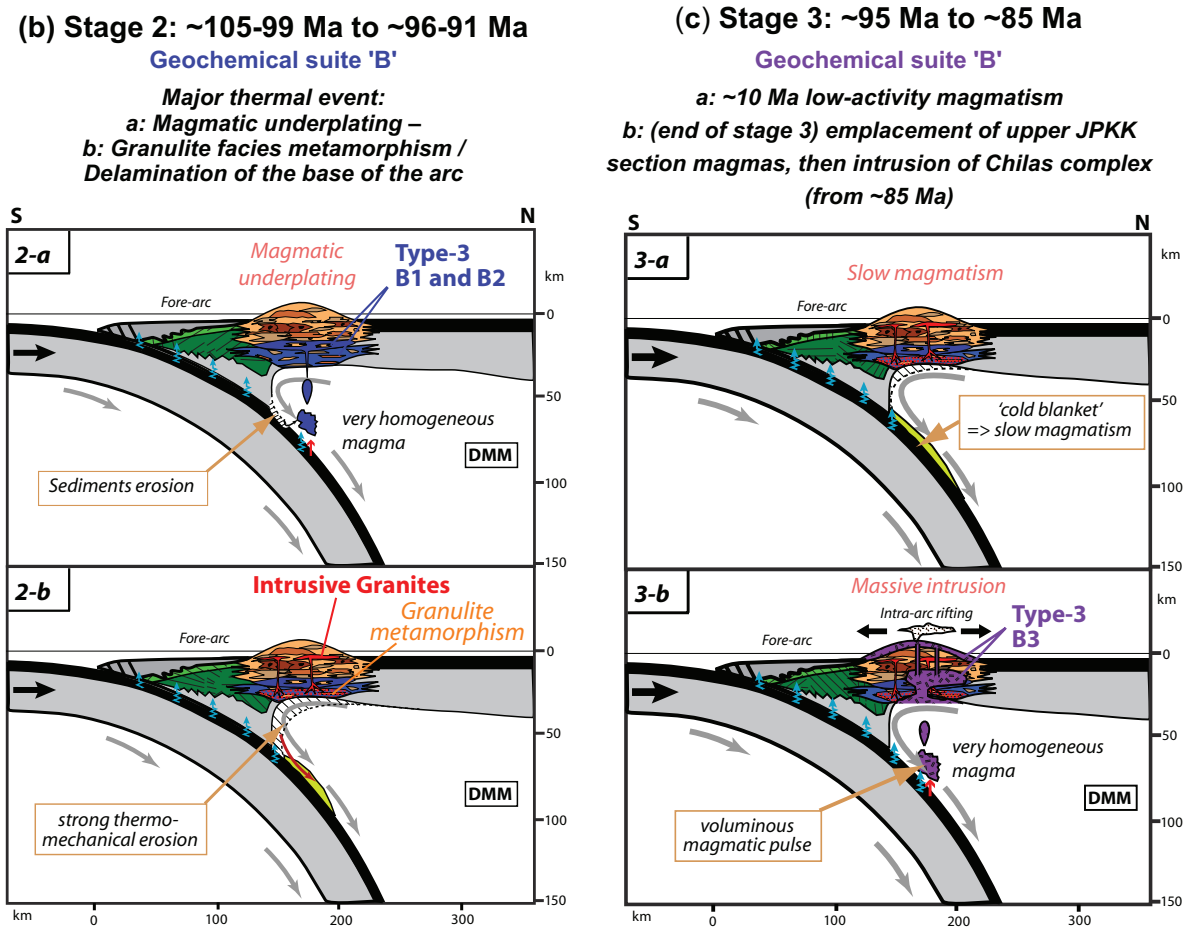

Fig. 15. Continued

volcanic arc evolved. The increasing influence of a slab melt component is probably related to the activation of convection in the mantle wedge, allowing a continuous 'circulation' of hot mantle at the slab surface (e.g. Kincaid & Sacks, 1997; van Keken *et al.*, 2002). The conductive heating of the slab surface by the overlying asthenospheric mantle caused it to partially melt (i.e. the sediments ± the underlying altered oceanic crust), followed by the injection of slab melts into the mantle wedge

Stage 2 (~105–99 Ma to 96–91 Ma): major thermal event: magmatic underplating, granulite-facies metamorphism and erosion-delamination of the arc base

The initiation of Stage 2 is associated with the development of suite B. Two major events occurred at around 100 Ma, just after the building of the volcanic part of the arc, and over a period of ~10 Myr.

(1) Magmatic underplating of the arc crust (Fig. 15b, Stage 2-a), caused the emplacement of large volumes of gabbroic rocks with B1 and then B2 geochemical signatures: these represent approximately 20% and 10% of the total thickness of the JPKK crustal section, respectively. This event resulted in significant crustal thickening (P_{max} = 1·4–2·1 GPa, Jan & Howie, 1981; Yamamoto, 1993; Ringuette *et al.*, 1999). The evolved character of the underplated magmas (43 < Mg-number < 59, Table 1) implies that there was likely to have been a thick cumulate sequence [up to 30–35 km (Garrido *et al.*, 2007)], which is not preserved in the obducted section of the Kohistan arc (Dhuime *et al.*, 2007; Garrido *et al.*, 2007).

Compared with suite A, suite B rocks (Stage 2-a) have a rather homogeneous composition, despite the large volumes of magma involved. Their enriched Nd and $^{207}Pb/^{204}Pb$ isotope compositions indicate significant changes in the magmatic source during the transition from suite A to suite B. The isotopic enrichment of suite B rocks can be explained by the 'subduction erosion' of forearc metasediments (e.g. von Huene & Scholl, 1991, 1993; Ranero & von Huene, 2000) and the mixing between these sediments and DMM-type asthenospheric mantle. This mixed, enriched material was later dragged down by corner flow towards the magma source region of suite B

(Fig. 15b, Stage 2-b), accounting for the progressive geochemical enrichment observed for this suite.

(2) Granulite-facies metamorphism at the base of the arc sequence (Fig. 15b, stage 2-b) occurred in association with dehydration-melting of hornblende-bearing mafic and ultramafic rocks and the development of granitic melts. The migration of these granitic melts to shallower crustal levels, and their interaction with their host-rocks, constitutes the main mechanism for intra-crustal differentiation in the Kohistan arc (Garrido *et al.*, 2006); as well as in Cenozoic paleo-arc complexes such as the Hidaka Metamorphic Belt in Japan (Kemp *et al.*, 2007).

The distinct Sr–Nd–Pb isotopic signature of the garnet-bearing rocks (i.e. garnet granulites and garnet hornblendites) at the roots of the Kohistan arc invalidates claims that these rocks are cogenetic high-pressure, garnet-bearing cumulates (Alonso Perez *et al.*, 2008). The absence in the exhumed section of the Kohistan arc of cogenetic ultramafic cumulates with the evolved gabbroic rocks formed in Stage 2-a points to their removal at Stage 2-b either by gravitational collapse (Kay & Kay, 1985, 1993; Tatsumi, 2000; Jull & Kelemen, 2001) or by thermo-mechanical erosion of the infra-arc lithosphere (Eberle *et al.*, 2002; Morency & Doin, 2004; Arcay *et al.*, 2005, 2006)

The time span (~15–20 Myr) between the volcanic arc stage (~110 Ma) and the granulite-facies metamorphism (~96–91 Ma) is too short for the development of gravitational instabilities leading to delamination (Jull & Kelemen, 2001; Kelemen *et al.*, 2003). In our model, magmatic underplating and granulite-facies metamorphism result from a single event, associated with an increase of mantle convection efficiency. The water-dependent modification of asthenospheric mantle rheology (Mackwell *et al.*, 1985; Karato *et al.*, 1986; Hirth & Kohlstedt, 1996; Mei & Kohlstedt, 2000*a*, 2000*b*; Karato, 2003), induced by fluids from a dehydrating subducted slab (Billen & Gurnis, 2001; Billen *et al.*, 2003; Honda & Saito, 2003; van Keken, 2003), have been inferred to trigger an acceleration of convection in the mantle wedge (Arcay *et al.*, 2005). This acceleration of the convection process causes thermo-mechanical erosion and dragging of the 'cold walls' of the mantle wedge (i.e. along the upper part of the slab and the base of the overriding plate). Numerical models suggest that thermo-mechanical erosion provides a good explanation for the removal of the missing cumulates (Arcay *et al.*, 2006) and could happen within 15 Myr.

Stage 3 (~95–85 Ma): low magmatic activity, emplacement of the upper JPKK magmas, and intrusion of the Chilas complex from 85 Ma (last stage of magmatism in intra-oceanic setting)

The rocks associated with Stage 3 constitute the most isotopically enriched magmas of suite B (B3). These rocks are found in the uppermost part of the JPKK section (~20% of the total thickness of the JPKK crustal section) and in the Chilas complex (see Fig. 12). The Chilas ultramafic–mafic complex was emplaced in an intra-arc rift setting at ~85 Ma (Zeitler *et al.*, 1981; Bard, 1983; Coward *et al.*, 1987; Khan *et al.*, 1989; Treloar *et al.*, 1996; Burg *et al.*, 1998; Schaltegger *et al.*, 2002; Jagoutz *et al.*, 2006). It is intrusive into the uppermost JPKK rocks, suggesting an older age for those rocks. However, given the apparent geochemical similarity between the upper JPKK and the Chilas gabbroic–dioritic rocks (see Figs 4, 13 and 14), the ~85 Ma zircon age for the Chilas gabbroic rocks (Zeitler *et al.*, 1981; Schaltegger *et al.*, 2002) is probably the best estimate for the maximum age of the B3 magmas. Such an age implies an ~10 Myr period of 'low magmatic activity' (Fig. 15c, Stage 3-a) between the ~96–91 Ma granulite-facies metamorphism and associated mechanical erosion (Fig. 15b, Stage 2-b), and the formation of the B3 magmas (Fig. 15c, Stage 3-b).

The B3 magmas are associated with the final stage of thermo-mechanical erosion of the arc base. The thinning of the overriding plate at the arc base level could have provoked the rifting of the arc after a significant period (<10 Myr) of stagnation and homogenization of a large volume of magma. Recent numerical models of subduction zones (Kincaid & Sacks, 1997; Arcay *et al.*, 2007) suggest the formation of a thermal shield—or 'cold blanket'—above the slab surface. A similar scenario could account for the period of low magmatic activity observed in the Kohistan arc. In our model, a shield was formed when the eroded 'cold walls' (see Stage 2 above) were progressively dragged into the zone of melt generation through convection in the mantle wedge (see Fig. 15c, Stage 3-a). The cold blanket inhibited the dehydration and partial melting of subducted material, and thus the partial melting of the mantle wedge. This continued until the cold blanket was removed by corner flow and/or was thermally re-equilibrated, before the emplacement of the B3 magmas (Fig. 15c, Stage 3-b).

CONCLUSIONS

The detailed study of the JPKK crustal section of the Kohistan Arc Complex, from the Moho transition zone to the contact with the Chilas complex has, for the first time, characterized the geochemistry of a continuous ~30 km thick section of lower- to middle-arc crust. The results suggest that the intra-oceanic evolution of the Kohistan arc occurred over a period of ~30 Myr (117 Ma > $t_{initiation-collision}$ > 85 Ma). Three major stages characterize its evolution: (1) the progressive building of a 'volcanic arc' between ~117 Ma and ~105 Ma; (2) magmatic underplating of large quantities of magma in the arc base (~100 Ma) and the development of a major granulite-facies metamorphic event in the lower arc crust (~96–91 Ma); (3)

a period of 'low magmatic activity' between ~95 Ma and ~85 Ma before a final magmatic pulse at ~85 Ma preceding arc–continent collision.

The transition between Stages 1 and 2 was probably induced by the progressive hydration of the mantle wedge, which modified its rheology and induced convection. This resulted in thermo-mechanical erosion of the lower parts of the crustal section and, at least in part, provided the heat required to trigger granulite-facies metamorphism at the arc base. As the main process for recycling lower arc crust into the mantle, thermo-mechanical erosion has the advantage over classical models of delamination by gravitational collapse of being compatible with the relatively short duration of the magmatic activity in the Kohistan arc.

The bulk chemical composition of the arc magmas can be interpreted in terms of mixing, in different proportions, between a depleted 'DMM-like' mantle component and a subduction component. The latter has a geochemical composition that reflects the involvement of sediments from the Indian Ocean and altered oceanic crust. Depending on the stage of evolution of the subduction system, the subduction component is transported initially in dehydration fluids and then later in silicate melts. The latter are related to the activation of convection in the mantle wedge and the circulation of hot mantle at the slab surface, leading eventually to partial melting of the uppermost levels of the slab (i.e. sediments ± altered oceanic crust).

ACKNOWLEDGEMENTS

This work has benefited from financial support from the 'Institut National des Sciences de l'Univers du Centre National de la Recherche Scientifique' ('DyETI Program, Thème IV') in 2004 and 2006 to D.B. and from a PhD grant of 3 years from the research ministry to B.D. C.J.G. acknowledges funding from the Spanish 'Ministerio de Ciencia e Innovación' (research grants CGL2006-04440/BTE, CGL2007-61205 and PCI2006-A9-0580) and the 'Junta de Andalucía' (research group RMN131). We would like to thank Béatrice Galland for technical assistance in the chemistry clean room, Simone Pourtalès for help during ICP-MS analyses, and J. P. Burg and G. Zeilinger for providing some samples. The technical assistance of Philippe Télouk during Nd and Pb data acquisition (Service Commun National, ENS, Lyon) and of Patrick Verdoux during Sr isotope analyses (GIS laboratory, Nîmes) has been greatly appreciated. This paper benefited from helpful reviews from R. Price and an anonymous reviewer. The authors greatly appreciate discussions with D. Arcay, S. Guillot, C. J. Hawkesworth, S. Lallemand and R. Maury. Special thanks go to S. Mullin for improving the quality of English.

SUPPLEMENTARY DATA

Supplementary data for this paper are available at *Journal of Petrology* online.

REFERENCES

Alonso-Perez, R., Müntener, O. & Ulmer, P. (2008). Igneous garnet and amphibole fractionation in the roots of island arcs: experimental constraints on andesitic liquids. *Contributions to Mineralogy and Petrology* doi:10.1007/s00410-008-0351-8.

Anczkiewicz, R. & Vance, D. (1997). Chronology of subduction, collision and regional metamorphism in Kohistan, NW Himalaya, Pakistan. *Terra Nova* **9**, 345.

Anczkiewicz, R. & Vance, D. (2000). Isotopic constraints on the evolution of metamorphic conditions in the Jijal–Patan Complex and Kamila Belt of the Kohistan Arc, Pakistan Himalaya. In: Khan, M. A., Treloar, P. J., Searle, M. P. & Jan, M. Q. (eds) *Tectonics of the Nanga Parbat Syntaxis and the Western Himalaya. Geological Society, London, Special Publications* **170**, 321–331.

Anczkiewicz, R., Thirlwall, M. & Platt, J. (2002). Influence of inclusions and leaching techniques on Sm–Nd and Lu–Hf garnet chronology. *Geochimica et Cosmochimica Acta* **66**(19).

Arcay, D., Tric, E. & Doin, M.-P. (2005). Numerical simulations of subduction zones—Effect of slab dehydration on the mantle wedge dynamics. *Physics of the Earth and Planetary Interiors* **149**, 133–153.

Arcay, D., Doin, M.-P., Tric, E., Bousquet, R. & de Capitani, C. (2006). Overriding plate thinning in subduction zones: Localized convection induced by slab dehydration. *Geochemistry, Geophysics, Geosystems* **7**, Q02007, doi:10.1029/2005GC001061.

Arcay, D., Tric, E. & Doin, M.-P. (2007). Slab surface temperature in subduction zones: Influence of the interplate decoupling depth and upper plate thinning processes. *Earth and Planetary Science Letters* **255**, 324–338.

Arculus, R. J. (1994). Aspects of magma genesis on arcs. *Lithos* **33**, 189–208.

Arculus, R. J. & Powell, R. (1986). Source component mixing in the regions of arc magma generation. *Journal of Geophysical Research—Solid Earth and Planets* **91**, 5913–5926.

Bard, J.-P. (1983). Metamorphism of an obducted island arc: example of the Kohistan sequence (Pakistan) in the Himalayan collided range. *Earth and Planetary Science Letters* **65**, 133–144.

Bard, J.-P., Maluski, H., Matte, P. & Proust, F. (1980). The Kohistan sequence; crust and mantle of an obducted island arc. In: Tahirkheli, R. A. K., Jan, M. Q. & Majid, M. (eds) *Proceedings of the International Committee on Geodynamics, Group 6 Meeting*. Peshawar: University of Peshawar: Department of Geology, pp. 87–93.

Barker, F. & Grantz, A. (1982). Talkeetna Formation in the southeastern Talkeetna Mountains, southern Alaska: An early Jurassic andesitic intraoceanic island arc. *Geological Society of America, Abstracts with Programs* **14**, 147.

Ben Othman, D., White, W. M. & Patchett, J. (1989). The geochemistry of marine sediments, island arc magmas genesis, and crust–mantle recycling. *Earth and Planetary Science Letters* **94**, 1–21.

Bignold, S. M., Treloar, P. J. & Petford, N. (2006). Changing sources of magma generation beneath intra-oceanic island arcs: An insight from the juvenile Kohistan island arc, Pakistan Himalaya. *Chemical Geology* **233**, 46–74.

Billen, M. & Gurnis, M. (2001). A low viscosity wedge in subduction zones. *Earth and Planetary Science Letters* **193**, 227–236.

Billen, M., Gurnis, M. & Simons, M. (2003). Multiscale dynamics of the Tonga–Kermadec subduction zones. *Geophysical Journal International* **153**, 359–388.

Brenan, J. M., Shaw, H. F. & Ryerson, F. J. (1995). Experimental evidence for the origin of lead enrichment in convergent-margin magmas. *Nature* **378**, 54–56.

Burg, J.-P., Bodinier, J.-L., Chaudhry, S., Hussain, S. & Dawood, H. (1998). Infra-arc mantle–crust transition and intra-arc mantle diapirs in the Kohistan Complex (Pakistani Himalaya): petro-structural evidence. *Terra Nova* **10**, 74–80.

Chauvel, C., Marini, J.-C., Plank, T. & Ludden, J (2009). Hf–Nd input flux in the Izu–Mariana subduction zone and recycling of subducted material in the mantle. *Geochemistry, Geophysics, Geosystems*, **10**, Q01l0l, doi:l0.1029/2008GC002101.

Condie, K. C. & Chomiak, B. (1996). Continental accretion: contrasting Mesosoic and Early Proterozoic tectonic regimes in North America. *Tectonophysics* **265**, 101–126.

Coward, M. P., Jan, M. Q., Rex, D., Tarney, J., Thirlwall, M. F. & Windley, B. F. (1982). Geo-tectonic framework of the Himalaya of N Pakistan. *Journal of the Geological Society, London* **139**, 299–308.

Coward, M. P., Windley, B. F., Broughton, R. D., Luff, I. W. & Petterson, M. G. (1986). Collision tectonics in the NW Himalayas. In: Coward, M. P. & Ries, A. C. (eds) *Collision Tectonics. Geological Society, London, Special Pubications* **19**, 203–219.

Coward, M. P., Butler, R. W. H., Khan, M. A. & Knipe, R. J. (1987). The tectonic history of Kohistan and its implications for Himalayan structure. *Journal of the Geological Society, London* **144**, 377–391.

Crawford, A. J., Briqueu, L., Laporte, C. & Hasenaka, T. (1995). Coexistence of Indian and Pacific oceanic upper mantle reservoirs beneath the central New Hebrides island arc. In: Taylor, B. & Natland, J. P. (eds) *Active Margins and Marginal Basins of the Western Pacific. Geophysical Monograph, American Geophysical Union* **88**, 199–217.

Davidson, J. P. (1987). Crustal contamination versus subduction zone enrichment: examples from the Lesser Antilles and implications for mantle source compositions of island arc volcanic rocks. *Geochimica et Cosmochimica Acta* **51**, 2185–2198.

Davies, J. H. & Stevenson, D. J. (1992). Physical model of source region of subduction zone volcanics. *Journal of Geophysical Research* **97**, 2037–2070.

DeBari, S. M. & Coleman, R. G. (1989). Examination of the deep levels of an island-arc—evidence from the Tonsina ultramafic–mafic assemblage, Tonsina, Alaska. *Journal of Geophysical Research—Solid Earth and Planets* **94**, 4373–4391.

Debon, F. & Khan, N. A. (1996). Alkaline orogenic plutonism in the Karakorum batholith: The Upper Cretaceous Koz Sar complex (Karambar valley, N Pakistan). *Geodinamica Acta* **9**, 145–160.

Dhuime, B., Bosch, D., Bodinier, J.-L., Bruguier, O., Garrido, C. J., Hussain, S. & Dawood, H. (2006). Isotopic anatomy of an intraoceanic arc crust: Example from the Jijal–Patan–Dasu area (Kohistan arc, Indus Valley, N Pakistan). *Geophysical Research Abstracts* **8**, 05698.

Dhuime, B., Bosch, D., Bodinier, J.-L., Garrido, C. J., Bruguier, O., Hussain, S. S. & Dawood, H. (2007). Multistage evolution of the Jijal ultramafic–mafic complex (Kohistan, N Pakistan): Implications for building the roots of island arcs. *Earth and Planetary Science Letters* **261**, 179–200.

Eberle, M., Grasset, O. & Sotin, C. (2002). A numerical study of the interaction between the mantle wedge, the subducting slab, and overriding plate. *Physics of the Earth and Planetary Interiors* **134**, 191–202.

Eisele, J., Sharma, M., Galer, S. J. G., Blichert-Toft, J., Devey, C. W. & Hofmann, A. W. (2002). The role of sediment recycling in EM-1 inferred from Os, Pb, Hf, Nd, Sr isotope and trace element systematics of the Pitcairn hotspot. *Earth and Planetary Science Letters* **196**, 197–212.

Ellam, R. M. & Hawkesworth, C. J. (1988). Elemental and isotopic variations in subduction related basalts: Evidence for a three component model. *Contributions to Mineralogy and Petrology* **98**, 72–80.

Elliott, T., Plank, T., Zindler, A., White, W. & Bourdon, B. (1997). Element transport from slab to volcanic front at the Mariana arc. *Journal of Geophysical Research—Solid Earth* **102**, 14991–15019.

Ewart, A. & Hawkesworth, C. J. (1987). The Pleistocene Recent Tonga Kermadec arc lavas—interpretation of new isotopic and rare-earth data in terms of a depleted mantle source model. *Journal of Petrology* **28**, 495–530.

Ewart, A., Collerson, K. D., Regelous, M., Wendt, J. I. & Niu, Y. (1998). Geochemical evolution within the Tonga–Kermadec–Lau arc–back-arc systems: the role of varying mantle wedge composition in space and time. *Journal of Petrology* **39**, 331–368.

Faure, G. (1986). *Principles of Isotope Geology*, 2nd edn. New York: John Wiley.

Fraser, J. E., Searle, M. P., Parrish, R. R. & Noble, S. R. (2001). Chronology of deformation, metamorphism, and magmatism in the southern Karakoram Mountains. *Geological Society of America Bulletin* **113**, 1443–1455.

Gamble, J., Woodhead, J., Wright, I. & Smith, I. (1996). Basalt and sediment geochemistry and magma petrogenesis in a transect from oceanic island arc to rifted continental margin arc: the Kermadec–Hikurangi margin, SW Pacific. *Journal of Petrology* **37**, 1523–1546.

Garrido, C. J., Sanchez-Vizcaino, V. L., Gomez-Pugnaire, M. T., Trommsdorff, V., Alard, O., Bodinier, J. L. & Godard, M. (2005). Enrichment of HFSE in chlorite-harzburgite produced by high-pressure dehydration of antigorite-serpentinite: Implications for subduction magmatism. *Geochemistry, Geophysics, Geosystems* **6**, Q01J15.

Garrido, C. J., Bodinier, J.-L., Burg, J.-P., Zeilinger, G., Hussain, S., Dawood, H., Chaudhry, M. N. & Gervilla, F. (2006). Petrogenesis of mafic garnet granulite in the lower crust of the Kohistan Paleo-arc Complex (Northern Pakistan): Implications for intra-crustal differentiation of island arcs and generation of continental crust. *Journal of Petrology* **47**, 1873–1914.

Garrido, C. J., Bodinier, J.-L., Dhuime, B., Bosch, D., Chanefo, I., Bruguier, O., Hussain, S., Dawood, H. & Burg, J.-P. (2007). Origin of the island arc Moho transition zone via melt–rock reaction and its implications for intracrustal differentiation of island arcs: Evidence from the Jijal complex (Kohistan complex, northern Pakistan). *Geology* **35**, 683–686.

Gill, J. (1981). *Orogenic Andesites and Plate Tectonics*. Berlin: Springer.

Hart, S. R. (1984). A large-scale isotopic anomaly in the Southern Hemisphere mantle. *Nature* **309**, 753–757.

Hart, S. R. (1988). Heterogeneous mantle domains: signatures, genesis and mixing chronologies. *Earth and Planetary Science Letters* **90**, 273–296.

Hart, S. R. & Dunn, T. (1993). Experimental Cpx melt partitioning of 24 trace-elements. *Contributions to Mineralogy and Petrology* **113**, 1–8.

Hawkesworth, C. J. (1982). Isotope characteristics of magmas erupted along destructive plate margins. In: Thorpe, R. S. (ed.) *Andesites: Orogenic Andesites and Related Rocks*. Chichester: John Wiley, pp. 549–571.

Hawkesworth, C. J., Hergt, J. M., Ellam, R. M. & McDermott, F. (1991). Element fluxes associated with subduction related magmatism. *Philosophical Transactions of the Royal Society of London, Series A* **335**, 393–405.

Hawkesworth, C. J., Gallagher, K., Hergt, J. M. & McDermott, F. (1993). Mantle and slab contributions in arc magmas. *Annual Review of Earth and Planetary Sciences* **21**, 175–204.

Hawkesworth, C. J., Turner, S. P., McDermott, F., Peate, D. W. & van Calsteren, P. J. (1997*a*). U–Th isotopes in arc magmas: implications for element transfer from the subducted slab. *Science* **276**, 551–555.

Hawkesworth, C. J, Turner, S. P., Peate, D., McDermott, F. & van Calsteren, P. J. (1997*b*). Elemental U and Th variations in island arc rocks: implications for U-series isotopes. *Chemical Geology* **139**, 207–221.

Hermann, J. & Green, D.H. (2001). Experimental constraints on high pressure melting in subducted crust. *Earth and Planetary Science Letters* **188**, 149–168.

Hermann, J. & Spandler, C. (2008). Sediment melts at sub-arc depths: an experimental study. *Journal of Petrology* **49**, 717–740.

Hermann, J., Spandler, C., Hack, A. & Korsakov, A. (2006). Aqueous fluids and hydrous melts in high-pressure and ultra-high pressure rocks: Implications for element transfer in subduction zones. *Lithos* **92**, 399–417.

Hirth, G. & Kohlstedt, D. (1996). Water in the oceanic upper mantle: implications for rheology, melt extraction and the evolution of the lithosphere. *Earth and Planetary Science Letters* **144**, 93–108.

Hofmann, A. W. (1988). Chemical differentiation of the Earth—the relationship between mantle, continental-crust, and oceanic-crust. *Earth and Planetary Science Letters* **90**, 297–314.

Hofmann, A. W. (2003). Sampling mantle heterogeneity through oceanic basalts: Isotopes and trace elements. In: Holland, H. D. & Turekian, K. K. (eds) *Treatise on Geochemistry*. Oxford: Elsevier–Pergamon, pp. 61–101.

Honda, S. & Saito, M. (2003). Small-scale convection under the back-arc occurring in the low viscosity wedge. *Earth and Planetary Science Letters* **216**, 703–715.

Jagoutz, O., Müntener, O., Burg, J.-P., Ulmer, P. & Jagoutz, E. (2006). Lower continental crust formation through focused flow in km-scale melt conduits: The zoned ultramafic bodies of the Chilas Complex in the Kohistan island arc (NW Pakistan). *Earth and Planetary Science Letters* **242**, 320–342.

Jan, M. Q. (1979). Petrography of the Jijal Complex, Kohistan. In: Tahirkheli, R. A. K. & Jan, M. Q. (eds) *Geology of Kohistan, Karakoram Himalaya, Northern Pakistan*. Peshawar: University of Peshawar, pp. 31–49.

Jan, M. Q. & Howie, R. A. (1981). The mineralogy and geochemistry of the metamorphosed basic and ultrabasic rocks of the Jijal Complex, Kohistan, NW Pakistan. *Journal of Petrology* **22**, 85–126.

Jan, Q. M. (1988). Geochemistry of amphibolites from the southern part of the Kohistan Arc, N. Pakistan. *Mineralogical Magazine* **52**, 147–159.

Jull, M. & Kelemen, P. B. (2001). On the conditions for lower crustal convective instability. *Journal of Geophysical Research* **106**, 6423–6446.

Kamenetsky, V. S., Crawford, A. J., Eggins, S. & Muhe, R. (1997). Phenocryst and melt inclusion chemistry of near-axis seamounts, Valu Fa Ridge, Lau Basin: insight into mantle wedge melting and addition of subduction components. *Earth and Planetary Science Letters* **151**, 205–223.

Karato, S.-I. (2003). Mapping Water Content in the Upper Mantle. In: Eiler, J. (ed.) *Inside the Subduction Factory*. Washington, DC: Geophysical Monograph, pp. 135–152.

Karato, S.-I., Paterson, M. & FitzGerald, J. (1986). Rheology of synthetic olivine aggregates: influence of grain size and water. *Journal of Geophysical Research* **91**, 8151–8176.

Kay, R. W. (1980). Volcanic arc magmas—implications of a melting–mixing model for element recycling in the crust–upper mantle system. *Journal of Geology* **88**, 497–522.

Kay, S. M. & Kay, R. W. (1985). Role of crystal cumulates and the oceanic-crust in the formation of the lower crust of the Aleutian Arc. *Geology* **13**, 461–464.

Kay, R. W. & Kay, S. M. (1993). Delamination and delamination magmatism. *Tectonophysics* **219**, 177–189.

Kelemen, P. B., Hanghøj, K. & Greene, A. R. (2003). One view of the geochemistry of subduction-related magmatic arcs, with an emphasis on primitive andesite and lower crust. In: Rudnick, R. L. (ed.) *Geochemistry of the Crust*. Amsterdam: Elsevier, pp. 593–659.

Kemp, A. I. S., Shimura, T. & Hawkesworth, C. J. (2007). Linking granulites, silicic magmatism, and crustal growth in arcs: Ion microprobe (zircon) U–Pb ages from the Hidaka metamorphic belt, Japan. *Geology* **35**, 807–810.

Khan, M. A., Jan, M. Q., Windley, B. F., Tarney, J. & Thirlwall, M. F. (1989). The Chilas mafic-ultramafic igneous complex: the root of the Kohistan island arc in the Himalaya of northern Pakistan. In: Malinconico, L. L., Jr. & Lillie, R. J. (eds) *Tectonics of the western Himalayas*. Boulder, CO, United States: Geological Society of America, pp. 75–94.

Khan, M. A., Jan, M. Q. & Weaver, B. L. (1993). Evolution of the lower arc crust in Kohistan, N. Pakistan: temporal arc magmatism through early, mature and intra-arc rift stages. In: Treloar, P. J. & Searle, M. P. (eds) *Himalayan Tectonics. Geological Society, London Special Publications* **74**, 123–138.

Khan, M. A., Stern, R. J., Gribble, R. F. & Windley, B. F. (1997). Geochemical and isotopic constraints on subduction polarity, magma sources, and palaeogeography of the Kohistan intra-oceanic arc, northern Pakistan Himalaya. *Journal of the Geological Society, London* **154**, 935–946.

Kincaid, C. & Sacks, I. (1997). Thermal and dynamical evolution of the upper mantle in subduction zones. *Journal of Geophysical Research* **102**, 12295–12315.

Klimm, K., Blundy, J. & Green, T. H. (2008). Trace element partitioning and accessory phase saturation during H_2O-saturated melting of basalt with implications for subduction zone chemical fluxes. *Journal of Petrology* **49**, 523–553.

Kogiso, T., Tatsumi, Y. & Nakano, S. (1997). Trace element transport during dehydration processes in the subducted oceanic crust. 1. Experiments and implications for the origin of ocean island basalts. *Earth and Planetary Science Letters* **148**, 193–205.

Le Fort, P., Michard, A., Sonet, J. & Zimmermann, J. L. (1983). Petrography, geochemistry and geochronology of some samples from the Karakorum Axial Batholith (northern Pakistan). In: Shams, F. A. (ed.) *Granites of Himalayas, Karakorum and Hindu Kush*. Lahore: Institute of Geology, Punjab University, pp. 377–387.

Luais, B., Télouk, P. & Albarède, F. (1997). Precise and accurate neodymium isotopic measurements by plasma-source mass spectrometry. *Geochimica et Cosmochimica Acta* **61**, 4847–4854.

Mackwell, S., Kohlstedt, D. & Paterson, M. (1985). The role of water in the deformation of olivine single crystals. *Journal of Geophysical Research* **90**, 11319–11333.

Mahoney, J. J., Frei, R., Tejada, M. L. G., Mo, X. X., Leat, P. T. & Nägler, T. F. (1998). Tracing the Indian Ocean mantle domain through time: Isotopic results from old west Indian, east Tethyan, and south Pacific seafloor. *Journal of Petrology* **37**, 1285–1306.

Mahoney, J. J., Graham, D. W., Christie, D. M., Johnson, K. T. M., Hall, L. S. & Vonderharr, D. L. (2002). Between a hotspot and a coldspot: Isotopic variation in the southeast Indian ridge asthenosphere 86°E–118°E. *Journal of Petrology* **43**, 1155–1176.

Manhès, G., Allègre, C. J., Dupré, B. & Hamelin, B. (1980). Lead isotope study of basic–ultrabasic layered complexes: speculations about the age of the Earth and primitive mantle characteristics. *Earth and Planetary Science Letters* **47**, 370–382.

McCulloch, M. T. & Gamble, J. A. (1991). Geochemical and geodynamical constraints on subduction zone magmatism. *Earth and Planetary Science Letters* **102**, 358–374.

McLennan, S. M. & Taylor, S. R. (1985). *The Continental Crust: Its Composition and Evolution: An Examination of the Geochemical Record Preserved in Sedimentary Rocks*. Oxford: Blackwell Scientific.

Mei, S. & Kohlstedt, D. (2000*a*). Influence of water on plastic deformation of olivine aggregates. 1. Diffusion creep regime. *Journal of Geophysical Research* **105**, 21457–21469.

Mei, S. & Kohlstedt, D. (2000*b*). Influence of water on plastic deformation of olivine aggregates. 2. Dislocation creep regime. *Journal of Geophysical Research* **105**, 21471–21481.

Mikoshiba, M. U., Takahashi, Y., Takahashi, Y., Kausar, A. B., Khan, T., Kubo, K. & Shirahase, T. (1999). Rb–Sr isotopic study of the Chilas igneous complex, Kohistan, northern Pakistan. In: Macfarlane, A., Sorkhabi, R. B. & Quade, J. (eds) *Himalaya and Tibet; Mountain Roots to Mountain Tops. Geological Society of America, Special Papers* **328**, 47–57.

Miller, D. J. & Christensen, N. I. (1994). Seismic signature and geochemistry of an island arc: a multidisciplinary study of the Kohistan accreted terrane, northern Pakistan. *Journal of Geophysical Research* **99**, 11623–11642.

Miller, D. J., Loucks, R. R. & Ashraf, M. (1991). Platinum-group element mineralization in the Jijal layered ultramafic–mafic complex, Pakistani Himalayas. *Economic Geology* **86**, 1093–1102.

Miller, D. M., Goldstein, S. L. & Langmuir, C. H. (1994). Cerium–lead and lead-isotope ratios in arc magmas and the enrichment of lead in the continents. *Nature* **368**, 514–520.

Miyashiro, A. (1974). Volcanic rock series in island arcs and active continental margins. *American Journal of Science* **274**, 321–355.

Morency, C. & Doin, M.-P. (2004). Numerical simulations of the mantle lithosphere delamination. *Journal of Geophysical Research* **109**, B03410.

Morris, J. D. & Hart, S. R. (1983). Isotopic and incompatible element constraints on the genesis of island arc volcanics from Cold Bay and Amak Island, Aleutians, and implications for mantle structure. *Geochemica et Cosmochimica Acta* **47**, 2015–2030.

Münker, C. (2000). The isotope and trace element budget of the Cambrian Devil River arc system, New Zealand: Identification of four source components. *Journal of Petrology* **41**, 759–788.

Nicholls, I. A. & Ringwood, A. E. (1973). Effect of water on olivine stability in tholeiites and the production of silica-saturated magmas in the island-arc environment. *Journal of Geology* **81**, 285–300.

Padrón-Navarta, J. A., Garrido, C. J., Sánchez-Navas, A., Tommasi, A., López Sánchez-Vizcaíno, V., Gomez-Pugnaire, M. T. & Hussain, S. S. (2008). Oriented growth of garnet by topotactic reactions and epitaxy in high-pressure, mafic garnet granulite formed by dehydration melting of metastable hornblende-gabbronorite (Jijal Complex, Kohistan Complex, north Pakistan). *Journal of Metamorphic Geology* **26**, 855–870.

Pearce, J. A. (1982). Trace element characteristics of lavas from destructive plate boundaries. In: Thorpe, R. S. (ed.) *Andesites*. Chichester: John Wiley, pp. 525–547.

Pearce, J. A. & Parkinson, I. J. (1993). Trace element models for mantle melting: application to volcanic arc petrogenesis. In: Prichard, H. M., Alabaster, T., Harris, N. B. & Neary, C. R. (eds) *Magmatic Processes and Plate Tectonics. Geological Society, London, Special Publications* **76**, 373–403.

Pearce, J. A., Kempton, P. D. & Gill, J. B. (2007). Hf–Nd evidence for the origin and distribution of mantle domains in the SW Pacific. *Earth and Planetary Science Letters* **260**, 98–114.

Peate, D. W., Pearce, J. A., Hawkesworth, C. J., Colley, H., Edwards, C. M. H. & Hirose, K. (1997). Geochemical variations in Vanuatu arc lavas: the role of subducted material and a variable mantle wedge composition. *Journal of Petrology* **38**, 1331–1358.

Perfit, M. R., Gust, D. A., Bence, A. E., Arculus, R. J. & Taylor, S. R. (1980). Chemical characteristics of island-arc basalts—implications for mantle sources. *Chemical Geology* **30**, 227–256.

Petterson, M. G. & Windley, B. F. (1985). Rb–Sr dating of the Kohistan arc-batholith in the Trans-Himalaya of North Pakistan, and tectonic implications. *Earth and Planetary Science Letters* **74**, 45–57.

Pin, C., Briot, D., Bassin, C. & Poitrasson, F. (1994). Concomitant extraction of Sr and Sm–Nd for isotopic analysis in silicate samples based on specific extraction chromatography. *Analytica Chimica Acta* **298**, 209–217.

Plank, T. & Langmuir, C. H. (1993). Tracing trace elements from sediment input to volcanic output at subduction zones. *Nature* **362**, 739–743.

Plank, T. & Langmuir, C. H. (1998). The chemical composition of subducting sediment and its consequences for the crust and mantle. *Chemical Geology* **145**, 325–394.

Plank, T., Kelley, K. A., Murray, R. W. & Stern, L. Q. (2006). Chemical composition of sediments subducting at the Izu–Bonin trench. *Geochemistry, Geophysics, Geosystems* **8**, 1–16.

Pudsey, C. J. (1986). The Northern Suture, Pakistan—Margin of a Cretaceous island-arc. *Geological Magazine* **123**, 405–423.

Ranero, C. R. & von Huene, R. (2000). Subduction erosion along the Middle America convergent margin. *Nature* **404**, 748–755.

Regelous, M., Collerson, K.D., Ewart, A. & Wendt, J.I. (1997). Trace element transport rates in subduction zones: evidence from Th, Sr and Pb isotope data for Tonga–Kermadec arc lavas. *Earth and Planetary Science Letters* **150**, 291–302.

Ringuette, L., Martignole, J. & Windley, B. F. (1999). Magmatic crystallization, isobaric cooling, and decompression of the garnet-bearing assemblages of the Jijal Sequence (Kohistan Terrane, western Himalayas). *Geology* **27**, 139–142.

Ringwood, A. E. (1974). The petrological evolution of island arc systems. *Journal of the Geological Society, London* **130**, 183–204.

Rudnick, R. L. (1995). Making continental crust. *Nature* **378**, 571–578.

Rudnick, R. L. & Fountain, D. M. (1995). Nature and composition of the continental crust—a lower crustal perspective. *Reviews of Geophysics* **33**, 267–309.

Ryerson, F. J. & Watson, E. B. (1987). Rutile saturation in magmas—Implications for Ti–Nb–Ta depletion in island-arc basalts. *Earth and Planetary Science Letters* **86**, 225–239.

Saunders, A. D., Norry, M. J. & Tarney, J. (1991). Fluid influence on the compositions of subduction zone magmas. *Philosophical Transactions of the Royal Society of London, Series A* **335**, 377–392.

Schaltegger, U., Zeilinger, G., Frank, M. & Burg, J.-P. (2002). Multiple mantle sources during island arc magmatism: U–Pb and Hf isotopic evidence from the Kohistan arc complex, Pakistan. *Terra Nova* **14**, 461–468.

Schärer, U., Hamet, J. & Allègre, C. J. (1984). The Transhimalaya (Gangdese) plutonism in the Ladakh region: a U–Pb and Rb–Sr study. *Earth and Planetary Science Letters* **67**, 327–339.

Spandler, C., Mavrogenes, J. & Hermann, J. (2007). Experimental constraints on element mobility from subducted sediments using high-*P* synthetic fluid/melt inclusions. *Chemical Geology* **239**, 228–249.

Stern, R. J. (2004). Subduction initiation: spontaneous and induced. *Earth and Planetary Science Letters* **226**, 275–292.

Stern, R. J. & Bloomer, S. H. (1992). Subduction zone infancy: Examples from the Eocene Izu–Bonin–Mariana and Jurassic California arcs. *Geological Society of America Bulletin* **104**, 1621–1636.

Stolper, E. & Newman, S. (1994). The role of water in the petrogenesis of the Mariana trough magmas. *Earth and Planetary Science Letters* **121**, 293–325.

Sun, S.-S. & McDonough, W. F. (1989). Chemical and isotopic systematics of oceanic basalts: implications for mantle composition and processes. In: Saunders, A. D. & Norry, M. J. (eds) *Magmatism in the Ocean Basins. Geological Society, London, Special Publications* **42**, 313–345.

Tahirkheli, R. A. K. (1979). Geotectonic evolution of Kohistan. In: Tahirkheli, R. A. K. & Jan, M. Q. (eds) *Geology of Kohistan, Karakoram Himalaya, northern Pakistan*. Peshawar: University of Peshawar, pp. 113–130.

Tahirkheli, R. A. K., Mattauer, M., Proust, F. & Tapponier, P. (1979). The Indian–Eurasia suture in northern Pakistan. Synthesis and interpretation of data on plate scale. In: Farah, A. & Dejong, K. (eds) *Geodynamics of Pakistan*. Quetta: Geological Survey of Pakistan, pp. 125–130.

Takahashi, Y., Mikoshiba, M. U., Takahashi, Y., Kausar, A. B., Khan, T. & Kubo, K. (2006). Geochemical modelling of the Chilas Complex in the Kohistan Terrane, northern Pakistan. *Journal of Asian Earth Sciences* doi:10.1016/j.jseaes.2006.04.007.

Tatsumi, Y. (1989). Migration of fluid phases and genesis of basalt magmas in subduction zones. *Journal of Geophysical Research—Solid Earth and Planets* **94**, 4697–4707.

Tatsumi, Y. (2000). Continental crust formation by delamination in subduction zones and complementary accumulation of the enriched mantle I component in the mantle. *Geochemistry, Geophysics, Geosystems* **1**, 1–17.

Tatsumi, Y. & Kogiso, T. (1997). Trace element transport during dehydration processes in the subducted oceanic crust. 2. Origin of chemical and physical characteristics in arc magmatism. *Earth and Planetary Science Letters* **148**, 207–221.

Tatsumi, Y., Hamilton, D. L. & Nesbitt, R. W. (1986). Chemical characteristics of fluid phase released from a subducted lithosphere and origin of arc magmas: Evidence from high-pressure experiments and natural rocks. *Journal of Volcanology and Geothermal Research* **29**, 293–309.

Taylor, S. R. & McLennan, S. M. (1985). *The Continental Crust: Its Composition and Evolution*. Oxford: Blackwell.

Tera, F., Brown, L., Morris, J. & Sacks, I. S. (1986). Sediment incorporation in island-arc magmas: Inferences from ^{10}Be. *Geochimica et Cosmochimica Acta* **50**, 535–550.

Treloar, P. J., Broughton, R. D., Williams, M. P., Coward, M. P. & Windley, B. F. (1989). Deformation, metamorphism and imbrication of the Indian Plate, south of the Main Mantle Thrust, North Pakistan. *Journal of Metamorphic Geology* **7**, 111–125.

Treloar, P. J., Brodie, K. H., Coward, M. P., Jan, M. Q., Khan, M. A., Knipe, R. J., Rex, D. C. & Williams, M. P. (1990). The evolution of the Kamila shear zone, Kohistan, Pakistan. In: Salisbury, M. H. & Fountain, D. M. (eds) *Exposed Cross-sections of the Continental Crust*. Dordrecht: Kluwer Academic, pp. 175–214.

Treloar, P. J., Petterson, M. G., Jan, M. Q. & Sullivan, M. A. (1996). A re-evaluation of the stratigraphy and evolution of the Kohistan arc sequence, Pakistan Himalaya: Implications for magmatic and tectonic arc-building processes. *Journal of the Geological Society, London* **153**, 681–693.

Turner, S. & Hawkesworth, C. J. (1997). Constraints on flux rates and mantle dynamics beneath island arcs from Tonga–Kermadec lava geochemistry. *Nature* **389**, 568–573.

Turner, S., Hawkesworth, C. J., van Calsteren, P., Heath, E., Macdonald, R. & Black, S. (1996). U-series isotopes and destructive plate margin magma genesis in the Lesser Antilles. *Earth and Planetary Science Letters* **142**, 191–207.

Turner, S., Hawkesworth, C. J., Rogers, N., Bartlett, J., Worthington, T., Hergt, J., Pearce, J. & Smith, I. (1997). ^{238}U–^{230}Th disequilibria, magma petrogenesis, and flux rates beneath the depleted Tonga–Kermadec island arc. *Geochimica et Cosmochimica Acta* **61**, 4855–4884.

Van Keken, P. E. (2003). The structure and dynamics of the mantle wedge. *Earth and Planetary Science Letters* **215**, 323–338.

Van Keken, P. E., Kiefer, B. & Peacock, S. (2002). High-resolution models of subduction zones: implications for mineral dehydration reactions and the transport of water into the deep mantle. *Geochemistry, Geophysics, Geosystems* **3**, 1056, doi:10.1029/2001GC000256.

von Huene, R. & Scholl, D. W. (1991). Observations at convergent margins concerning sediment subduction, subduction erosion, and the growth of continental crust. *Reviews of Geophysics* **29**, 279–316.

von Huene, R. & Scholl, D. W. (1993). The return of sialic material to the mantle indicated by terrigeneous material subducted at convergent margins. *Tectonophysics* **219**, 163–175.

White, W. M. & Patchett, P. J. (1984). Hf–Nd–Sr isotopes and incompatible element abundances in island arcs: implications for magma origin and crust–mantle evolution. *Earth and Planetary Science Letters* **67**, 167–185.

White, W. M., Albarède, F. & Télouk, P. (2000). High-precision analysis of Pb isotope ratios by multi-collector ICP-MS. *Chemical Geology* **167**, 257–270.

Woodhead, J. D. (1989). Geochemistry of the Mariana arc (western Pacific): source composition and processes. *Chemical Geology* **76**, 1–24.

Woodhead, J. D., Eggins, S.M. & Gamble, J. (1993). High field strength and transition element systematics in island arc and back-arc basin basalts: evidence for a multiphase melt extraction and a depleted mantle wedge. *Earth and Planetary Science Letters* **114**, 491–504.

Woodhead, J. D., Eggins, S. M. & Johnson, R.W. (1998). Magma genesis in the New Britain Island arc: further insights into melting and mass transfer processes. *Journal of Petrology* **39**, 1641–1668.

Yamamoto, H. (1993). Contrasting metamorphic *P–T*–time paths of the Kohistan granulites and tectonics of the western Himalayas. *Journal of the Geological Society, London* **150**, 843–856.

Yamamoto, H. & Nakamura, E. (1996). Sm–Nd dating of garnet granulites from the Kohistan Complex, northern Pakistan. *Journal of the Geological Society, London* **153**, 965–969.

Yamamoto, H. & Nakamura, E. (2000). Timing of magmatic and metamorphic events in the Jijal Complex of the Kohistan Arc deduced from Sm–Nd dating of mafic granulites. *Geological Society, London, Special Publications* **170**, 313–319.

Yamamoto, H., Nakamura, E., Kaneko, Y. & Kausar, A. B. (2005). U–Pb zircon dating of regional deformation in the lower crust of the Kohistan Arc. *International Geology Review* **47**, 1035–1047.

Yoshino, T., Yamamoto, H., Okudaira, T. & Toriumi, M. (1998). Crustal thickening of the lower crust of the Kohistan Arc (N. Pakistan) deduced from Al zoning in clinopyroxene and plagioclase. *Journal of Metamorphic Geology* **16**, 729–748.

Zeilinger, G. (2002). Structural and geochronological study of the lowest Kohistan Complex, Indus Kohistan region in Pakistan, NW Himalaya. PhD thesis, ETH, Zurich.

Zeitler, P. K., Tahirkheli, R. A. K., Naesser, C., Johnson, N. & Lyons, J. (1981). Preliminary fission track ages from the Swat valley, northern Pakistan. *Geological Bulletin, University of Peshawar* **13**, 63–65.

Zindler, A. & Hart, S. (1986). Chemical geodynamics. *Annual Review of Earth and Planetary Sciences* **14**, 493–571.